SAMPLED ANALOG RECURSIVE COMB FILTERS AND THEIR APPLICATION TO MTI- RADAR

Lars Terje Saetre

NAVAL POSTGRADUATE SCHOOL
Monterey, California

THESIS

SAMPLED ANALOG RECURSIVE COMB FILTERS
AND THEIR
APPLICATION TO MTI- RADAR
by

Lars Terje Sætre

December 1975

Thesis advisor: T.F. Tao

Approved for public release; distribution unlimited.

SECURITY CLASSIFICATION OF THIS PAGE (When Data Entered)

REPORT DOCUMENTATION PAGE

READ INSTRUCTIONS BEFORE COMPLETING FORM

1. REPORT NUMBER

2. GOVT ACCESSION NO.

3. RECIPIENT'S CATALOG NUMBER

4. TITLE (and Subtitle)

Sampled Analog Recursive Comb Filters and their Application to MTI- Radar

5. TYPE OF REPORT & PERIOD COVERED

Master's Thesis
December 1975

6. PERFORMING ORG. REPORT NUMBER

7. AUTHOR(s)

Lars Terje Sætre

8. CONTRACT OR GRANT NUMBER(s)

9. PERFORMING ORGANIZATION NAME AND ADDRESS

Naval Postgraduate School
Monterey, California 93940

10. PROGRAM ELEMENT, PROJECT, TASK AREA & WORK UNIT NUMBERS

11. CONTROLLING OFFICE NAME AND ADDRESS

Naval Postgraduate School
Monterey, California 93940

12. REPORT DATE

December 1975

13. NUMBER OF PAGES

14. MONITORING AGENCY NAME & ADDRESS(if different from Controlling Office)

15. SECURITY CLASS. (of this report)

Unclassified

15a. DECLASSIFICATION/DOWNGRADING SCHEDULE

16. DISTRIBUTION STATEMENT (of this Report)

Approved for public release; distribution unlimited.

17. DISTRIBUTION STATEMENT (of the abstract entered in Block 20, if different from Report)

18. SUPPLEMENTARY NOTES

19. KEY WORDS (Continue on reverse side if necessary and identify by block number)

Comb Filters
Sampled Analog Filters
MTI-canceller

20. ABSTRACT (Continue on reverse side if necessary and identify by block number)

The design of second order sampled analog filters using Z-transform techniques developed in digital theory was studied. A second order recursive CTD- filter was implemented and investigated. Deviation from theoretical frequency response was found to be partly due to frequency dependent circuitry.

DD FORM 1 JAN 73 1473 EDITION OF 1 NOV 65 IS OBSOLETE
S/N 0102-014-6601 |
(Page 1)

UNCLASSIFIED
SECURITY CLASSIFICATION OF THIS PAGE (When Data Entered)

(20. ABSTRACT Continued)

MTI- simulation was performed, and the ability of the CTD-filter to cancel clutter and pass doppler frequencies was demonstrated. Unexplained glitches in the filter output were noted.

Sampled Analog Recursive Comb Filters and their Application to MTI- Radar

by

Lars Terje Saetre
Lieutenant Commander, Royal Norwegian Navy
B.S., Royal Norwegian Naval Academy, 1964

Submitted in partial fulfillment of the
requirements for the degree of

MASTER OF SCIENCE IN ELECTRICAL ENGINEERING

FROM
from the

NAVAL POSTGRADUATE SCHOOL

December 1975

ABSTRACT

The design of second order sampled analog filters using Z-transform techniques developed in digital theory was studied. A second order recursive CTD- filter was implemented and investigated. Deviation from theoretical frequency response was found to be partly due to frequency dependent circuitry.
MTI- simulation was performed, and the ability of the CTD-filter to cancel clutter and pass doppler frequencies was demonstrated. Unexplained glitches in the filter output were noted.

TABLE OF CONTENTS

LIST OF TABLES

LIST OF FIGURES

ACKNOWLEDGEMENT

The author expresses his sincere appreciation to Dr. T.F. Tao for his inspiration and guidance in this study, LCDR Stacy Holmes for his assistance, and other members of the research team for their time and support.

I. INTRODUCTION

The field of Signal Processing is expanding rapidly, indicating an increasing importance. Today, digital signal processing is being extensively explored and employed. High speed digital computers with necessary peripheral equipment such as analog-to-digital and digital-to-analog converters are required. Traditional analog systems as radar and sonar are going digital. There exists a wealth of other digital signal processing applications.

For some applications, however, the use of digital processing may be termed "overkill", even if there is a distinct requirement for the inherent advantages of digital processing over analog processing.

A fairly new device technology, the Charge Transport Device technology (CTD's) offers new ways of signal processing which could be the answer for such cases.
Charge Transport Devices refer to several families of devices: Bucket Brigade Devices (BBD's), Charge Coupled Devices (CCD's), and Reticon Devices (i.e. SAD-100 and TAD-12) which are described in reference {3}.

The unique feature of CTD's is that the signal is represented by discrete charge packets, which are moved through the device at a speed determined by the clock frequency. The delay of the device is thus controlled by the clock frequency, and may be easily and momentarily changed. An excellent review of how the CCD works is given in reference {8}.
CTD's find wide applications in imaging (both low light, normal light and infrared), analog time delay, multiplexing, transversal filtering, with fixed and variable weighting, recursive filtering, correlators, chirp-z transformers and so on. The general advantages of CTD signal processors over conventional digital processing are lower cost, power, weight and size.

Comb filters are described by their periodic transfer characteristics in the frequency domain. They can be classified into two general types. The first type is the bandstop or canceller type shown in Table II. It has strong attenuation in a narrow neighbourhood of a series of periodically separated frequencies and good transmission in between. The second type is the bandpass, or integrator type (Table II). It has good transmission in a narrow neighbourhood of a series of periodically separated frequencies and strong attenuation in between. All possible implementation techniques for such comb filters use some kind of delay device.

In the analog case, a quartz delay line has been extensively used. It is, however, temperature dependent and results have in general not been very satisfactory. For the digital case the delay device is the shift register, in which the amount of delay is determined by the employed clock frequency.

Today a new family of comb filters is being developed, using the new CTD's. In these, analog signals are first sampled and then delayed. As a result of the sampling, these devices not only have standard analog properties but also some digital properties such as aliasing and stability of delay. A CTD consists of N serial delay stages. A signal will then be delayed N clock periods before it is fed back to the input in the recursive case. The frequency of recursive operation, f_r, is then only $\frac{1}{N}.f_c$, where f_c is the clock frequency, or sampling frequency. Therefore, in radar terms, f_r is equal to the Pulse Repetition Frequency (PRF), and there are $\frac{N}{2}$ teeth of the comb within the Nyquist frequency range from 0 to $f_c/2$.

So far recursive filtering using CCD's have not been extensively studied in the industry, since it was believed that it can only be done with extensive external electronic support such as fast and accurate operational amplifiers etc. {5}.

In fact, reference {4} was the only paper on CCD- recursive filters presented at the recent conference on CCD-applications in San Diego.
This thesis will study the second order recursive comb filter and employ a simulation scheme to study its application as a canceller in an MTI-radar.

II. SAMPLED ANALOG SECOND ORDER RECURSIVE COMB FILTERS

A. THEORY

1. Analog Filter

Since the sampled analog recursive filters are implemented by the same circuit configuration used for digital recursive filters, we may apply the existing well-developed theory for such filters. However, proper modifications must be made to account for the fact that the signal is now sampled analog and that there now are N delay stages instead of one. It is known that two general design approaches have been developed for the IIR (infinite impulse response) type digital recursive filter, namely the indirect and direct methods. The indirect method starts with the transfer function in the LaPlace transform variable s (H(s)), of a continuous filter and follows by performing another transform to obtain the corresponding transfer function in the discrete time variable z . Several different transforms are available for this purpose, for example mapping by differential transform, impulse invariant (standard z) transform, bilinear z-transform and matched z-transform.
The direct method is digital design in frequency or time domain using some type of computer aided design procedure.

Here the indirect approach will be used:
Given a prescribed response, there are several methods by which one can develop a transfer function in the variable s. Examples are: Butterworth, Chebyshev and elliptical filters etc{1}. In this thesis the Butterworth approach is used to obtain the transfer function in the s-domain.

a. For a Low Pass Filter

For the Butterworth filter in the second order case the equation is given as:

$$H(j\omega)^2 = \frac{1}{1 + \left(\frac{j\omega}{j\omega_x}\right)^2}$$

where ω_x is the 3-db cutoff frequency.

Converting to s-domain and expanding:

$$H(s) \cdot H(-s) = \frac{1}{1 + \left(\frac{s}{j\omega_x}\right)^{2N}} \qquad \text{Let } N = 2$$

By evaluating the poles in the s-plane and discarding the two poles in the right hand plane, one gets:

$$H(s) = \frac{1}{s^2 + 2\omega_x s + \omega_x^2}$$

This is the desired transfer function in the s-domain.

b. For High Pass Filter

A similar derivation for the high pass case gives:

$$H(s) = \frac{s^2}{s^2 + 2\omega_x s + \omega_x^2}$$

2. Transformation to Z-domain

a. Low Pass Filter

By indirect design method, using the bilinear z-transform:

$$s = \frac{2(z-1)}{T(z+1)}$$

one gets the following transfer function in z:

$$H(z) = \frac{\omega_x^2}{\left(\frac{2}{T}\,\frac{z-1}{z+1}\right)^2 + \frac{2}{T}\,\frac{z-1}{z+1}\,2\omega_x + \omega_x^2}$$

By employing a little algebra one will end up with this equation:

$$H(z) = \frac{K\,(a_o + a_1 z^{-1} + a_2 z^{-2})}{1 + b_1 z^{-1} + b_2 z^{-2}}$$

where:

$$K = \frac{T^2 \omega_x^2}{4 + 2\sqrt{2}\,\omega_x T + \omega_x^2 T^2}$$

$$a_o = 1$$

$$a_1 = 2$$

$$a_2 = 1$$

$$b_1 = \frac{2\omega_x^2 T^2 - 8}{4 + 2\sqrt{2}\,\omega_x T + \omega_x^2 T^2}$$

$$b_2 = \frac{4 + \omega_x^2 T^2 - 2\sqrt{2}\,\omega_x T}{4 + 2\sqrt{2}\,\omega_x T + \omega_x^2 T^2}$$

b. High Pass Filter

Starting from the s-domain equation:

$$H(s) = \frac{s^2}{s^2 + \sqrt{2}\,\omega_x\, s + \omega_x{}^2}$$

and using the bilinear transform again, one end up with:

$$H(z) = \frac{K(\, a_o + a_1\, z^{-1} + a_2\, z^{-2})}{1 + b_1\, z^{-1} + b_2\, z^{-2}}$$

where:

$$K = \frac{4}{4 + 2\sqrt{2}\,\omega_x T + \omega_x{}^2\, T^2}$$

$$a_o = a_2 = 1$$

$$a_1 = -2$$

$$b_1 = \frac{2\,\omega_x{}^2 T^2 - 8}{4 + 2\sqrt{2}\,\omega_x T + \omega_x{}^2 T^2}$$

$$b_2 = \frac{4 - 2\sqrt{2}\,\omega_x T + \omega_x{}^2 T^2}{4 + 2\sqrt{2}\,\omega_x{}^2 T + \omega_x{}^2 T^2}$$

It is noted that ω_x and T always occur together in the final expressions and that there are only two differences between the high pass and low pass cases: The size of K, and the sign of a_1. But K is merely a scaling factor, and has no influence upon the shape of the frequency response.

This means that when the coefficients are kept constant, the

TABLE I

$\omega_x T$	b_1	$\omega_x T$	b_2
0	-2.	0	1.
.1	-1.86	.5	.5
.5	-1.32	1.	.28
.7	-1.09	1.5	.18
1.	-.77	2.	.17
1.3	-.49	3.	.21
1.6	-.26	4.	.28
1.9	-.06	5.	.34
2.	0	6.	.4
3.	.47	7.	.46
4.	.77		
6.	1.24		

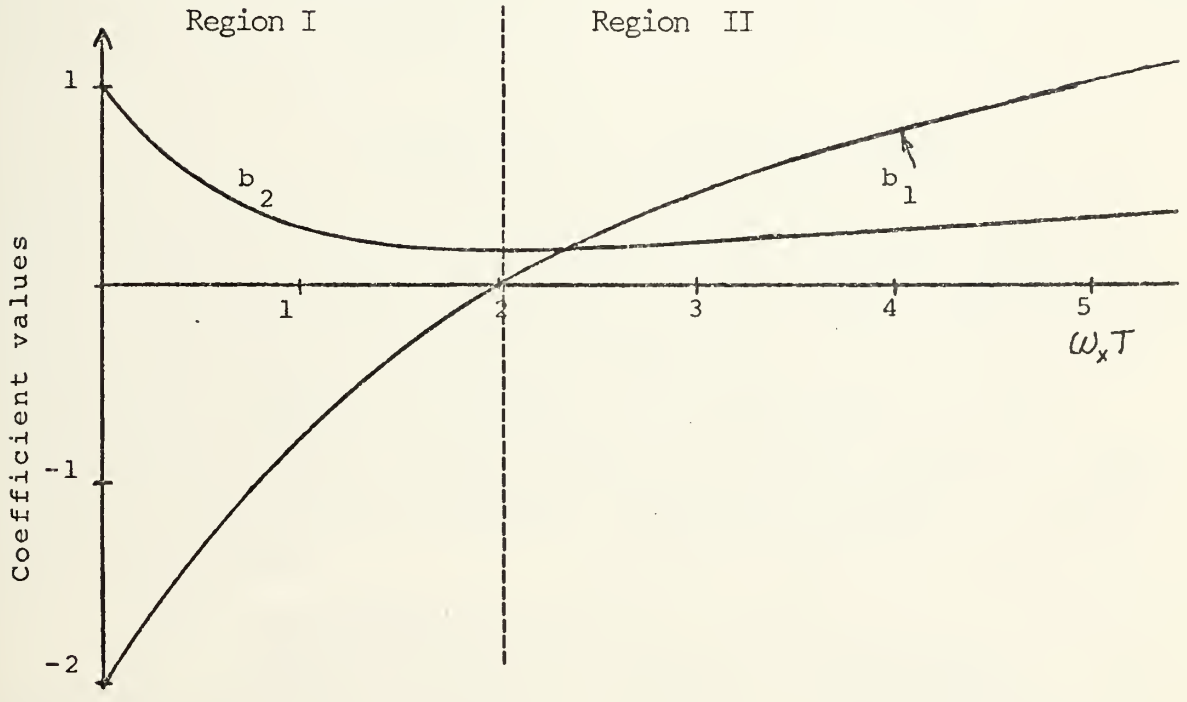

cutoff frequency will change by varying T.
Table I and Figure 2.1 shows how b_1 and b_2 varies with $\omega_x T$.
Table II is a summary of how the frequency response behave as $\omega_x T$ is varied, giving the ranges where the filter acts as integrator or canceller.
Since region I (Figure 2.1) is the area of interest in this thesis, the experimental study was carried out here.

3. Direct Design Method in Z-Domain

a. By Trial and Error Method

By carrying out the design in the z-domain, transformations from H(s) to H(z) can be avoided:

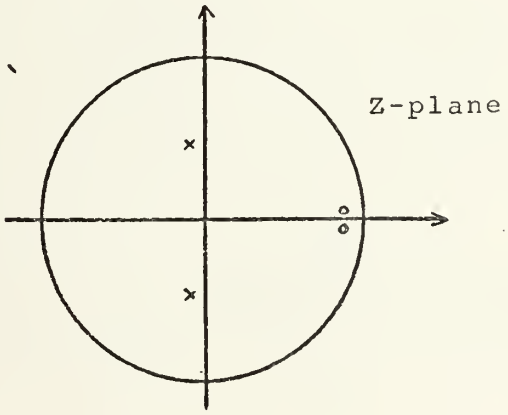

FIGURE 2.2. Z-Domain Unit Circle

Figure 2.2 shows the z-plane, where the entire left half of the s-plane has been transformed into the inside of the unit circle. By moving the two poles and two zeros (second order) around and using the geometric method {1} to calculate the amplitude- frequency response, it is possible to find a combination of the singularities that gives a response quite close to the desired response. Appendix A shows the result of such a study.

b. By Computer Approach

Several computer programs {1} have been developed that will optimize the search of coefficients,

TABLE II

Relationship between $\omega_x T$ and Filtertype for Highpass and lowpass filters using the bilinear z-transform method.

Filter Type	$\omega_x T$	Filter Shape
High Pass	<2 (Region I, Canceller)	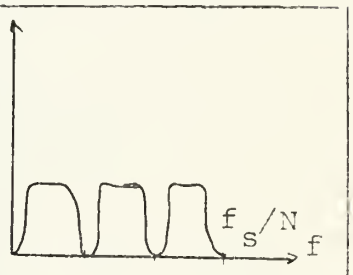
	>2 (Region II, Integrator)	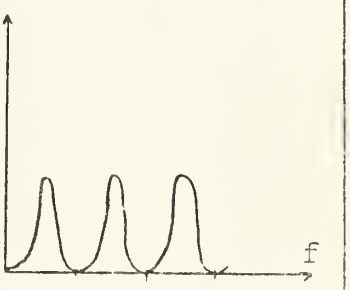
Low Pass	<2 (Region I, Integrator)	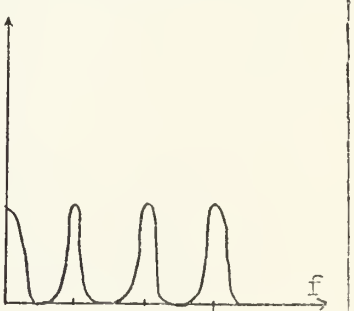
	>2 (Region II, Canceller)	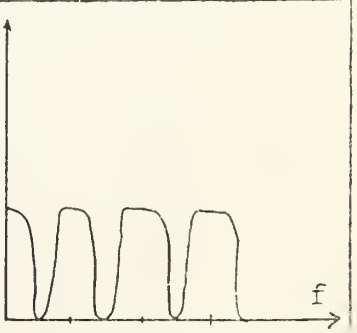

f_s = sampling frequency N= number of delay stages

based on different approaches in reducing the deviation between presented response and filter response.
This approach was not employed here.

B. EXPERIMENT

1. System Configuration

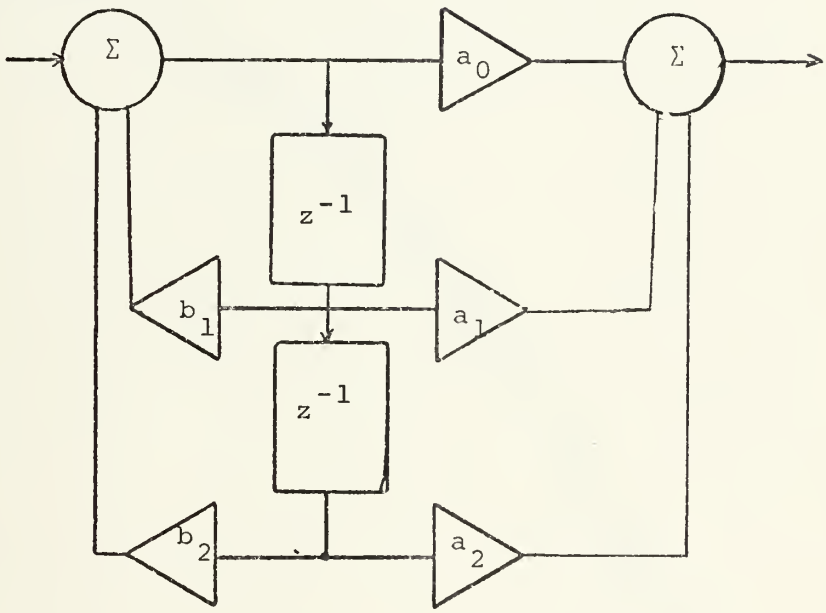

FIGURE 2.3. Second Order Recursive Filter

Figure 2.3 shows the block diagram of the canonical form of a second order recursive filter. Serial analog delay (SAD) from Reticon Co were used as delay lines. 20 K potentiometers were used to implement the coefficients. In the cases where coefficients greater than one were needed for the "a"-coefficients, the numerator in the transfer function H(z) was scaled down so that the "a"-coefficients were normalized. Several methods to implement the coefficients using the potentiometers are discussed in references {2} and {3}. In this work Figure 2.4 is presented, giving the calibration of potentiometer setting for desired coefficient value. This curve was obtained by simply measuring input and output

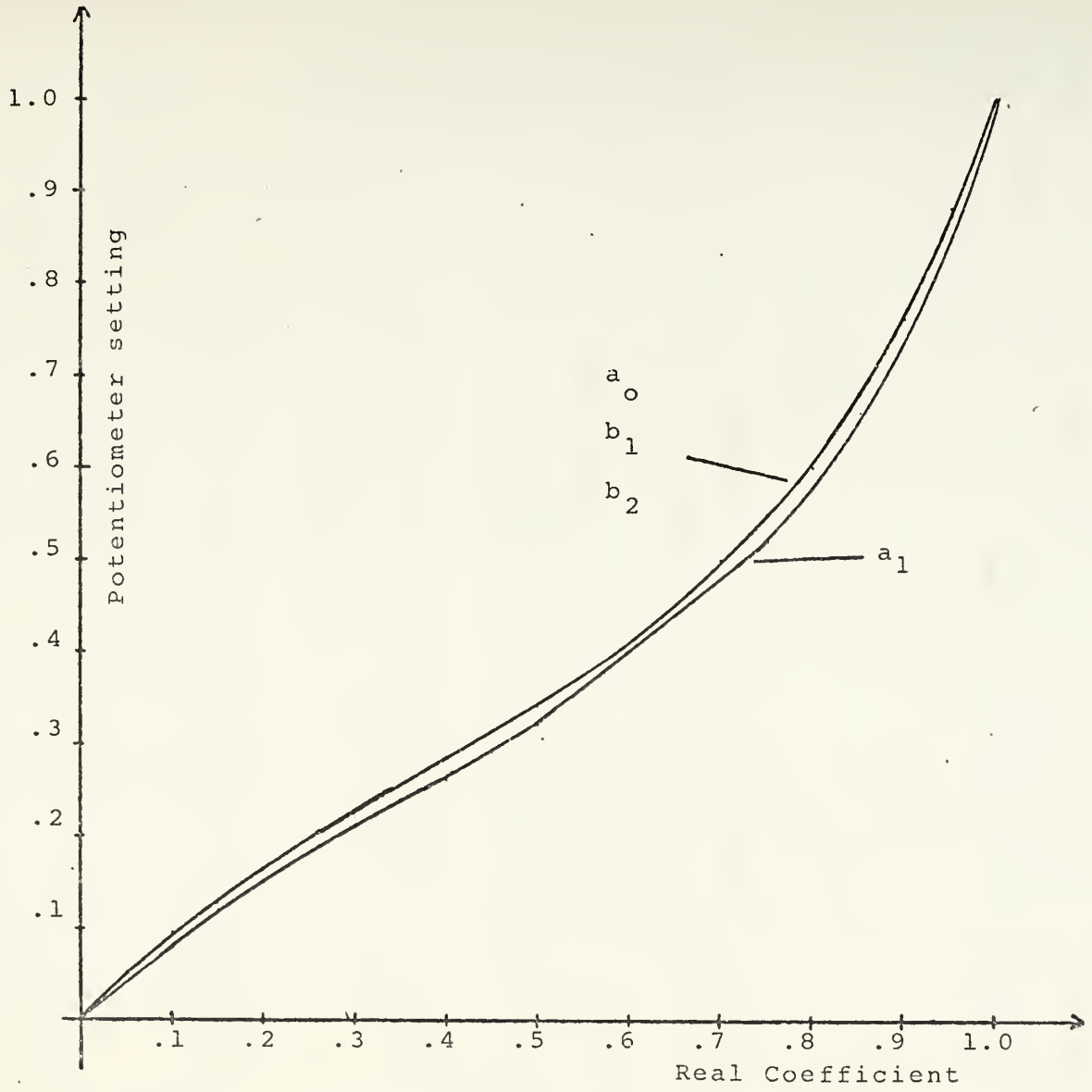

FIGURE 2.4. Potentiometer Calibration Curves.

across the potentiometer.

2. Results

The clock frequency for the SAD-100 (Reticon Co) device was 72 KHZ. Since the effective clock frequency was four times 72 KHZ, and there was 96 stages within the device, the corresponding nulls of a high pass comb filter should occur at multiples of:

$$\frac{72 \text{ KHZ} \cdot 4}{96} = 3 \text{ KHZ}$$

A computer program (APPENDIX B) was used to calculate and plot the theoretical frequency response curve,and also to superimpose the actual data points on the same plot.
The "a"- coefficients were kept fixed, and several combinations of b_1 and b_2 were used. They were selected from Figure 2.1, and b_1 was negative in all cases studied in this thesis.
By using the values of b_1 and b_2 corresponding to $\omega_x T$, the resulting response should be flat-topped in every case.
The implemented coefficients were:

	a_o	a_1	a_2	b_1	b_2
High Pass (Canceller)	.5	-1.0	.5	-1.0	.38
	.5	-1.0	.5	-0.7	.27
	.5	-1.0	.5	-0.4	.21
	.5	-1.0	.5	-0.3	.2
	.5	-1.0	.5	-0.2	.19
Low Pass (Integrator)	.5	1.0	.5	-1.0	.38
	.5	1.0	.5	-0.7	.27
	.5	1.0	.5	-0.4	.21
	.5	1.0	.5	-0.3	.2
	.5	1.0	.5	-0.2	.19

The coefficients b_1 and b_2 were all picked in Region I (Figure 2.1).
Figures 2.9 through 2.18 show the series of results.
There seemed to be the same problem with the second order filter as was experienced with the first order filter{2}, namely a skewness at higher frequencies. Also the results show an undesired dip in the passbands, indicating that the coefficients are not correctly implemented.
Suspecting that the experimental implementation inherently makes the system frequency dependent, several checks were made for its investigation. The gain of individual delay lines was checked for frequency dependence, using both the oscilloscope and a narrowband voltmeter.
The individual potentiometers input-output characteristics were measured when the filter loop was closed.
It was found that the gains of the delay lines were slightly frequency dependent as measured on the oscilloscope, and severely and inconsistently frequency dependent when measured on the narrowband voltmeter, indicating loading effects in the latter case; (the input impedance of the voltmeter was 100 Kohm).
Figures 2.5 through 2.8 show the calibration of the potentiometer settings including the frequency dependence for the coefficients used in the previous measurements.
Figures 2.19 through 2.21 show the frequency response when the frequency compensated coefficients are used.
The potentiometer settings were changed every 3 KHZ.
During several of the "runs" it can be seen that there is a slight shift in the position of the experimental curve relative to the theoretical curve. This is due to uncontrollable drift of the basic clock frequency in the course of the datataking.
The very latest set of data (Figure 2.21), was taken while adjusting a_o and a_2 at every null, after first having set all coefficients according to the curves given in Figures 2.5 -

2.8, at that null.

Table III shows the potentiometer settings for $a_o = 0.5$, $a_1 = -1.0$, $a_2 = 0.5$, $b_1 = -0.7$, $b_2 = 0.27$:

TABLE III

	From Curves				After readjusting		
Frequency	a_o	a_1	a_2	b_1	b_2	a_o	a_2
3 KHZ	.714	-1.0	.846	-.873	.407	.652	.885
6 "	.714	-1.0	.846	-.873	.405	.652	.885
9 "	.714	-1.0	.847	-.875	.403	.689	.863
12 "	.715	-1.0	.848	-.876	.4	.685	.859
15 "	.718	-1.0	.85	-0.877	.398	.685	.859
18 "	.722	-1.0	.852	-.877	.396	.68	.862

Figures 2.19 through 2.21 do not show any sign of the skewness of previous data sets, but the shape of the observed curves still deviate significantly from the theoretical curves, indicating that the proper coefficients have not been found for all frequencies.

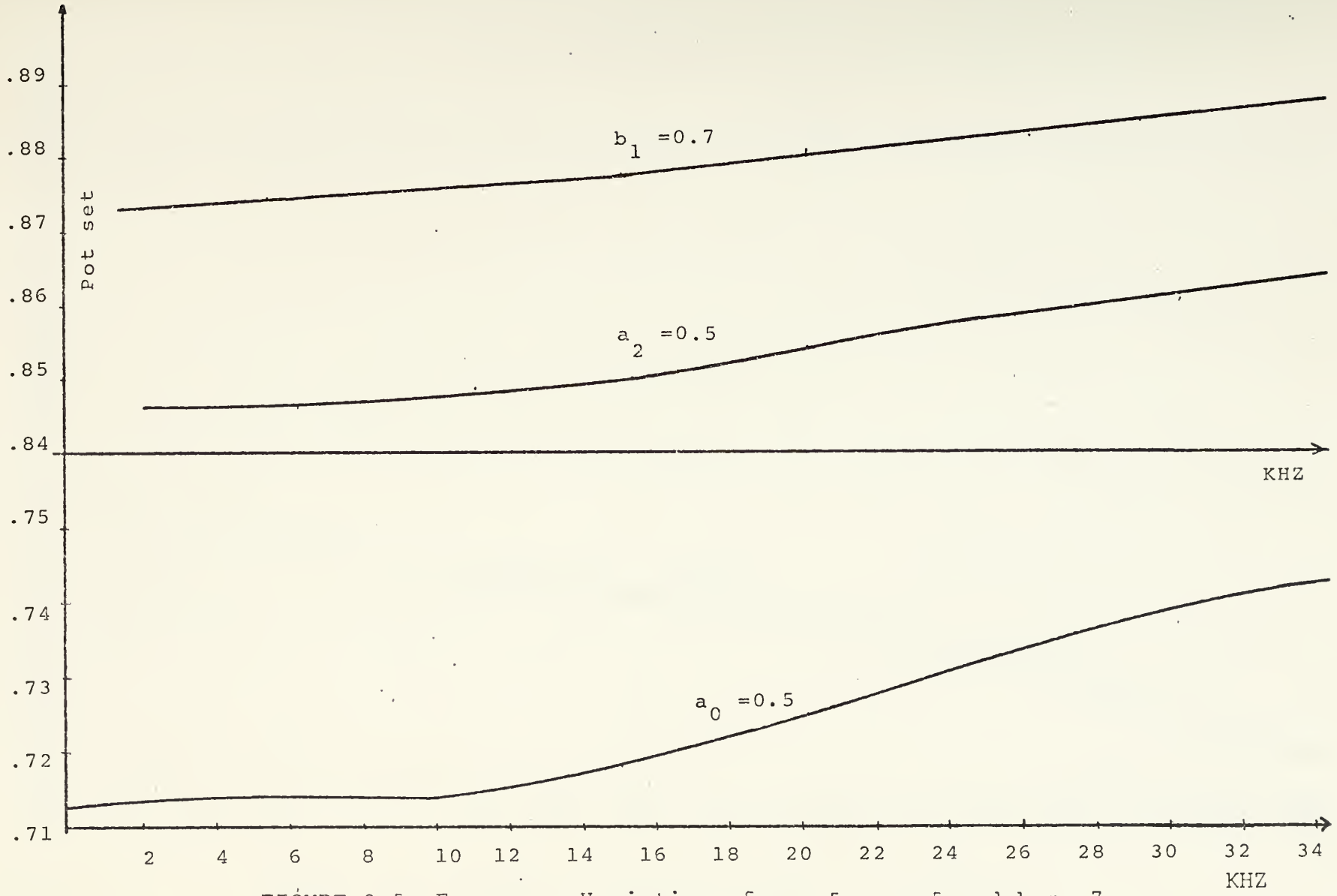

FIGURE 2.5. Frequency Variation of a_o=.5, a_2=.5 and b_1= .7

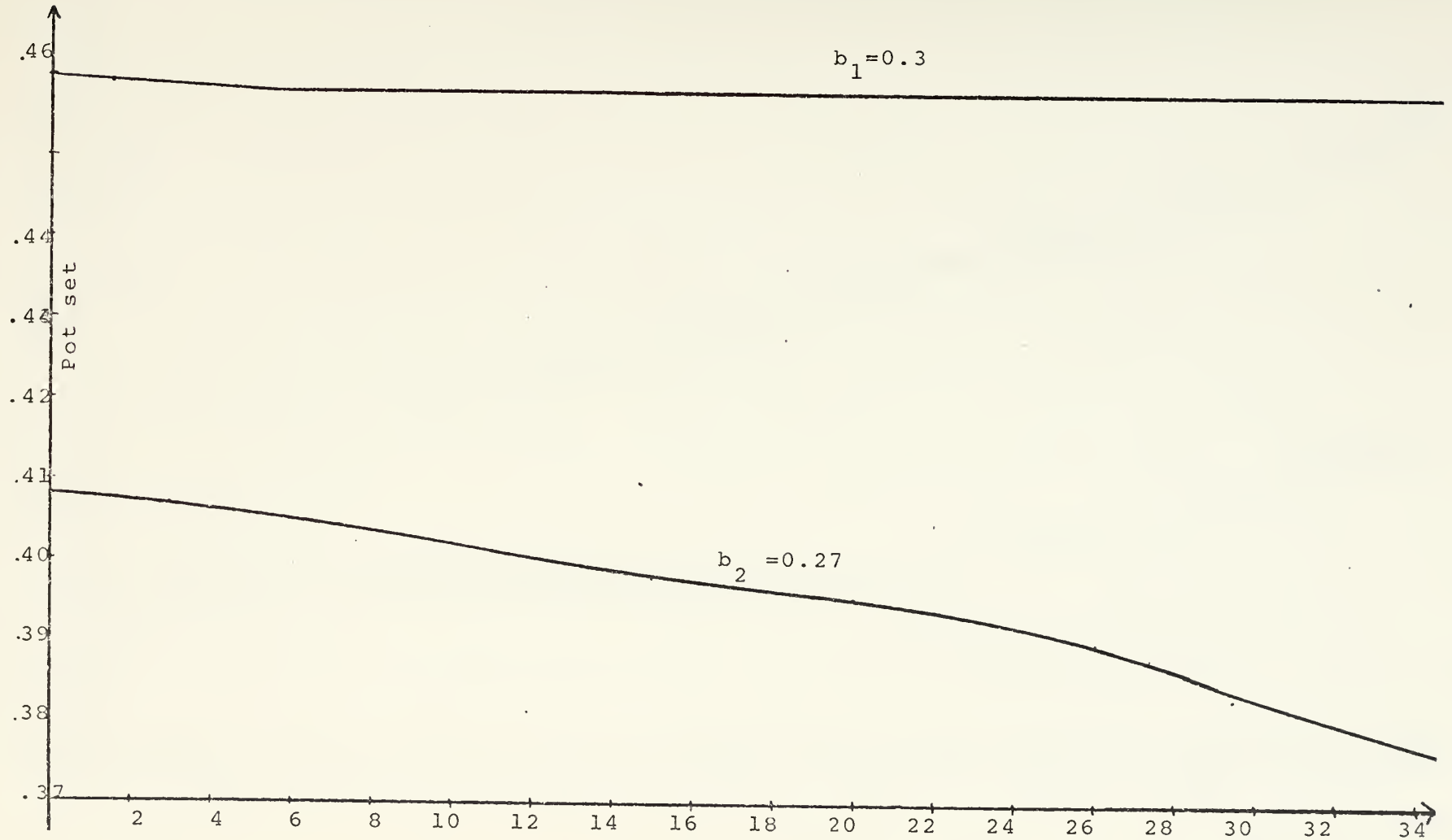

FIGURE 2.6. Frequency Variation of b_1= .3, and b_2= .27.

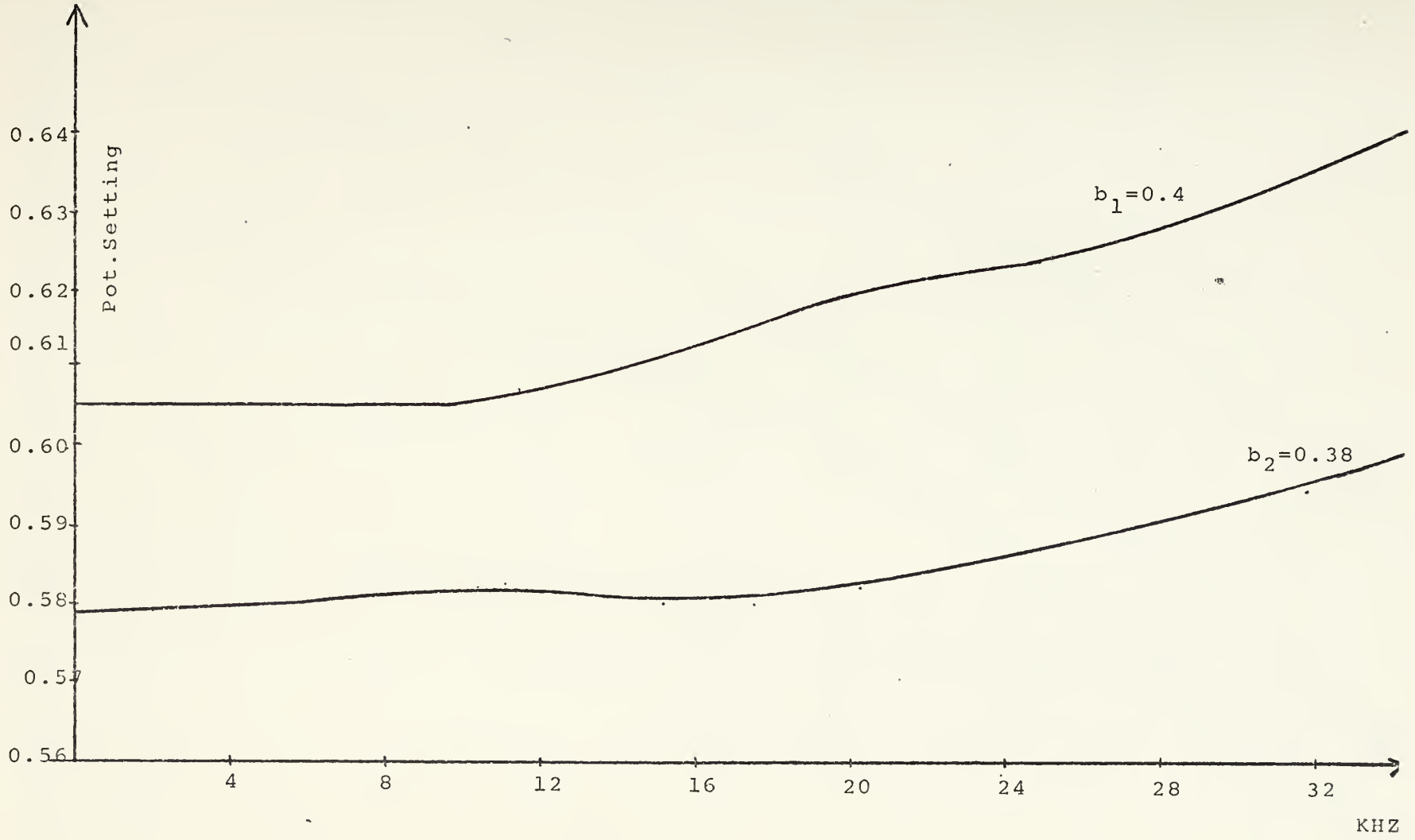

FIGURE 2.7. Frequency Variation of b_1= .4 and b_2= .38

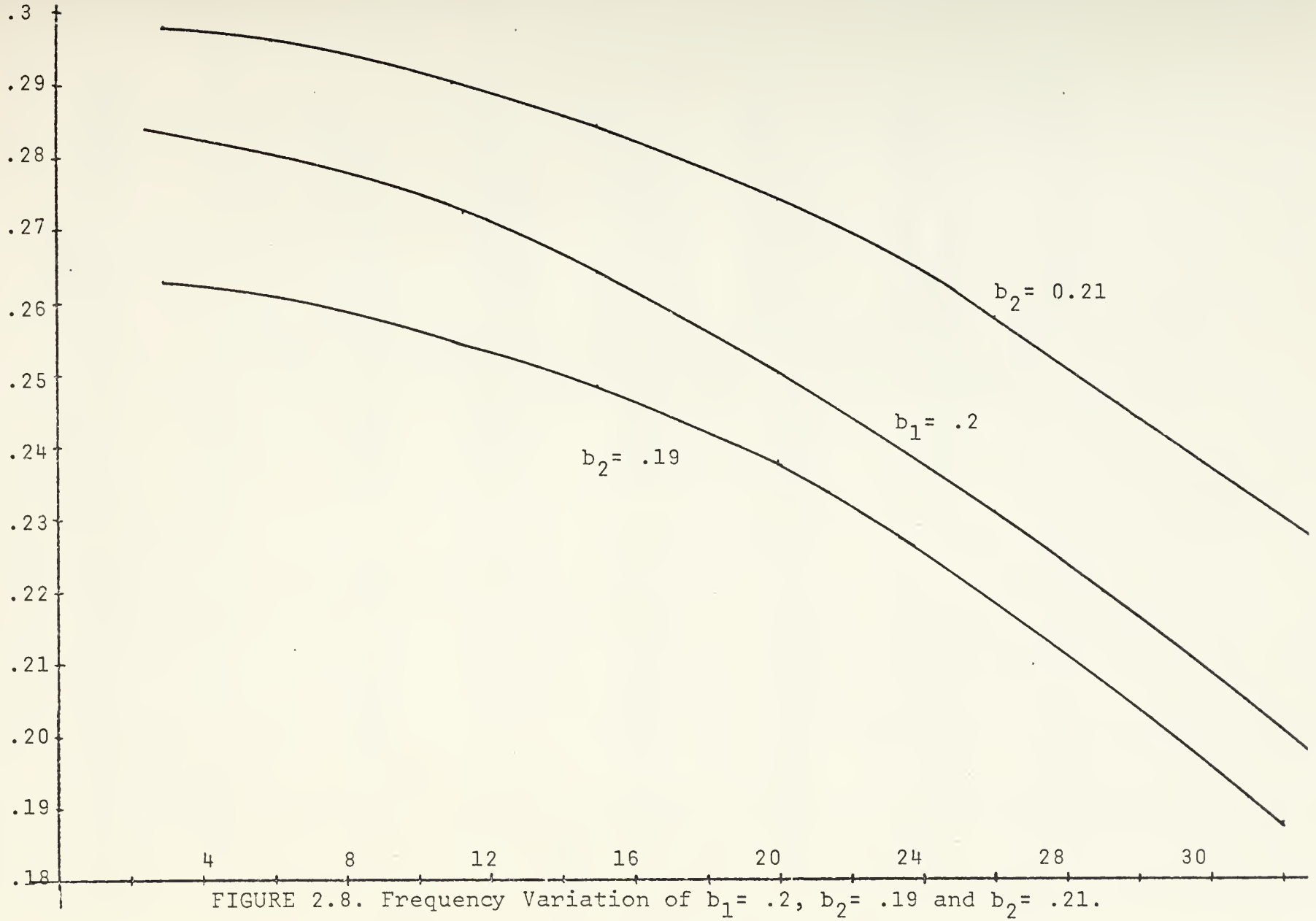

FIGURE 2.8. Frequency Variation of b_1= .2, b_2= .19 and b_2= .21.

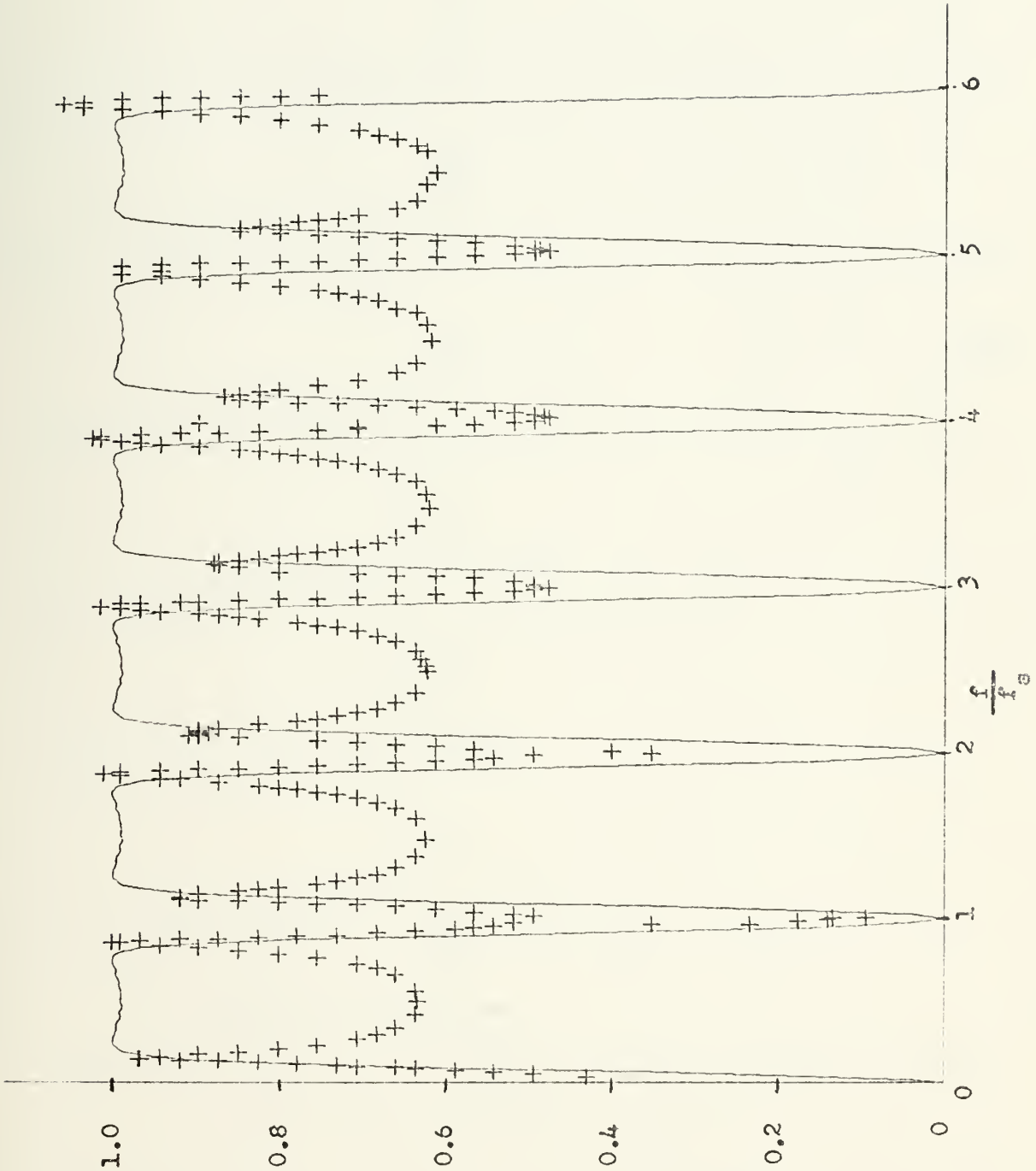

FIGURE 2.9a. Theoretical and Observed Frequency Response of High Pass Filter; $b_1 = -1.0$, $b_2 = 0.38$

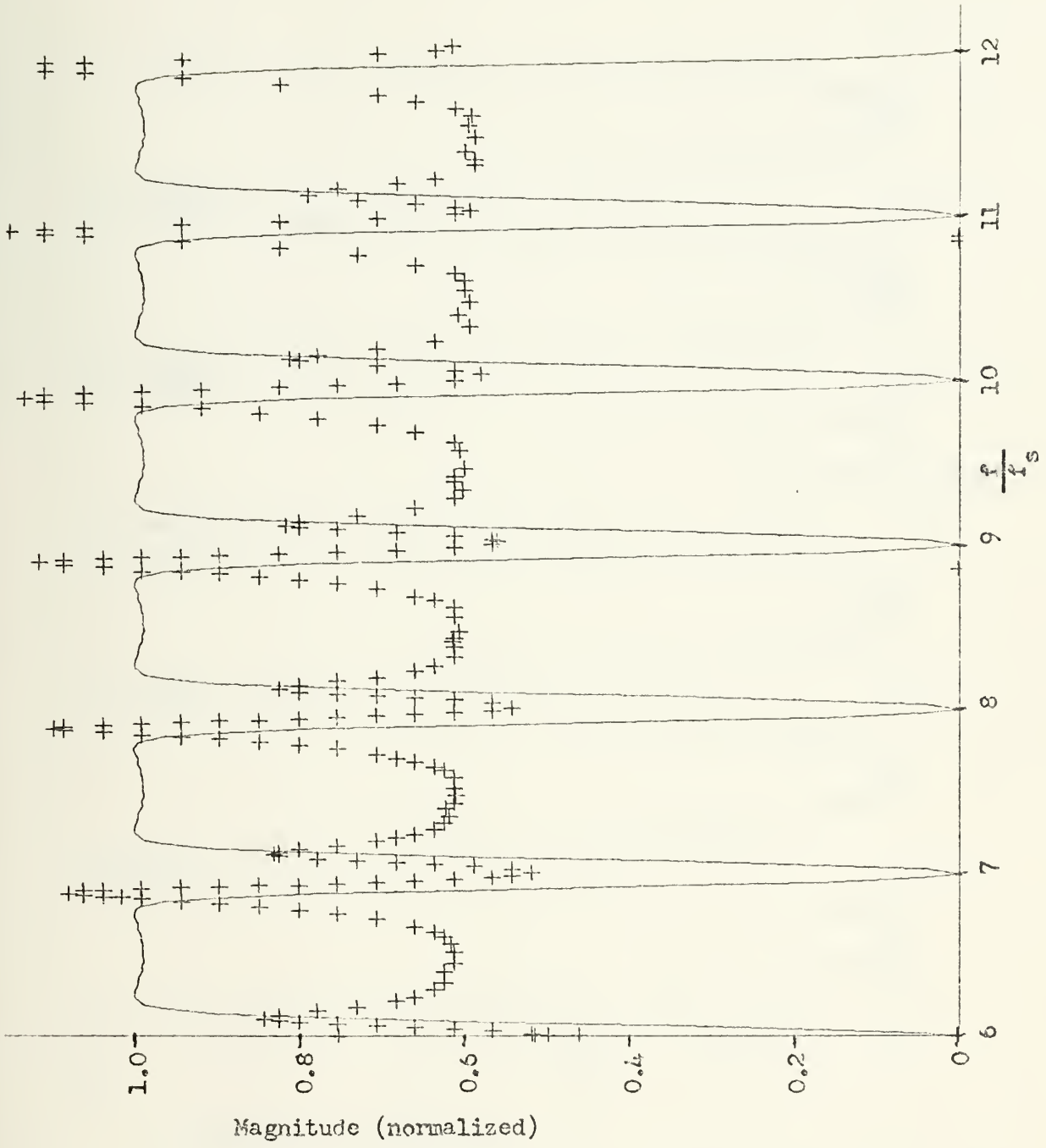

FIGURE 2.9b. Theoretical and Observed Response of High Pass Filter; $b_1 = -1.0$, $b_2 = 0.38$

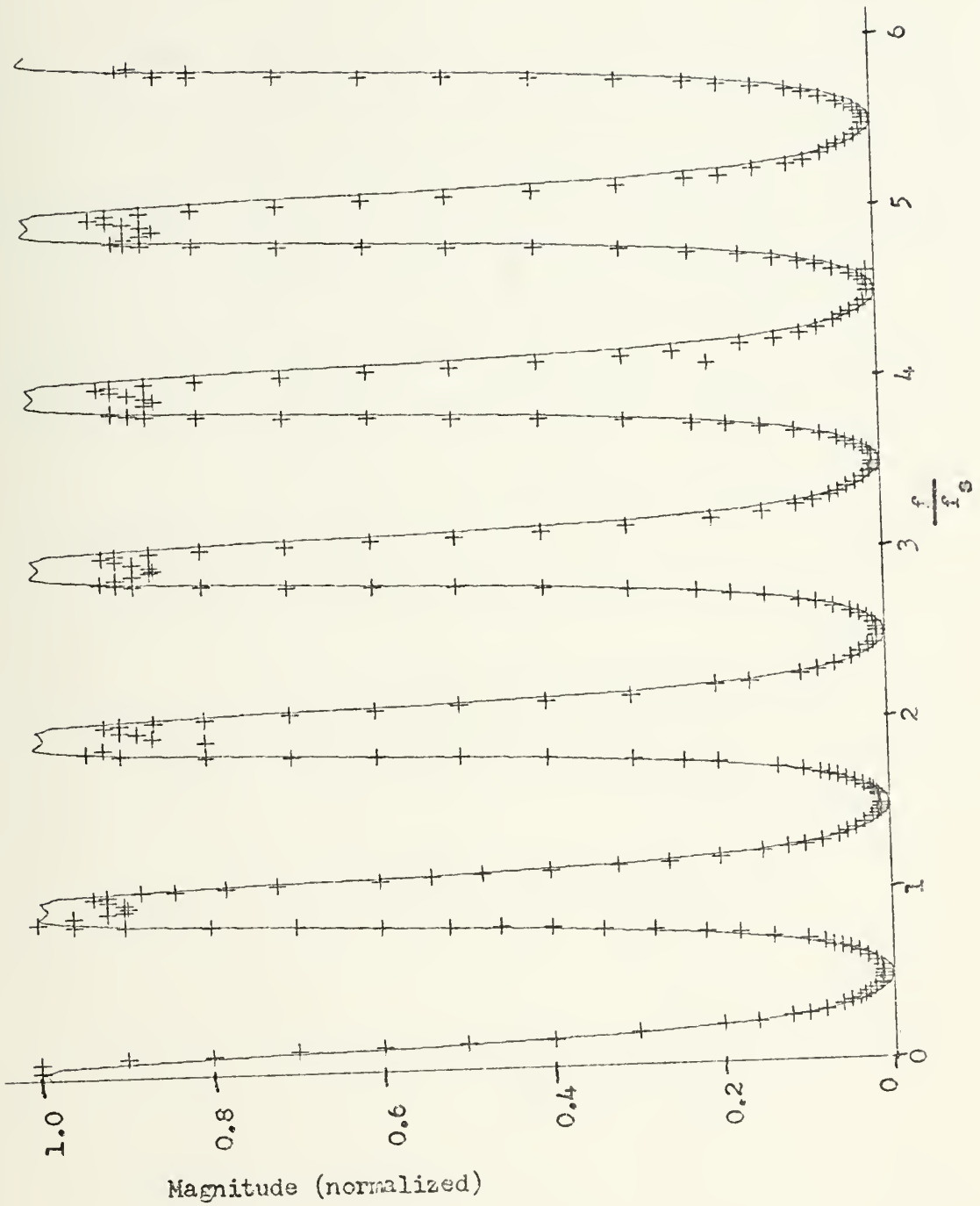

FIGURE 2.10a. Theoretical and Observed Response of Low Pass Filter;
$b_1 = 1.0$, $b_2 = 0.38$

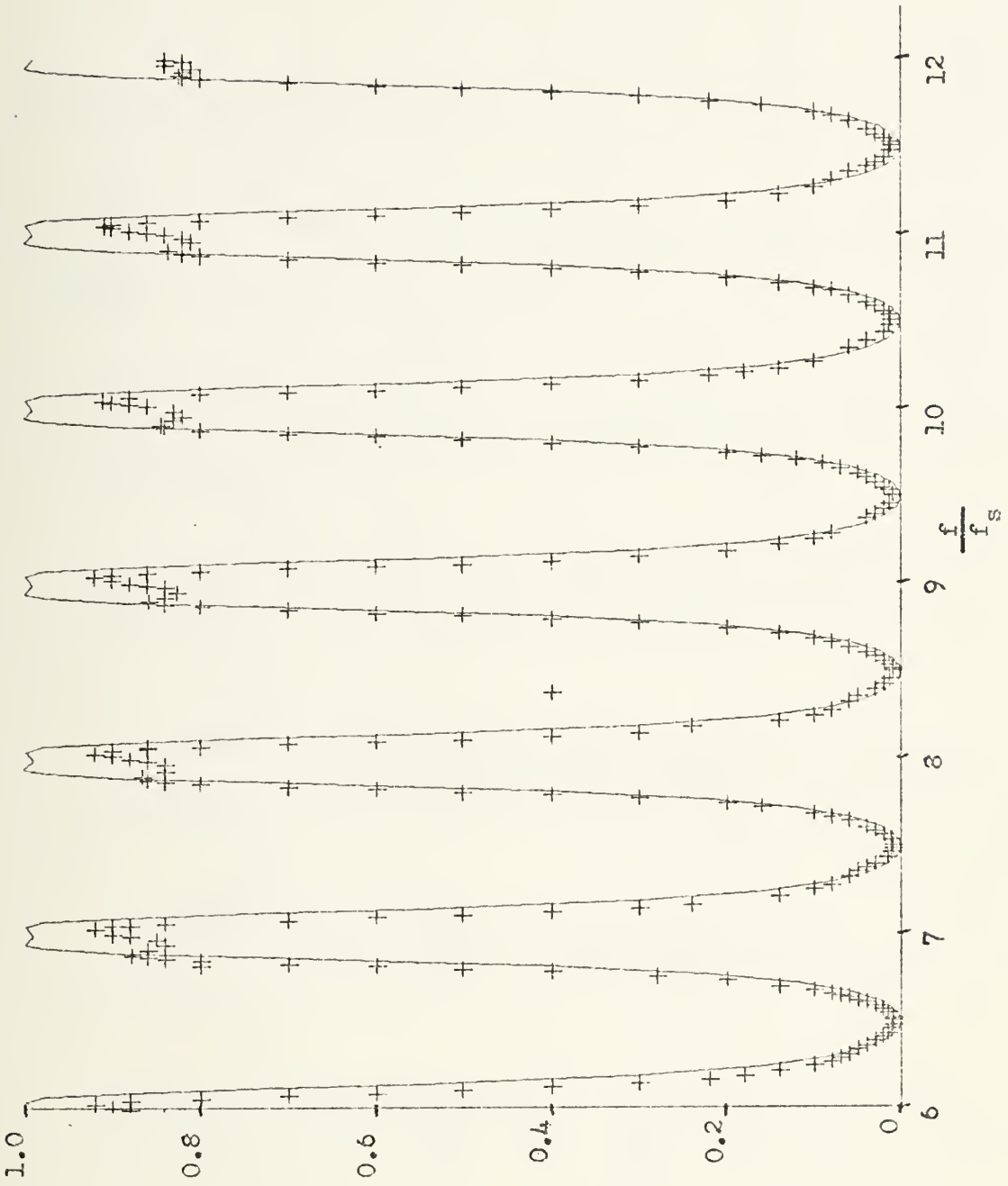

FIGURE 2.10b. Theoretical and Observed Response of Low Pass Filter; $b_1 = 1.0$, $b_2 = 0.38$

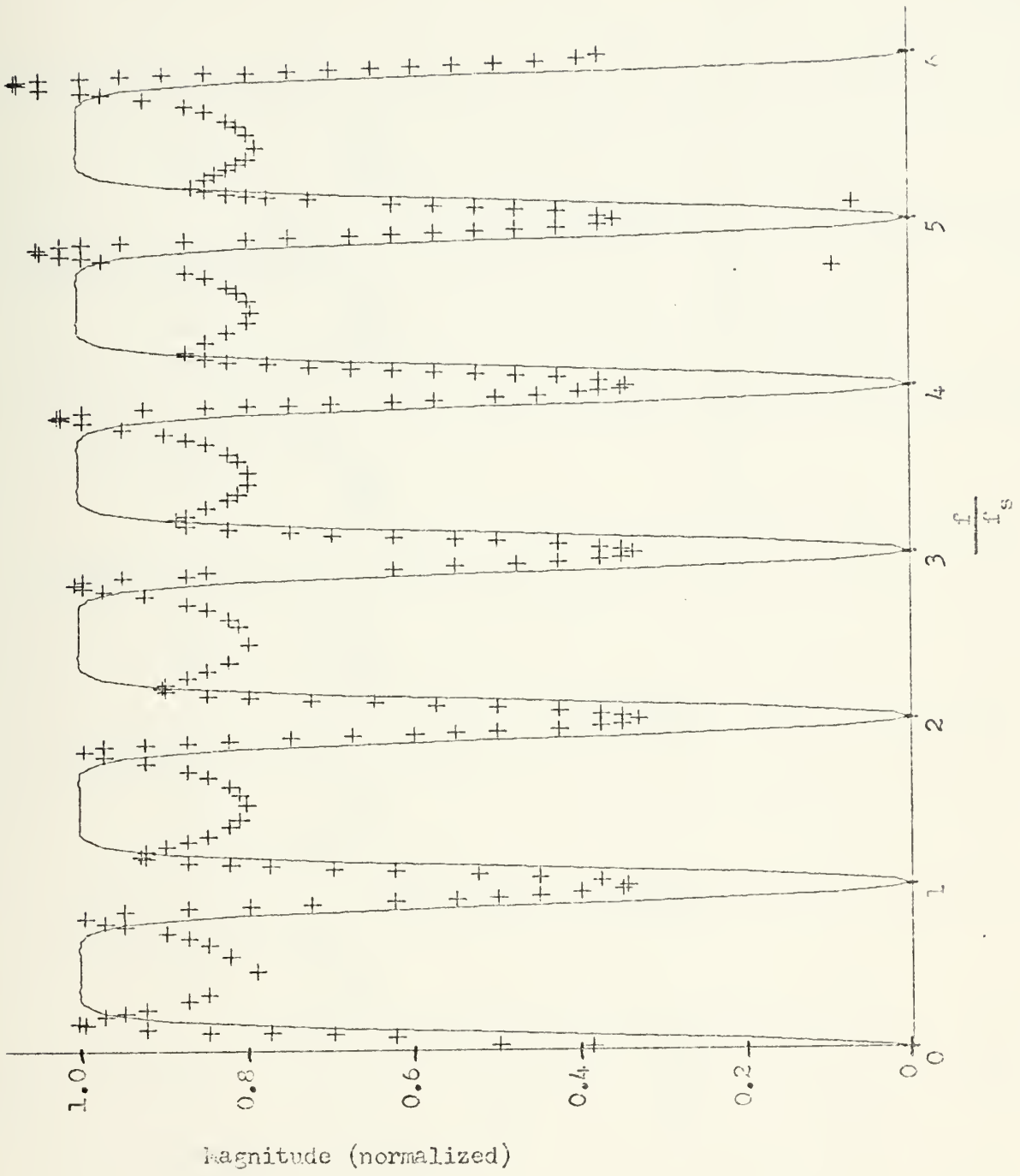

FIGURE 2.11a Theoretical and Observed Response of High Pass Filter; $b_1 = -0.7$, $b_2 = 0.27$

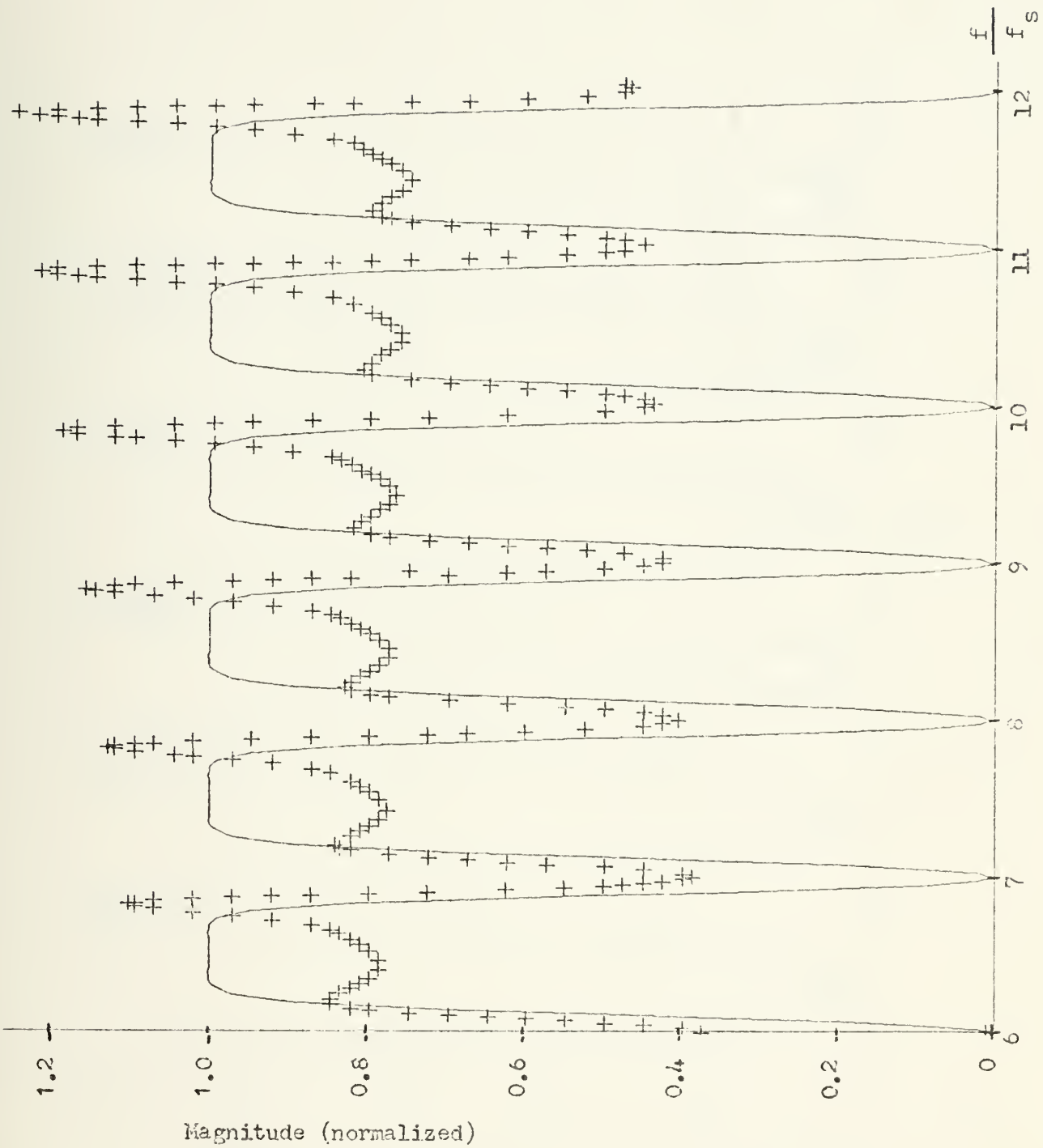

FIGURE 2.11b. Theoretical and Observed Response of High Pass Filter;
$b_1 = -0.7$, $b_2 = 0.27$

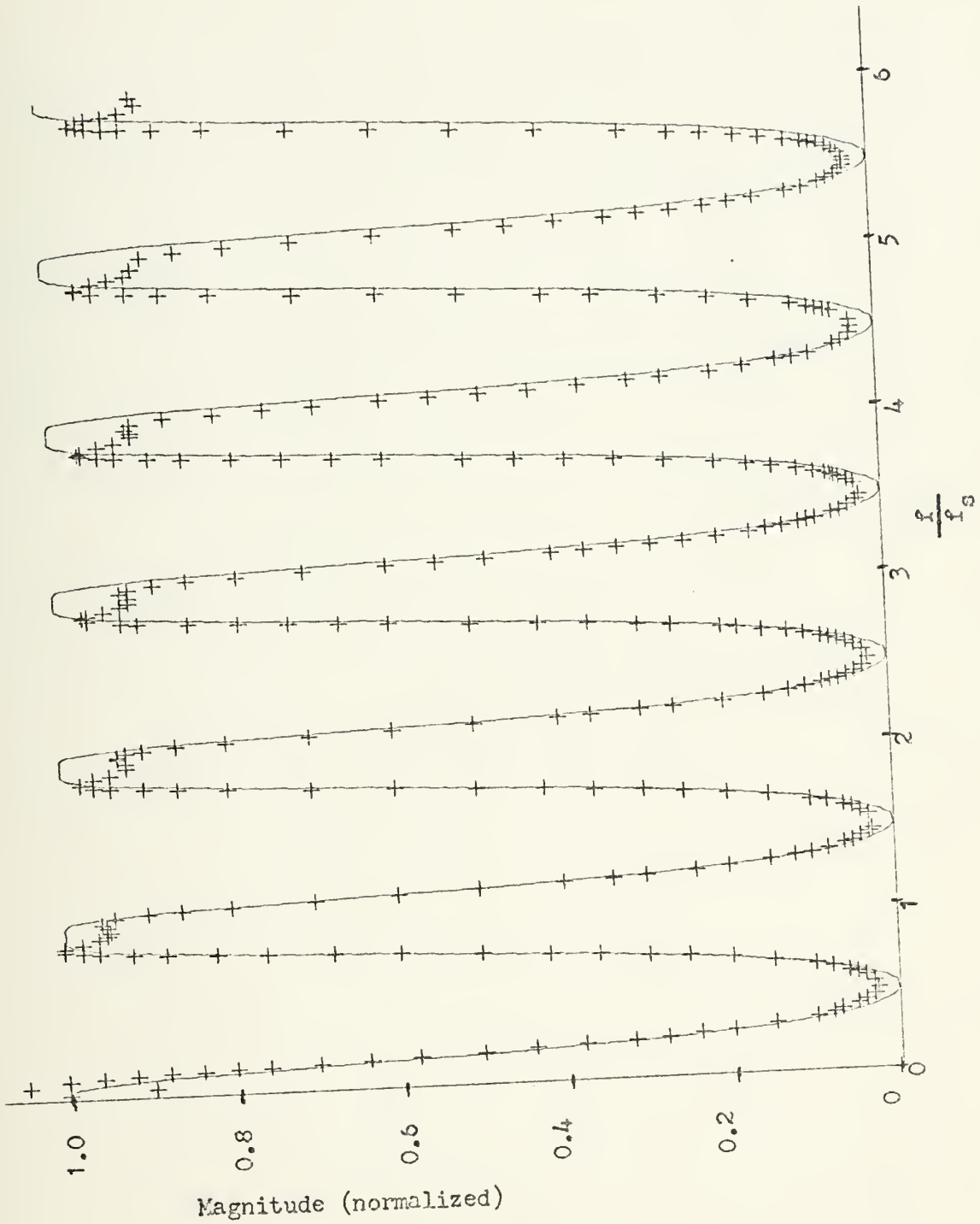

FIGURE 2.12a. Theoretical and Observed Response of Low Pass Filter;
$b_1 = 0.7$, $b_2 = 0.27$

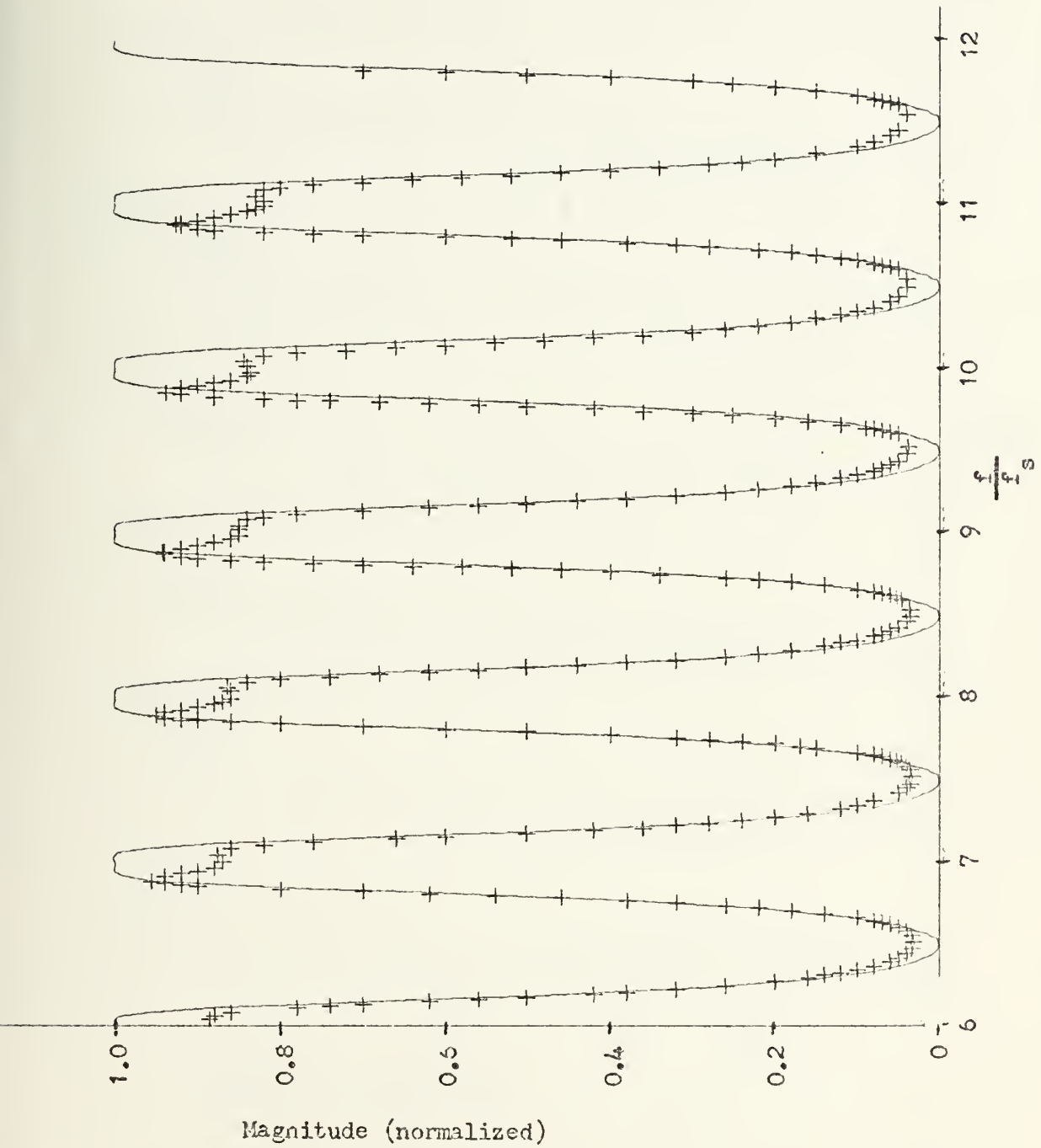

FIGURE 2.12b. Theoretical and Observed Response of Low Pass Filter;
$b_1 = 0.7, \quad b_2 = 0.27$

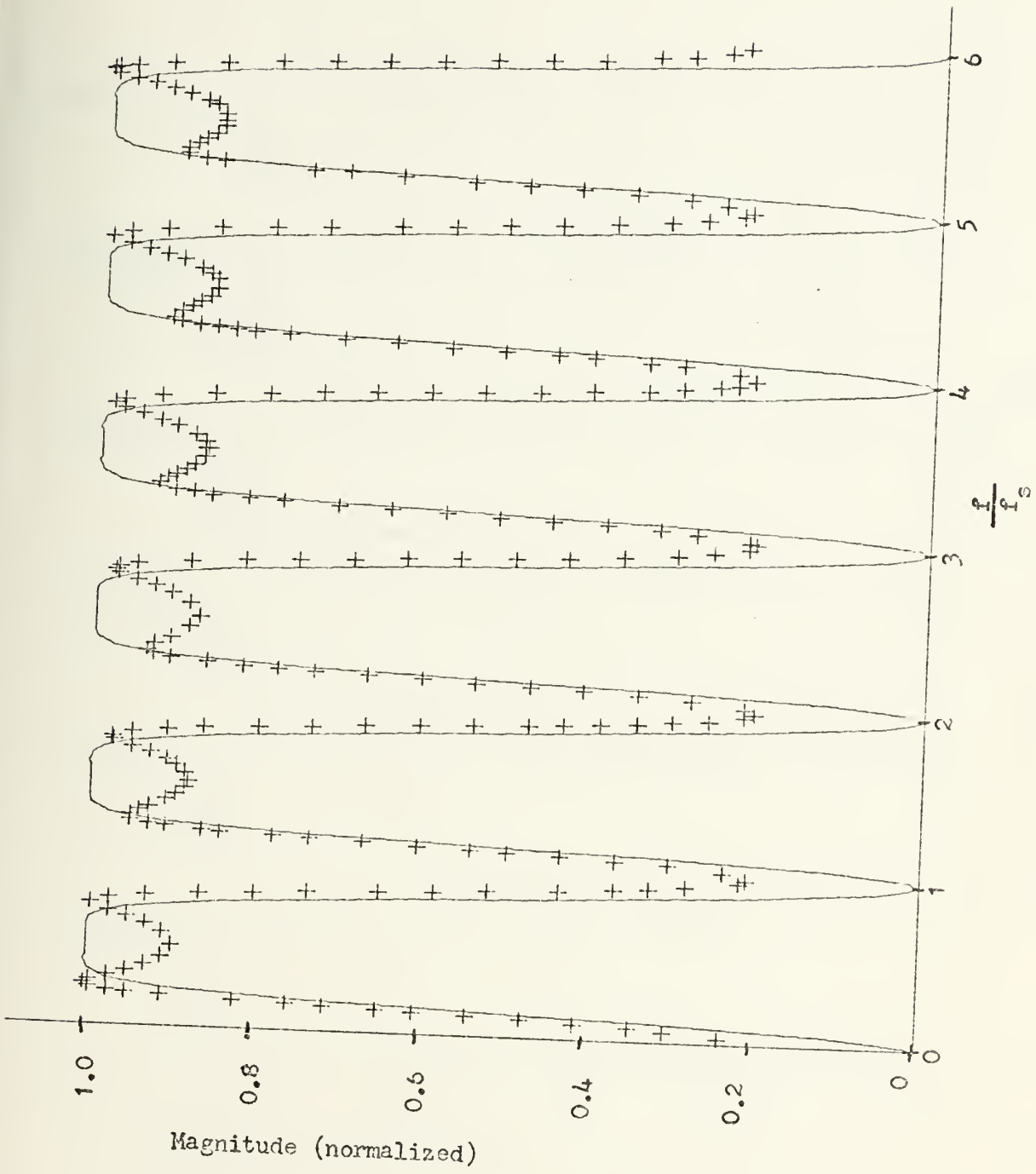

FIGURE 2.13a. Theoretical and Observed Response of High Pass Filter;
$b_1 = -0.4$, $b_2 = 0.21$

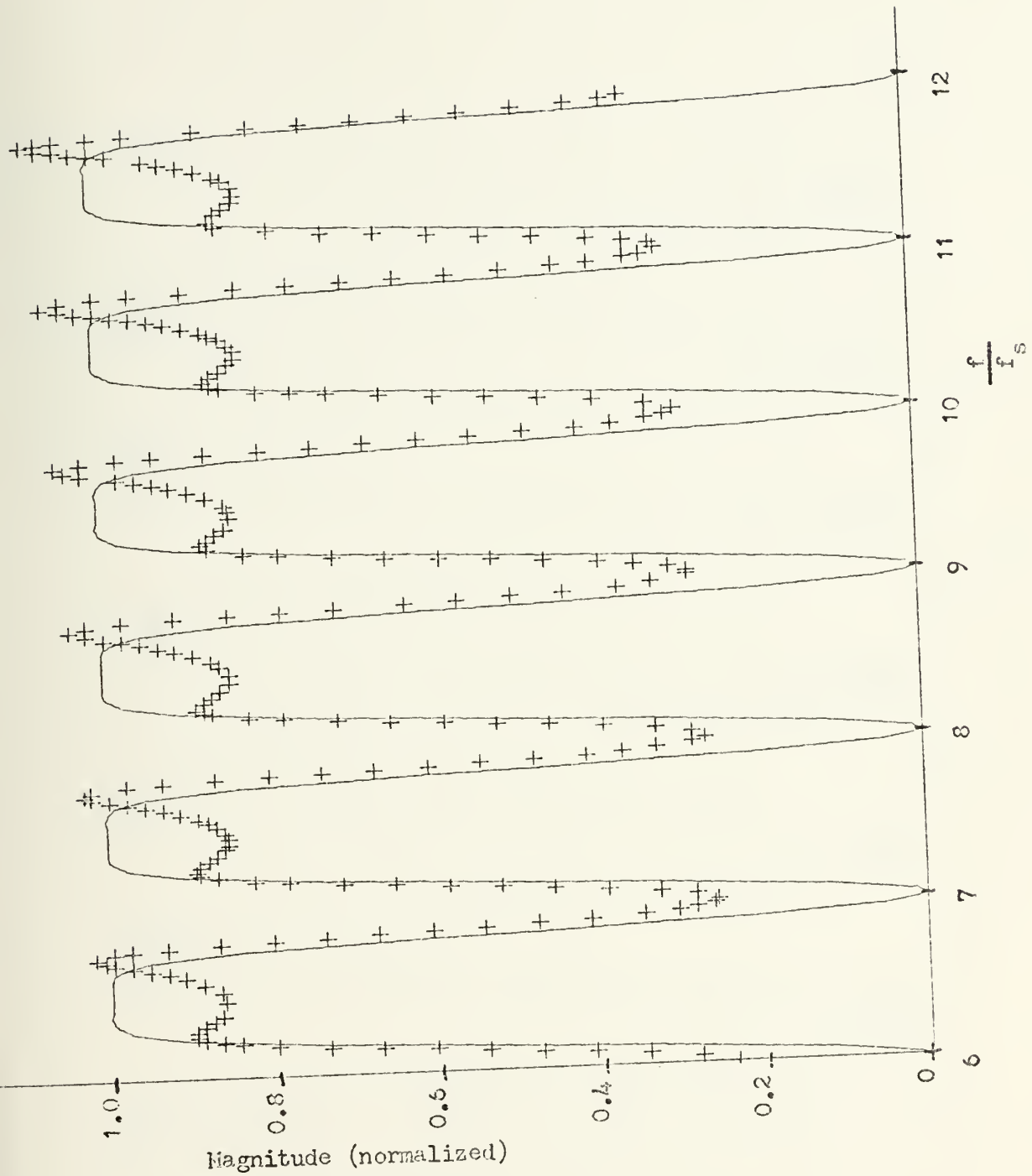

FIGURE 2.13b. Theoretical and Observed Response of High Pass Filter;
$b_1 = -0.4$, $b_2 = 0.21$

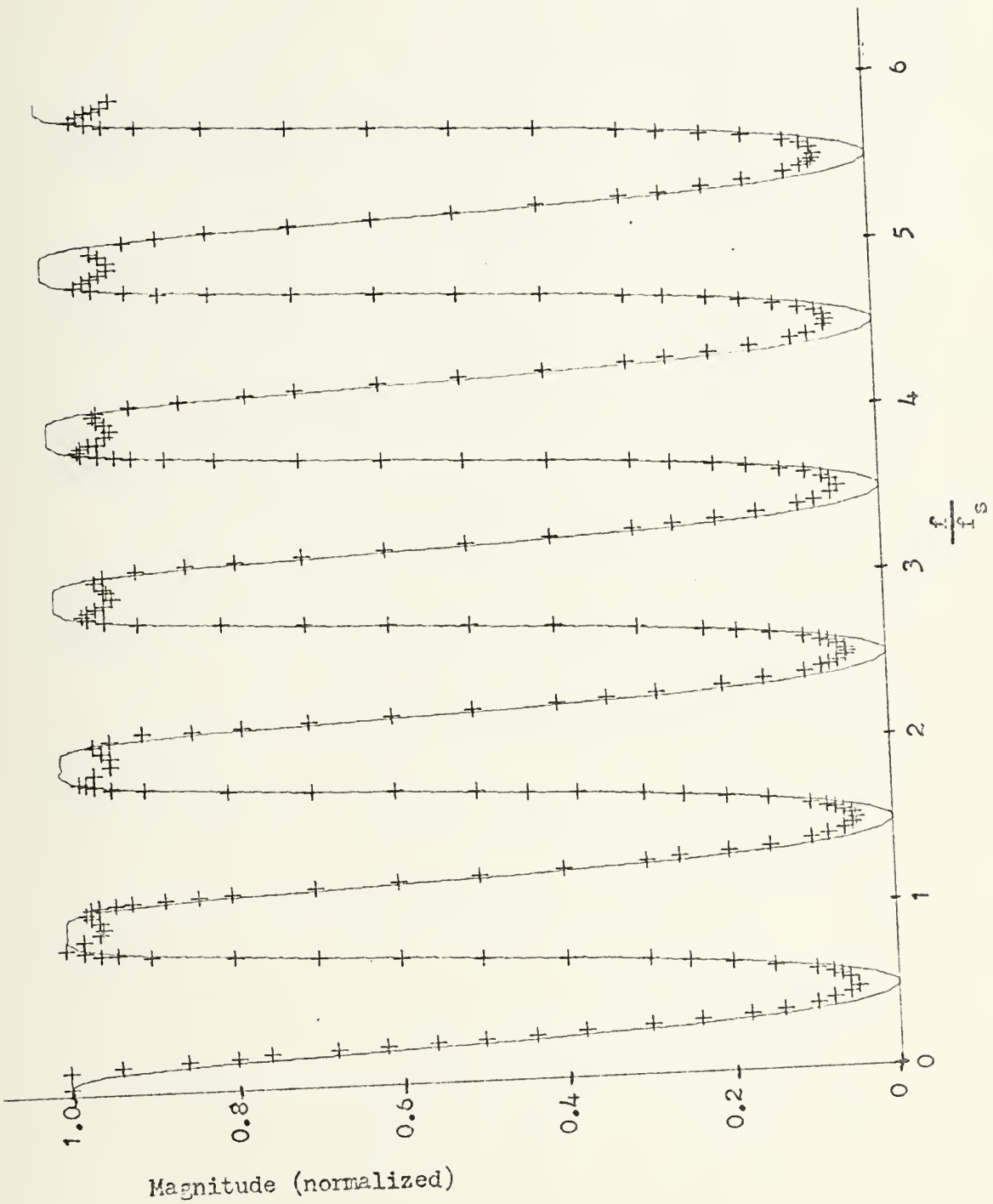

FIGURE 2.14a. Theoretical and Observed Response of Low Pass Filter;
$b_1 = 0.4, \quad b_2 = 0.21$

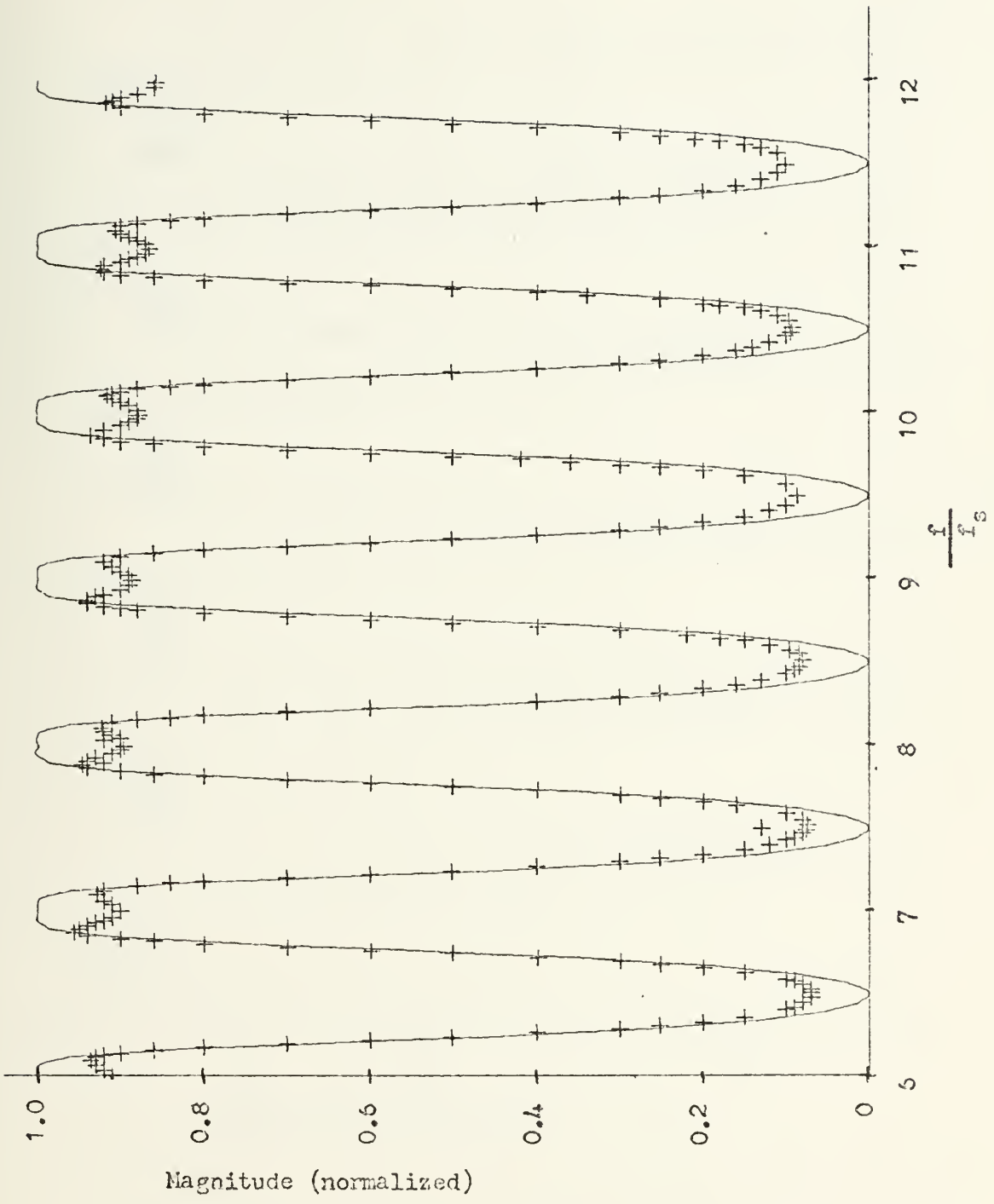

FIGURE 2.14b. Theoretical and Observed Response of Low Pass Filter;
$b_1 = 0.4$, $b_2 = 0.21$

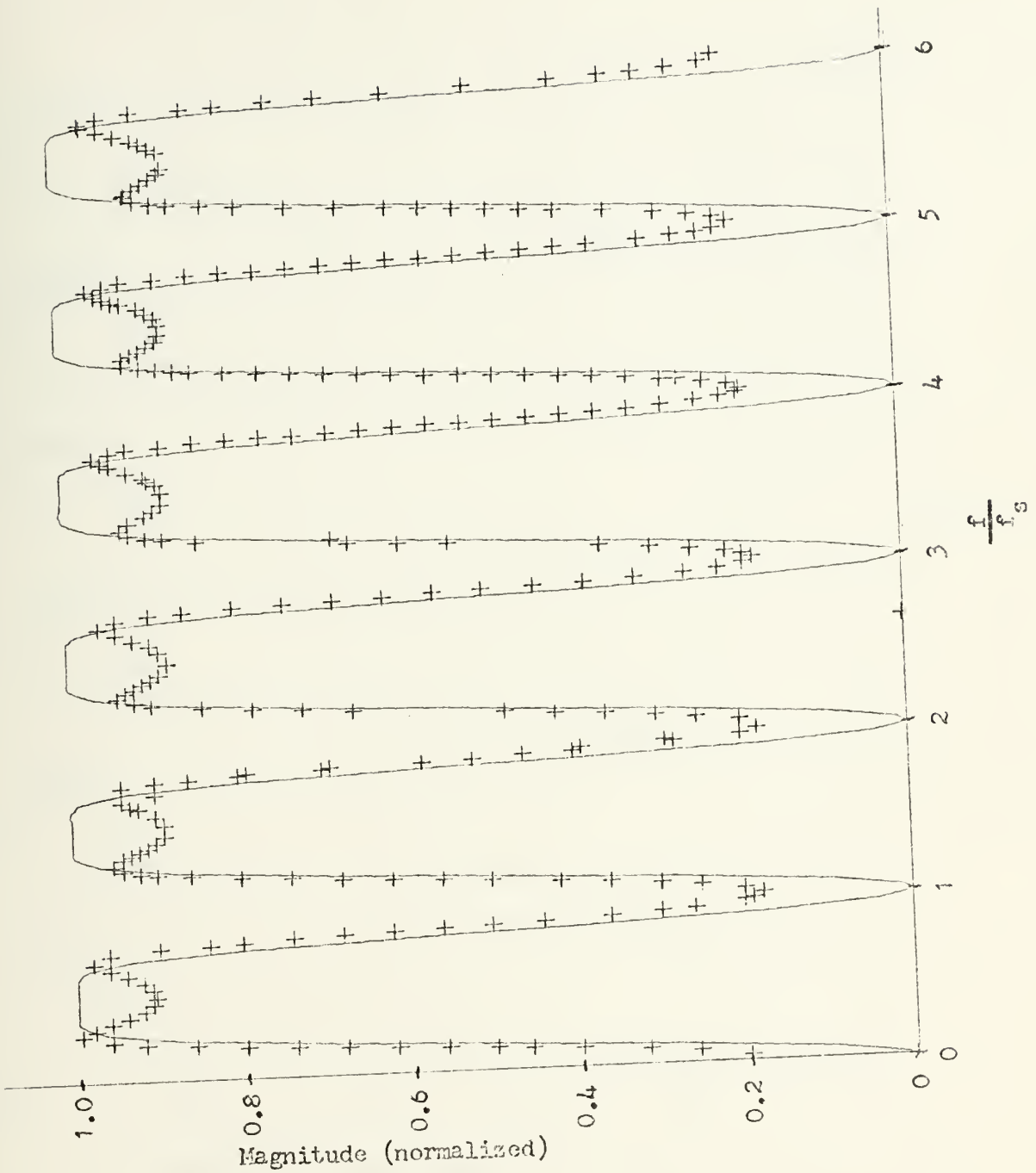

FIGURE 2.15a. Theoretical and Observed Response of High Pass Filter;
$b_1 = -0.3$, $b_2 = 0.2$

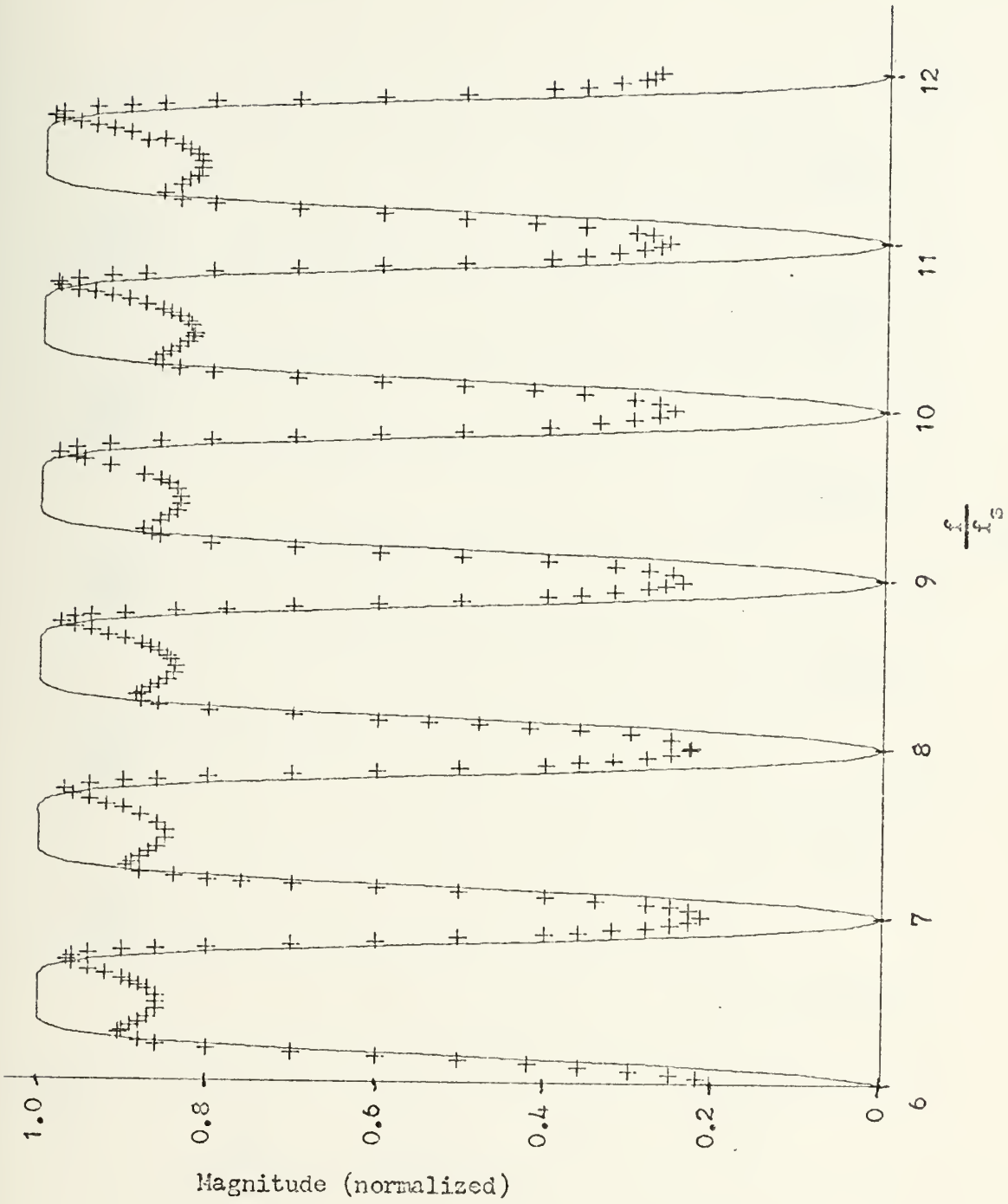

FIGURE 2.15b. Theoretical and Observed Response of High Pass Filter;
$b_1 = -0.3$, $b_2 = 0.2$

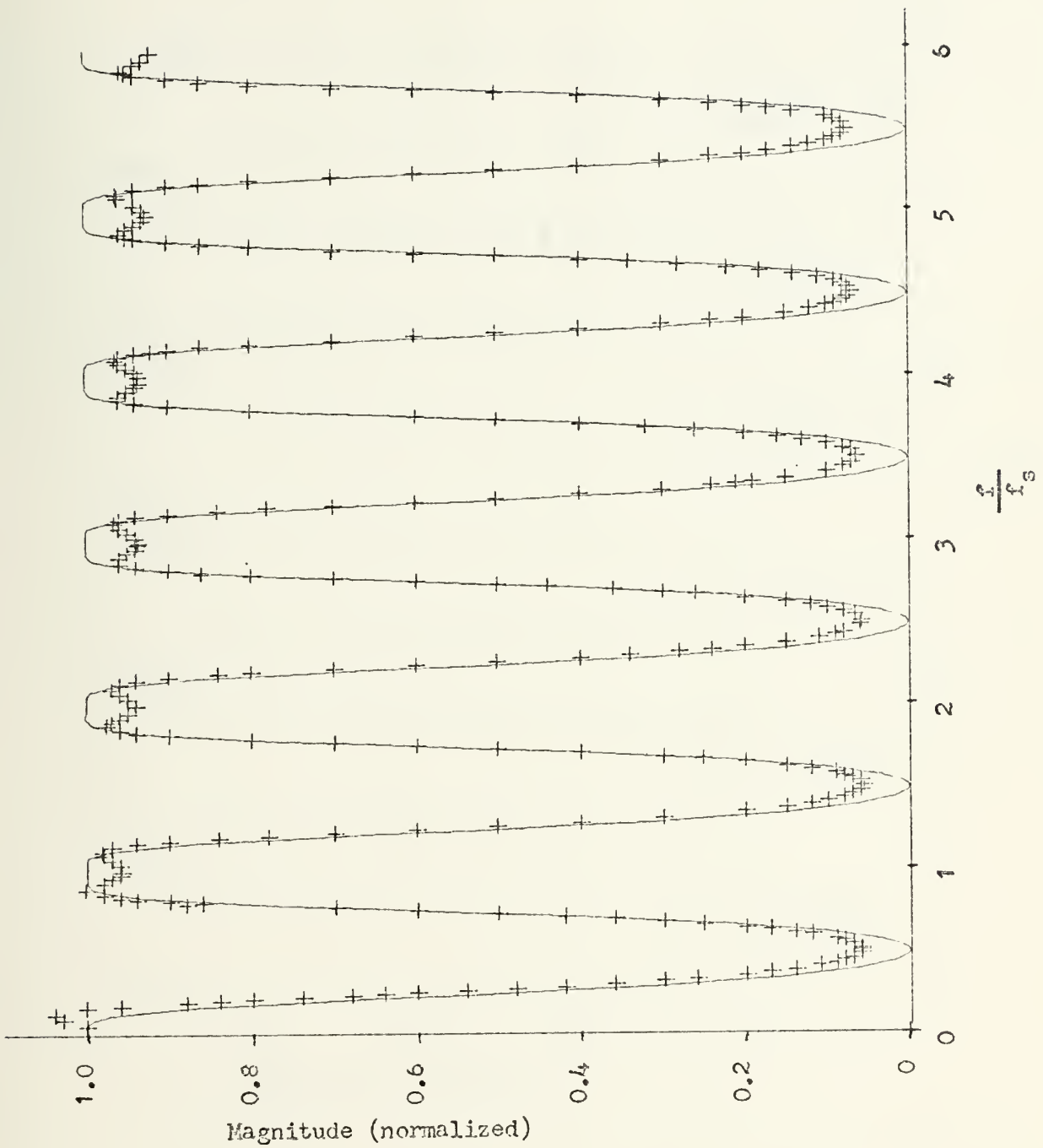

FIGURE 2.16a. Theoretical and Observed Response of Low Pass Filter;
$b_1 = 0.3, \quad b_2 = 0.2$

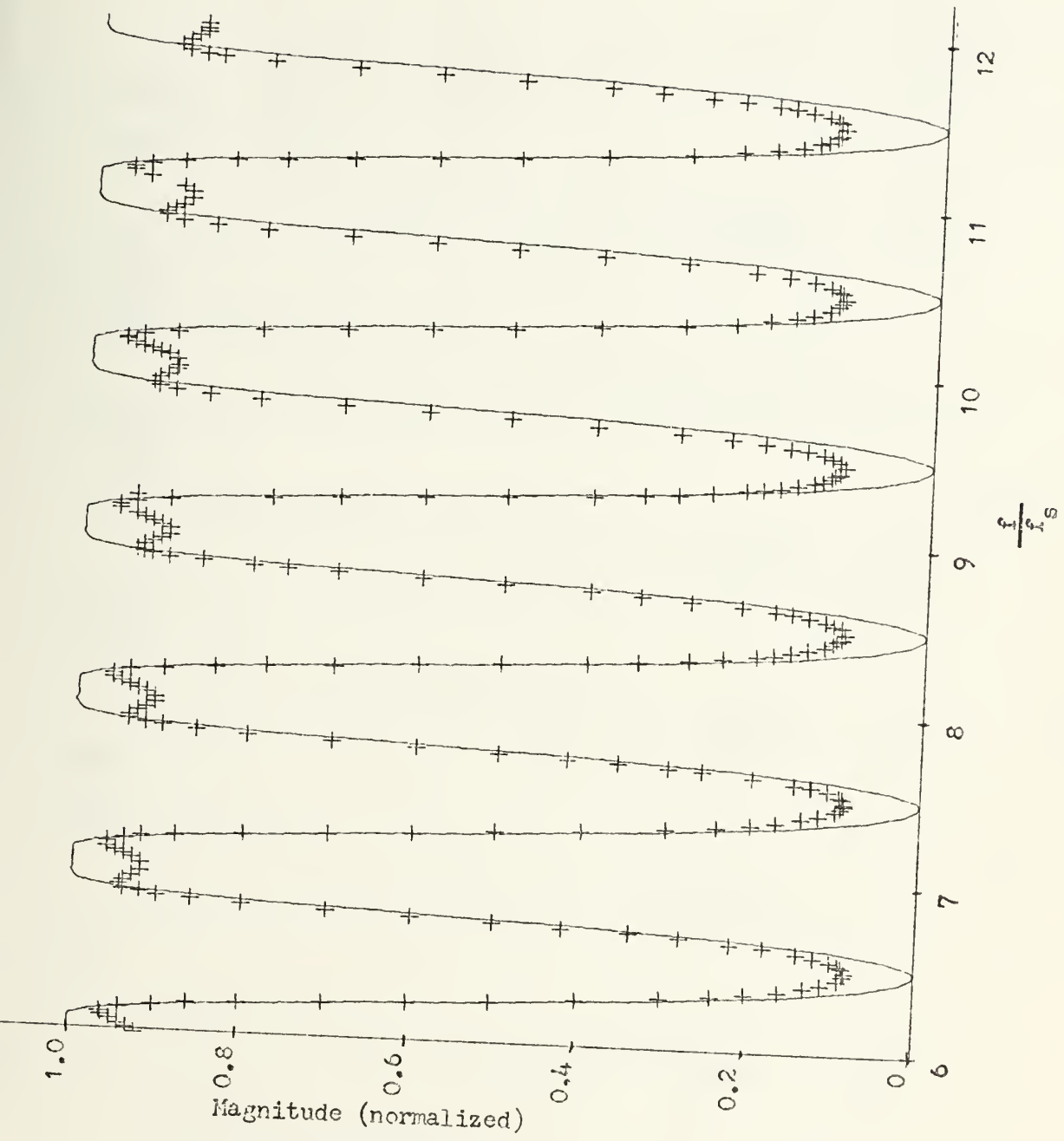

FIGURE 2.16b. Theoretical and Observed Response of Low Pass Filter;
$b_1 = 0.3$, $b_2 = 0.2$

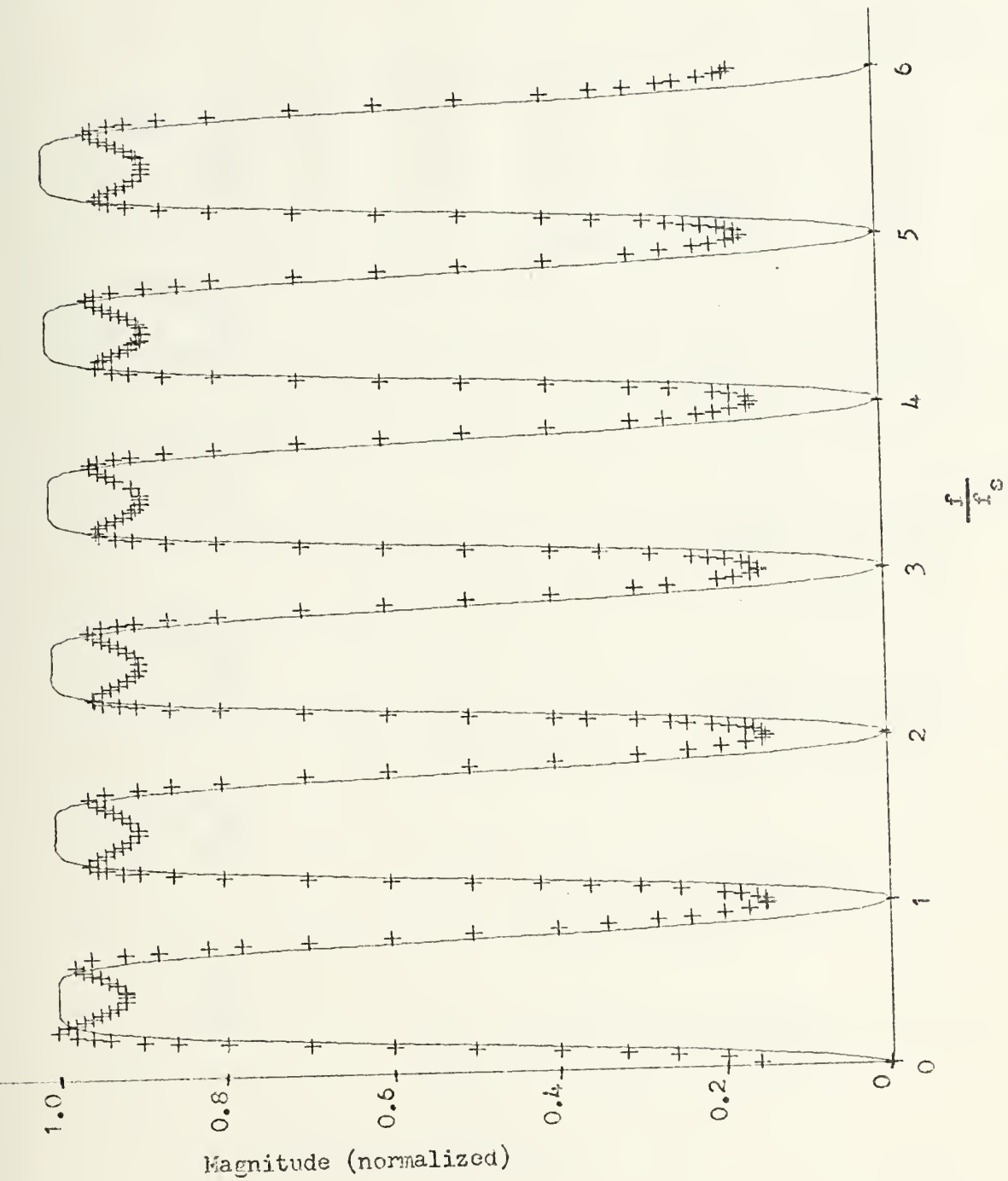

FIGURE 2.17a. Theoretical and Observed Response of High Pass Filter;
$b_1 = -0.2$, $b_2 = 0.19$

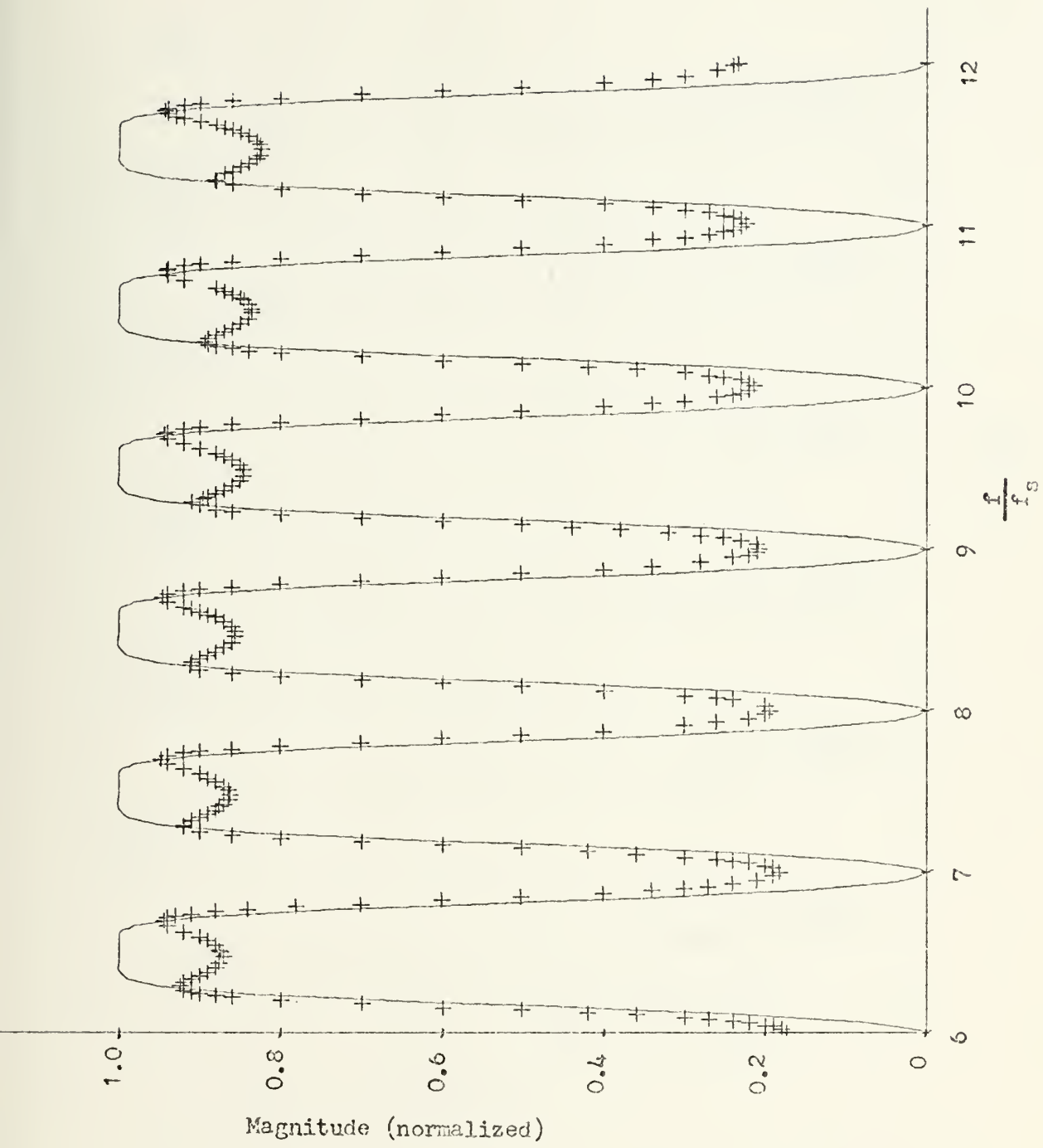

FIGURE 2.17b. Theoretical and Observed Response of High Pass Filter;
$b_1 = -0.2$, $b_2 = 0.19$

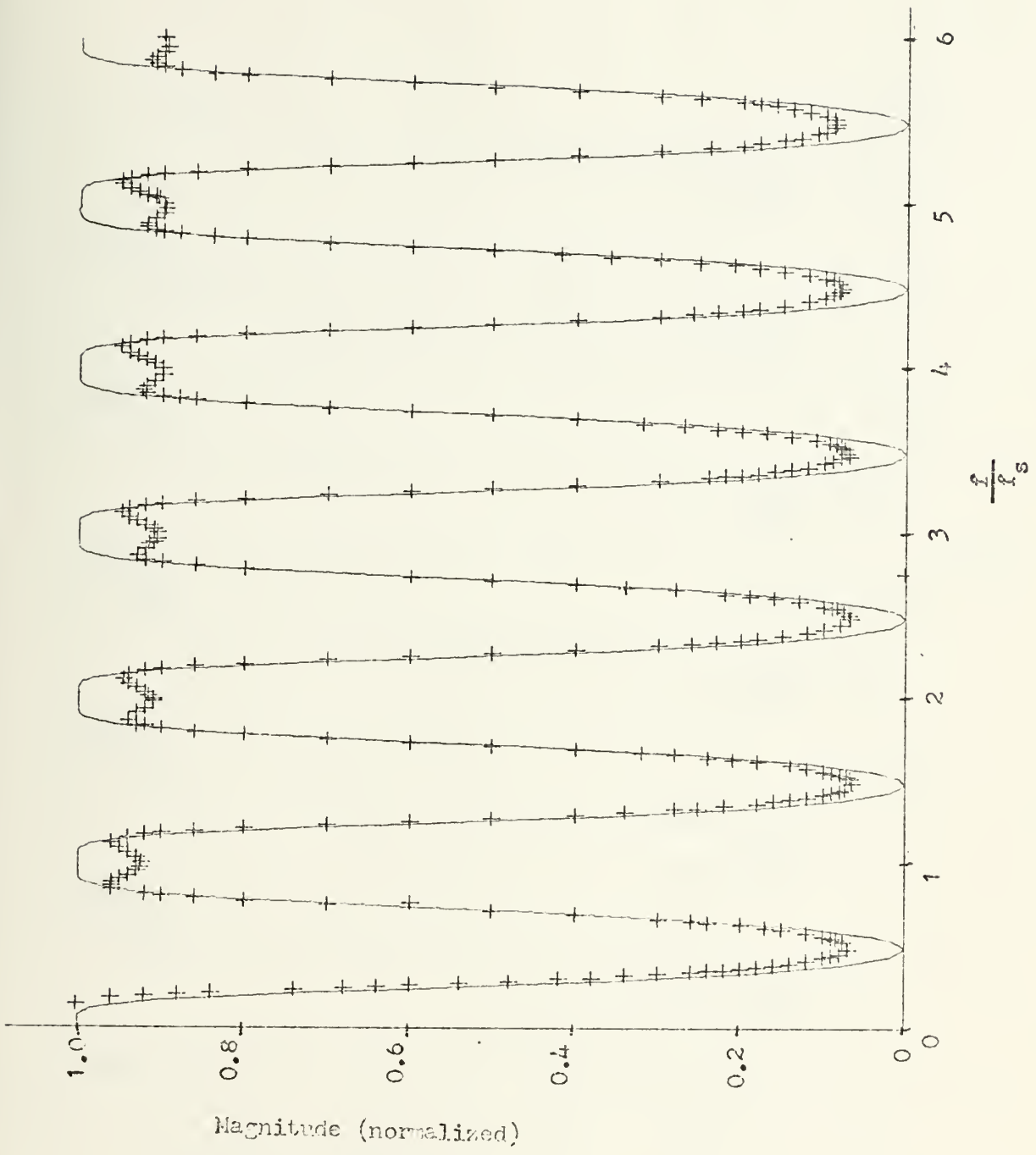

FIGURE 2.18a. Theoretical and Observed Response of Low Pass Filter;
$b_1 = 0.2, \quad b_2 = 0.19$

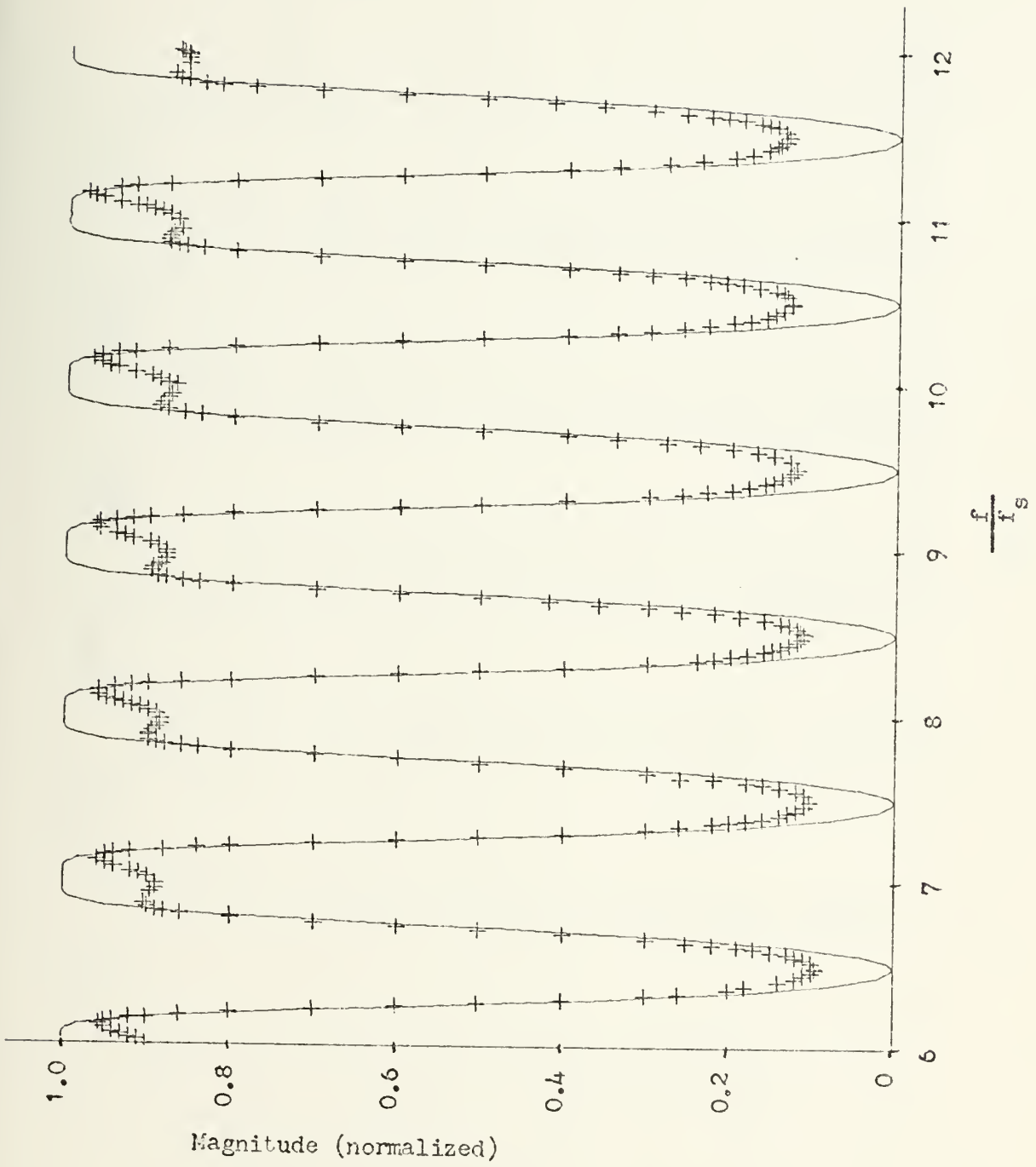

FIGURE 2.18b. Theoretical and Observed Response of Low Pass Filter;
$b_1 = 0.2, \quad b_2 = 0.19$

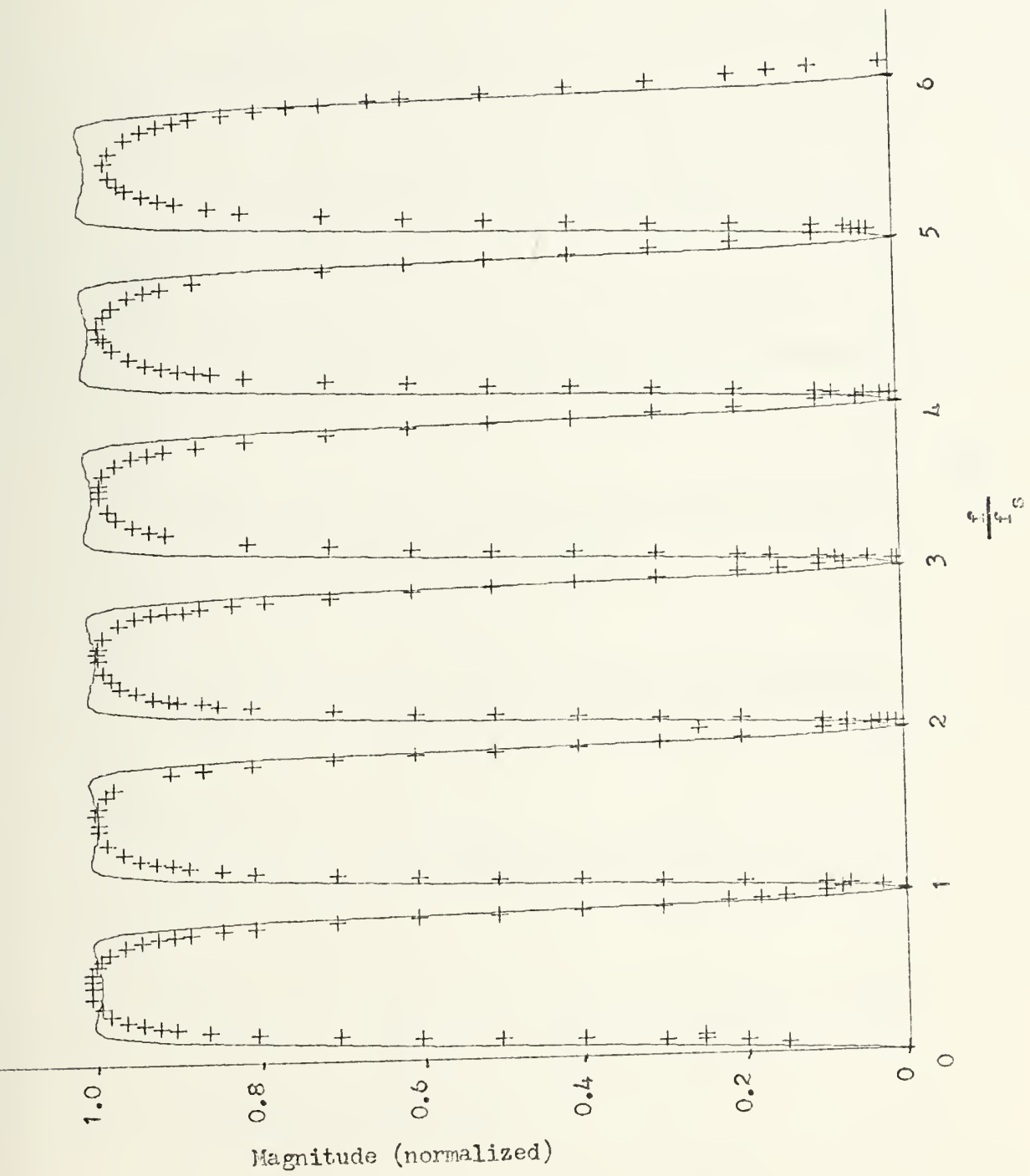

FIGURE 2.19a. Theoretical and Observed Response of High pass Filter;
$b_1 = -1.0$; $b_2 = 0.38$

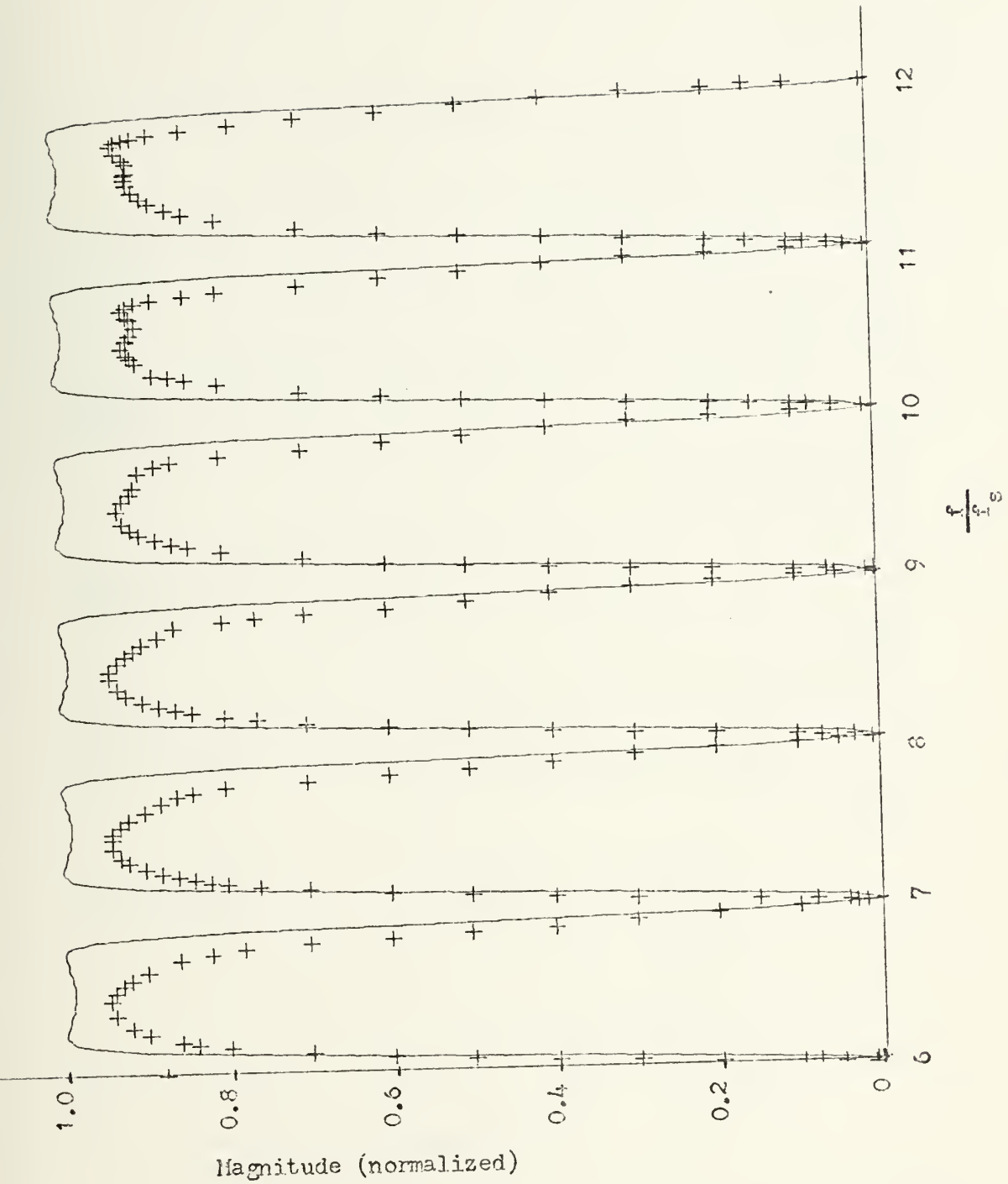

FIGURE 2.19b. Theoretical and Observed Response of High Pass Filter;
$b_1 = -1.0$, $b_2 = 0.38$

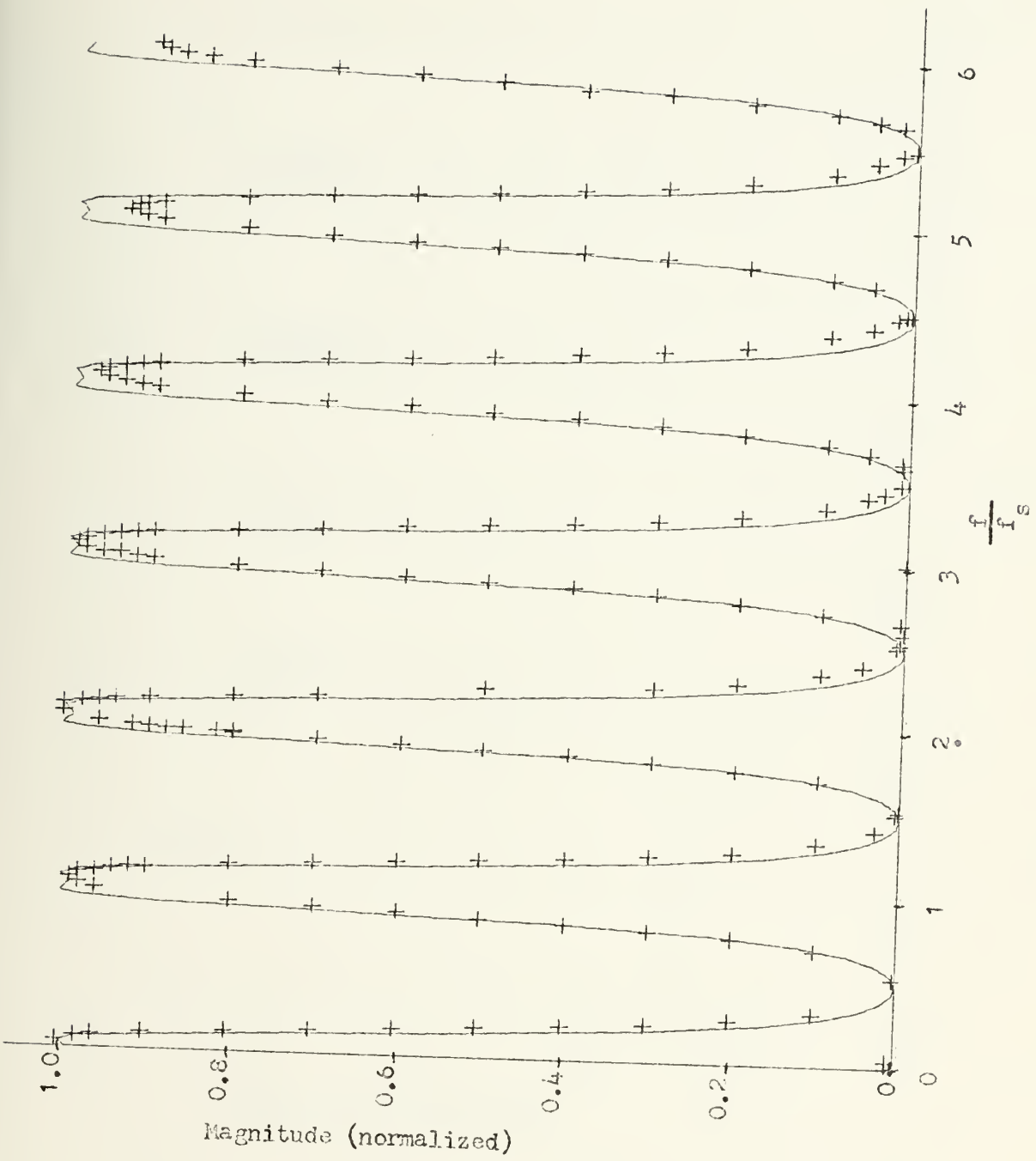

FIGURE 2.20a. Theoretical and Observed Response of Low Pass Filter;
$b_1 = +1.0$, $b_2 = 0.38$

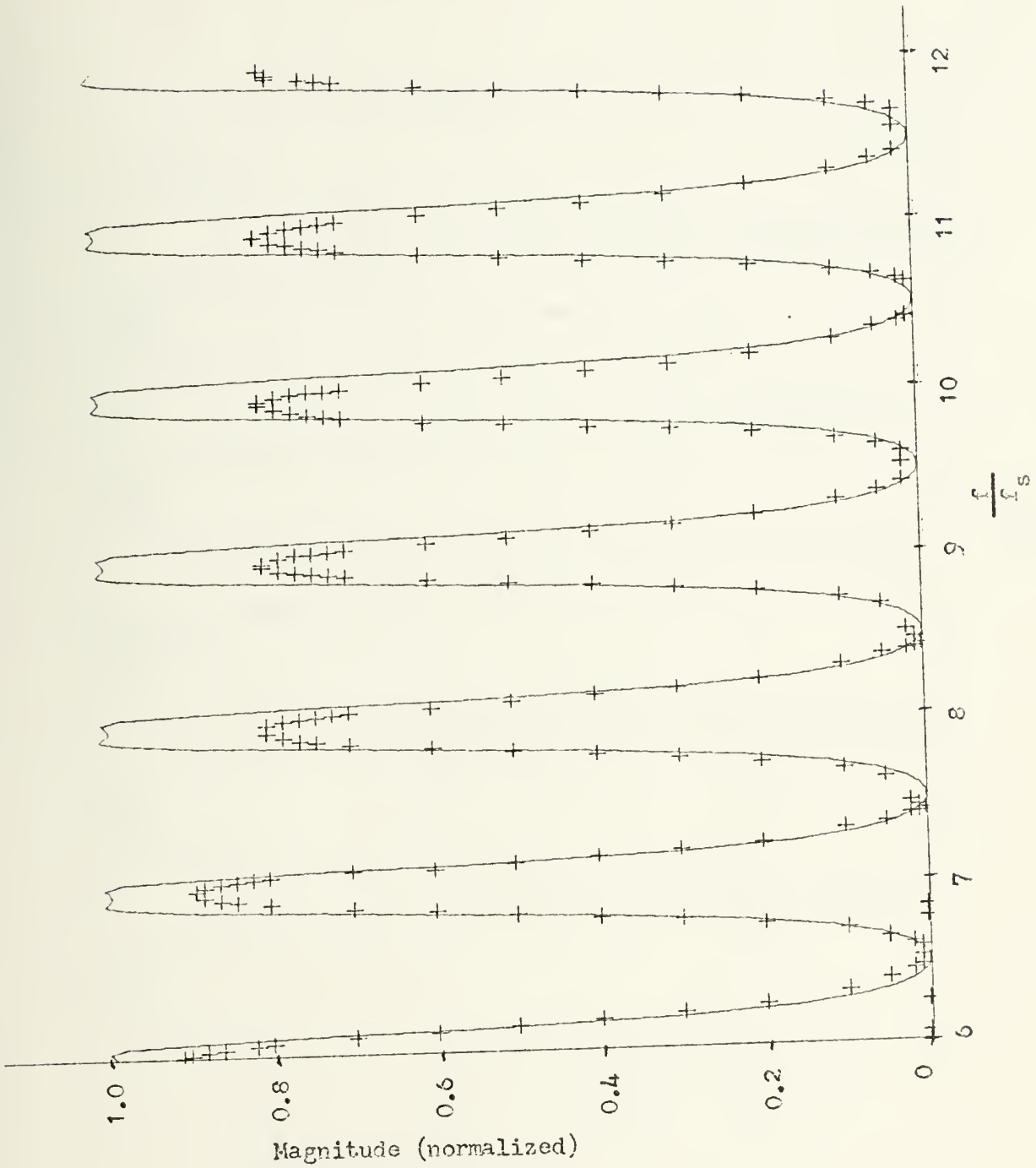

FIGURE 2.20b. Theoretical and Observed Response of Low Pass Filter;
$b_1 = -1.0, \quad b_2 = 0.38$

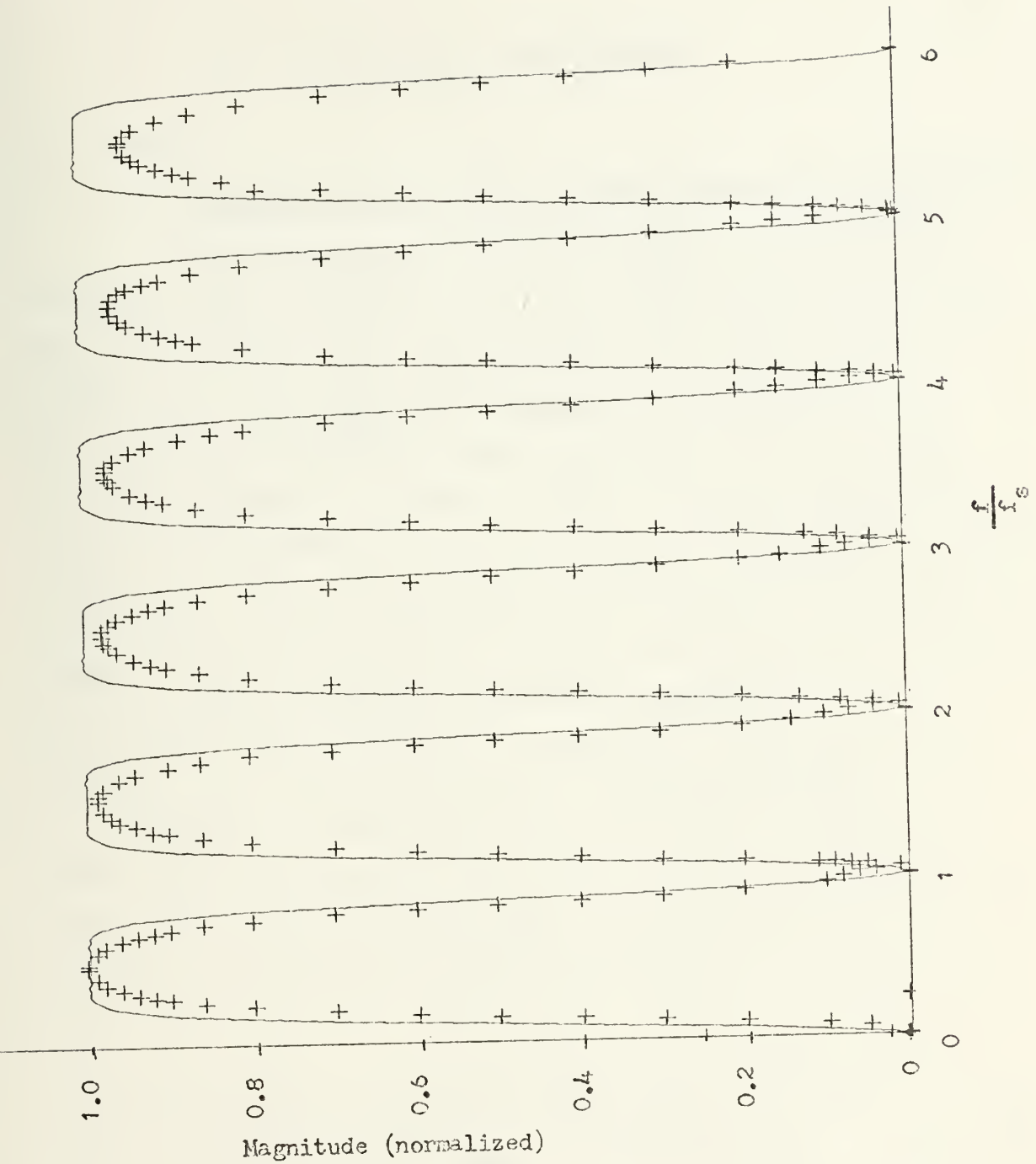

FIGURE 2.21. Theoretical and Observed Response of High Pass Filter;
$b_1 = -0.7$, $b_2 = 0.27$

III. APPLICATION TO MTI-RADAR

A. THEORY

1. Statement of the Radar Signal Processing Requirement

The majority of existing radars are pulsed radar systems. Thus the radar return is in effect a sampled signal, and the sampling width is the pulse width (PW) of the radar. Figure 3.1a. is a time-amplitude plot of radar signals. At multiples of $T = \frac{1}{PRF}$ the transmitted pulses are shown. The time interval between each transmitted pulse, called the Pulse Repetition Interval (PRI), target returns will appear. In Figure 3.1a two stationary targets and one moving target are shown. The stationary target return may be either positive or negative depending upon the phase of the returned signal. There is, however, no change from interval to interval, a fact which is exploited in the MTI canceller.
The moving target however, is changing in amplitude every interval, at a rate which is the doppler frequency.

Figure 3.1b shows how the pulse train of Figure 3.1a would look as presented on an oscilloscope or A-scope. Here every PRI is shown on top of each other, and the moving target is exibiting the socalled "Butterfly effect" {6} while the stationary targets remain fixed in amplitude and time.
To get the frequency representation of a periodic pulse train in the time domain, one can take the Fourier transform. The result would be a $\frac{\sin x}{x}$ -type waveshape. If only one pulse were transmitted, the frequency spectrum would be continuous, and the first null of the curve would appear at $\pm\frac{1}{PW}$. But when transmitting a train of pulses spaced in time at $T = \frac{1}{PRF}$, ideally each target will return a square pulse at PRI equal to T. The frequency spectrum of this periodic signal can be found from the Fourier series if the pulse

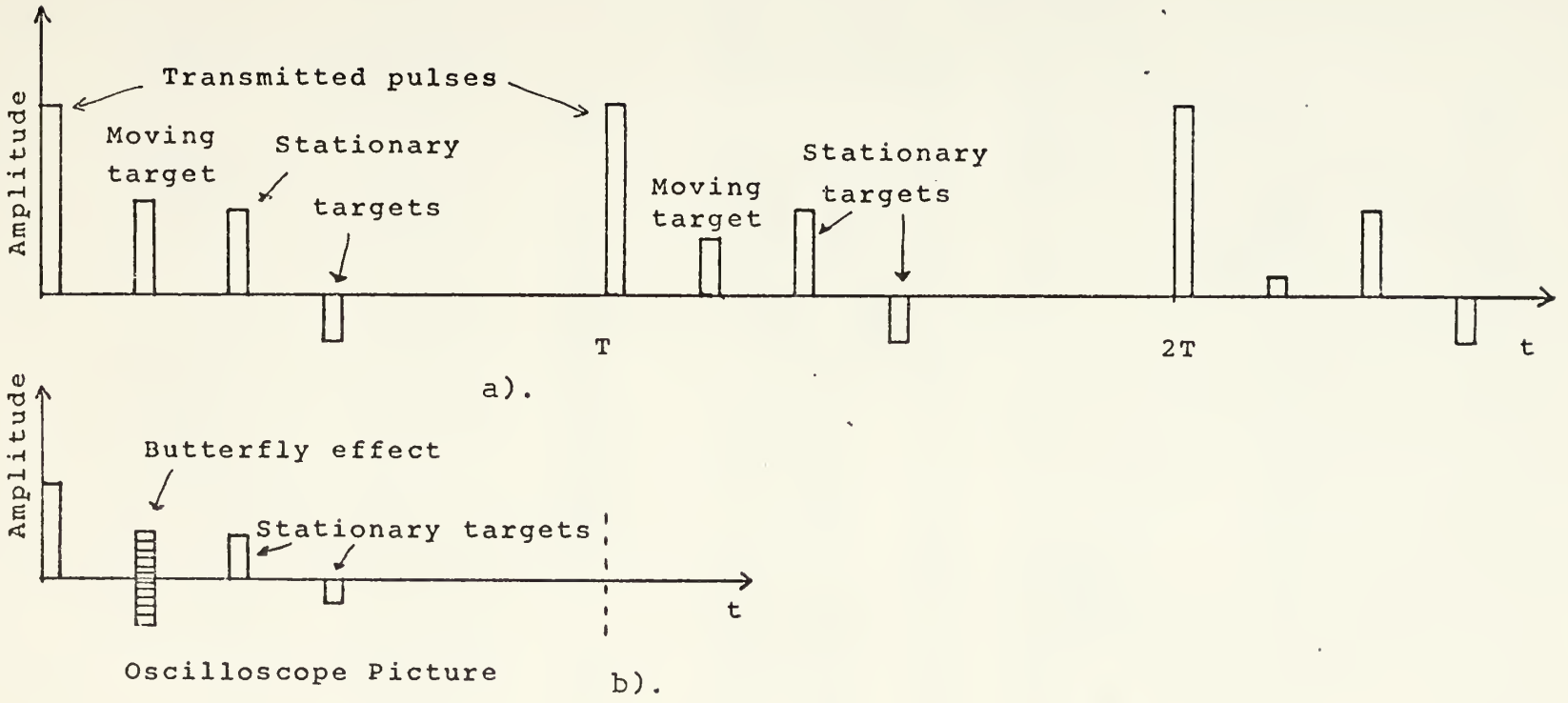

FIGURE 3.1. Infinite periodic Pulsetrain (a), and its appearance on an Oscilloscope (b).

train is infinite:

$$f(t) = \sum_{-\infty} C_n \, e^{jn\omega_1 t}$$

where

$$C_n = \frac{1}{T} \int_{-\frac{T}{2}}^{T/2} f(t) \, e^{-jn\omega_1 t} \, dt \quad , \omega_1 = \frac{2\Pi}{T}$$

C_n is shown in Figure 3.2, where the $\frac{\sin x}{x}$ modulation whose zero crossings with ω- axis are determined by the pulsewidth.

Example: For a radar with PRF of 800 HZ, a PW of 1.3μsec and wavelenght λ of 0.1 meter.
The first zero crossing of the envelope will occur at 769 KHZ. For a target radial speed (v_r) of 900 knots, using a formula from ref {6}; Doppler frequency; $f_d = \frac{2v_r}{\lambda}$.

$$f_d = \frac{2 \cdot 900 \cdot 1852/3600}{0.1} = 9.26 \text{ KHZ}$$

Thus it is obvious that the peaks of the repetitive "clutter spectrum" are essentially of equal amplitude in the frequency range of interest in MTI-radar (Figure 3.3).

Figure 3.3 is a small portion of Figure 3.2 (near the origin) and one moving target is introduced in this ideal frequency spectrum which consists of impulses.

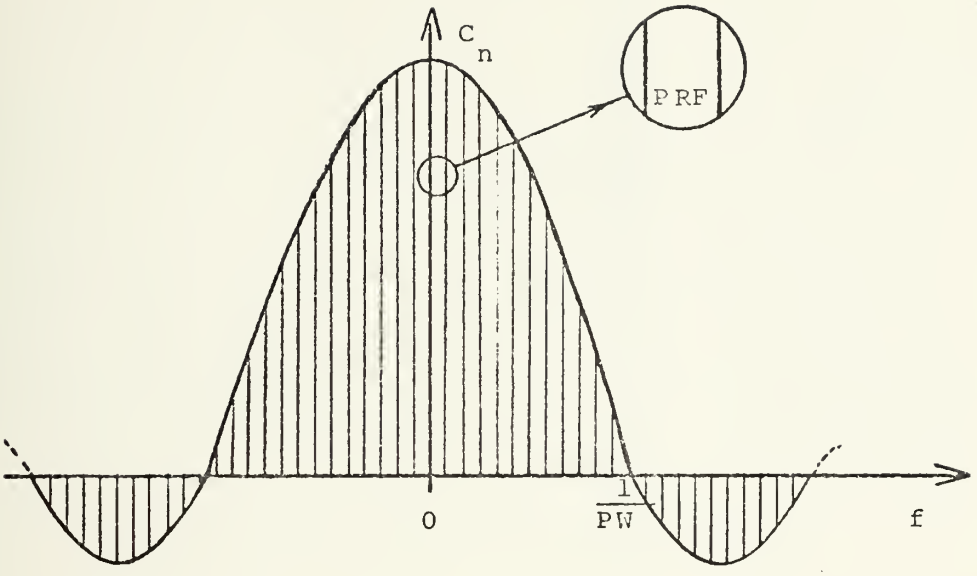

FIGURE 3.2. $\frac{\text{Sin } x}{x}$ envelope of many impulses at

$f = n \cdot PRF$

Figure 3.4 shows the "real" clutterspectrum, i.e. the impulses have been spread out in frequency. There are several reasons for the nonideal shape shown: The energy in the returned echoes is spread out in frequence due to land target movement (vegetation swaying in the wind), sea waves moving, platform noise (own irregular movement), and effects of a finite number of radar returns which stems from the fact that a radar antenna normally rotates.
Thus we do not have an infinite sequence of target pulses. Rather, the number of "hits" on a particular target may be, typically, from 10 to 50 per antenna rotation period.
Figure 3.5 shows the bursts of target echoes every time the antenna points at the target; the time between each burst is called the antenna rotation period.
In Figures 3.6 and 3.7 the Fourier transform of a finite number of 6, respectively 10 hits are shown. The mathematics is omitted here.
The fewer the number of hits, the more energy leaks into

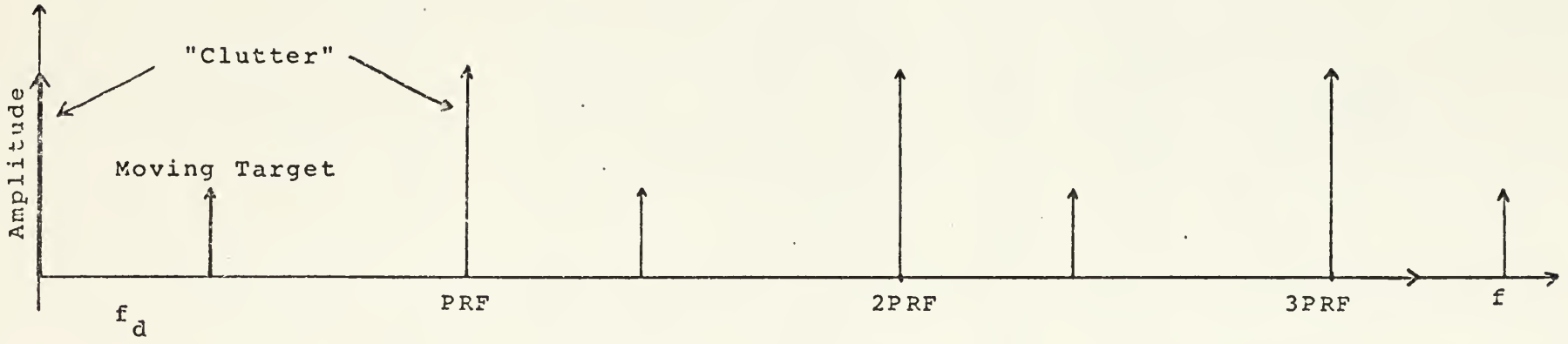

FIGURE 3.3. Ideal Frequency Spectrum of Clutter and One Moving Target.

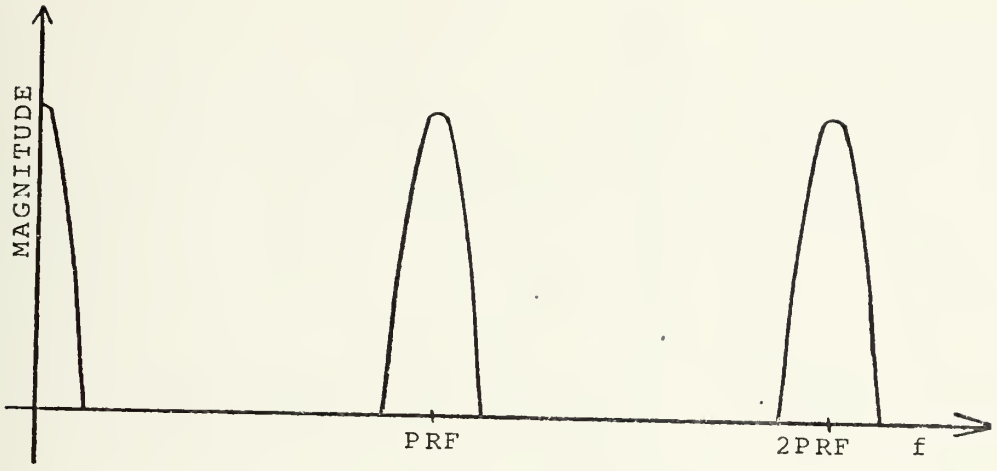

FIGURE 3.4. A "Real" Clutter Spectrum

frequencies where it may give raise to false alarm. Thus the finite number of hits not only leads to spreading of the clutter spectrum around multiples of PRF, but also reduces the maximum attainable cancellation ratio. For proper MTI operation, at least 10 hits per scan is needed. The Fourier transform of such a truncated series of target returns in which there is a moving target among heavy clutter return, is shown in Figure 3.8. Note that the component is also spread out from the ideal impulses, and the energy in the sidebands.

b. Time Response Approach to MTI-Radar Analysis

In this analysis we do not concern ourselves with the trailing edge of a typical echopulse, as our filter has no noticeable disadvantageous effect in this area. But since our filter is a recursive filter, the resirculation of signals lead to undesirable effects which must be investigated.

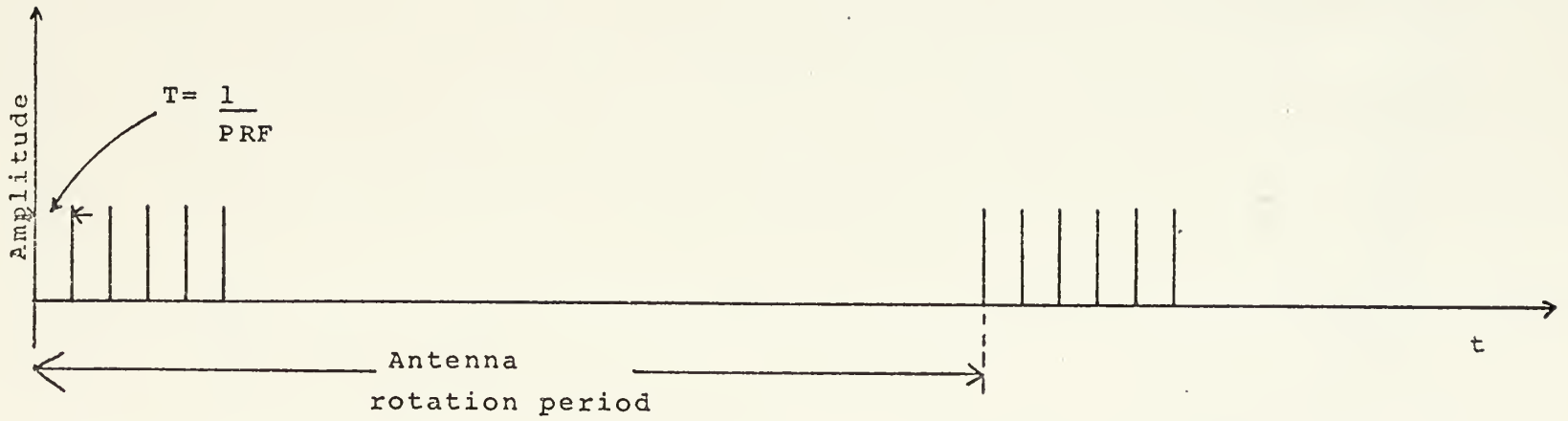

FIGURE 3.5. Finite Bursts of Target Echoes

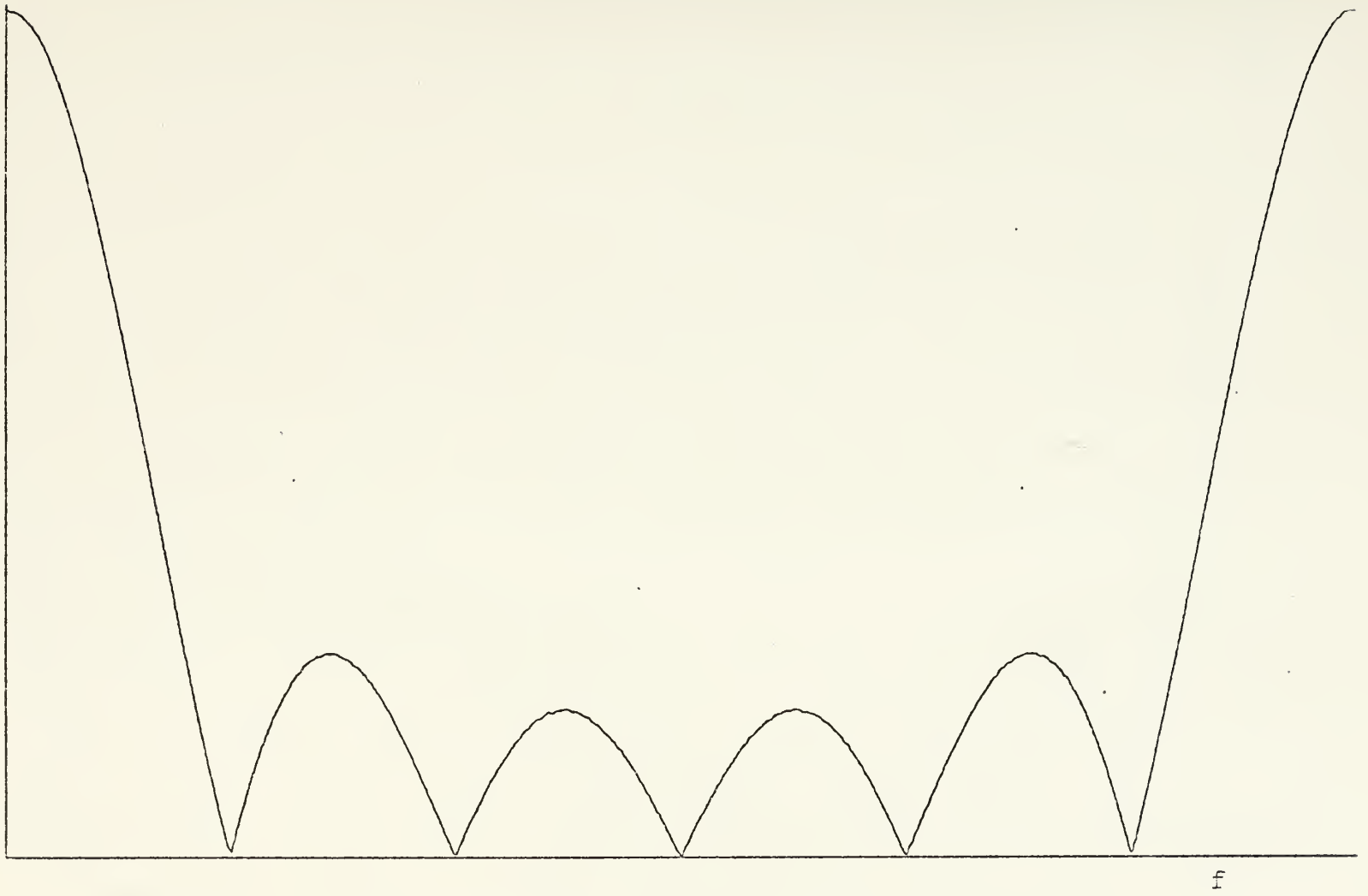

FIGURE 3.6. Fourier Transform of Periodic Bursts of 6 Pulses.

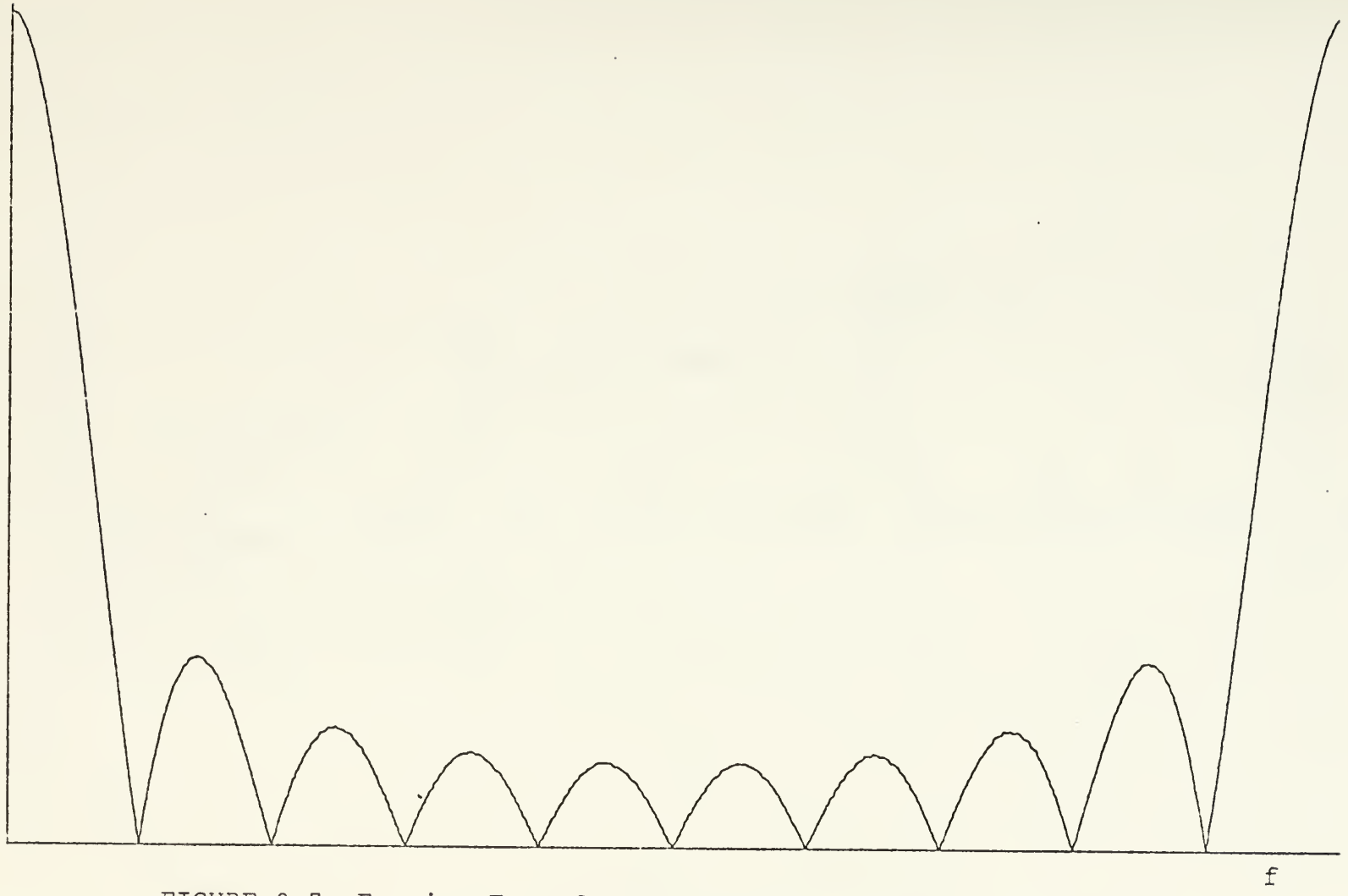

FIGURE 3.7. Fourier Transform of Periodic Bursts of 10 Pulses.

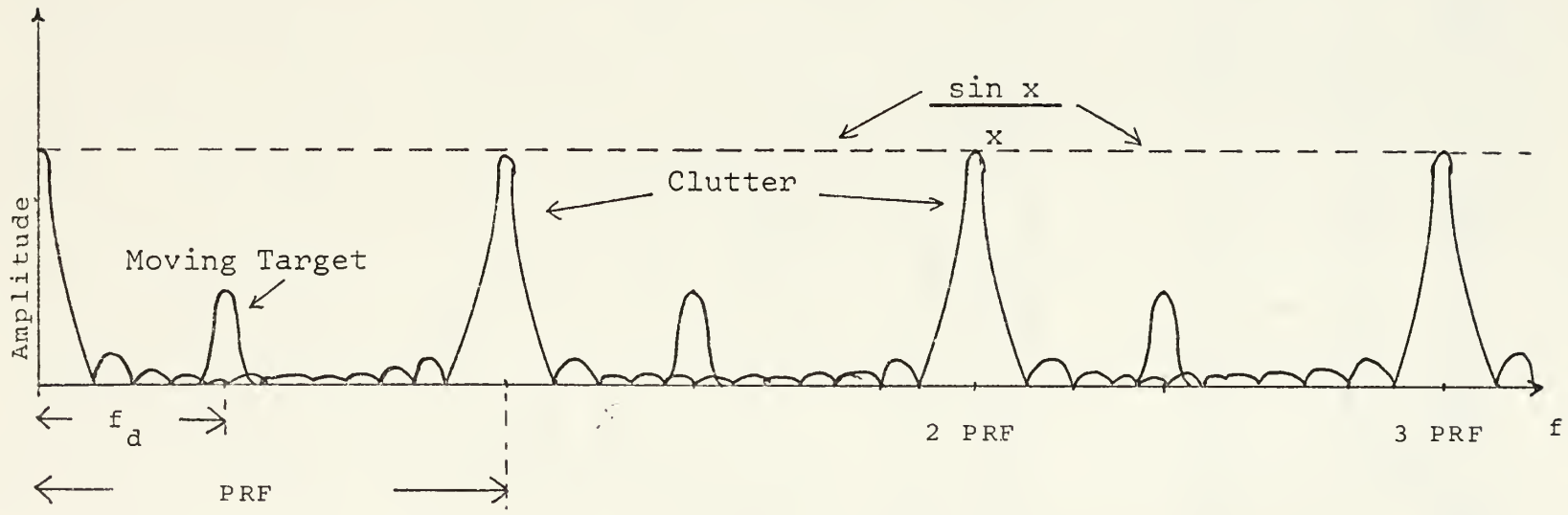

FIGURE 3.8. One Moving Target Among Heavy Clutter.

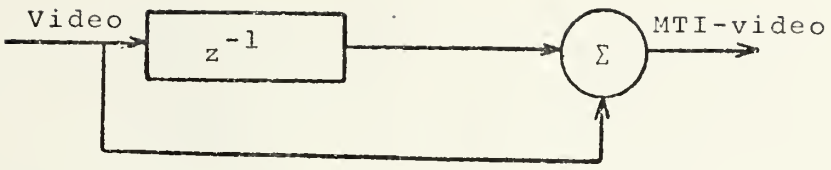

FIGURE 3.9. Delay Line Canceller

Figure 3.9 shows the blockdiagram of a conventional MTI delay-line canceller {6}. Cancellation is obtained only when two succeeding pulses are equal in amplitude. The first and last pulse in a pulse train of a finite number of pulses will be passed by this filter.

In the recursive CCD-filter of Figure 2.3, the first pulse of such a fixed amplitude pulse train will be passed, the second pulse will not be fully cancelled. After the pulse train input is terminated, it will take a finite time, depending upon the values of the feedback coefficients b_1 and b_2, before the filter output approaches zero. This time is measured in number of PRI's, and the effects in PPI presentation is that the target will spread out in azimuth in the direction of the antenna rotation.

Figures 3.10 and 3.11 illustrates typical unit impulse responses of a first order recursive filter with feedback coefficients equal to 0.3 and 0.9, respectively. Example: A typical antenna rotation rate is 20 revolutions per minute, which means 3 seconds/scan or 8.33 msec/degree. For the case where $b_1 = 0.9$ this means that the target would be extended 29/8.33 = 3.5 degrees beyond the actual position. This is considered to be a serious limitation,

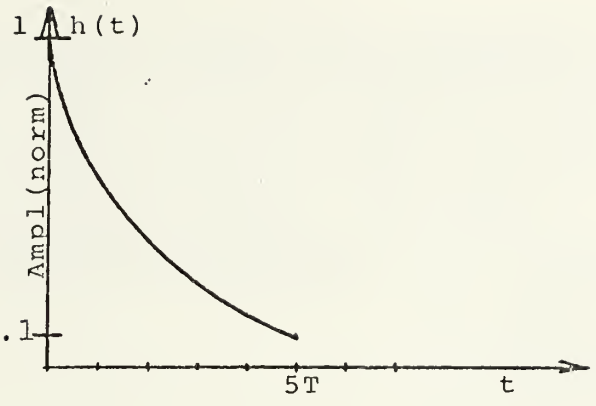

FIGURE 3.10. Time Response of First Order Recursive Filter, $b_1 = 0.3$

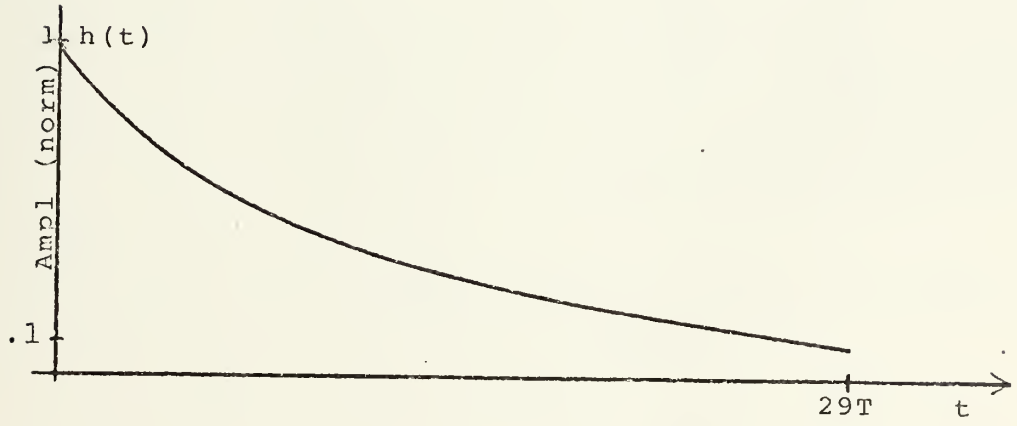

FIGURE 3.11. Time Response of First Order Recursive Filter, $b_1 = 0.9$

and consequently we have to keep this aspect in mind when designing filters of this type.

2. Applying the Comb Filter Technique.

The purpose of MTI -radar is to detect targets moving at or above a certain minimum speed, and suppress all echoes from stationary targets (clutter).
To do this, one exploits the well known doppler effect, namely that the frequency of a returned echo from such a target (moving), is different from the transmitted frequency. Using detection techniques in the receiver {6} , {7},only doppler frequencies are amplified and become the MTI-video which may be transmitted to a PPI for viewing.
Thus we need a comb filter (Figure 3.12), which can reject the clutter, and pass the doppler shifted signals.
One disadvantage is that when the target's radial velocity corresponds to some multiple of the PRF, it will be suppressed also (the target is then said to have a radial blind speed). To overcome this one must vary the PRI from pulse to pulse, by PRF-jitter (random variation of PRI), or PRF stagger (sequentially stepping the PRI between two values only).
A proposed method for building a CCD - filter to facilitate such a system is outlined in chapter IV.

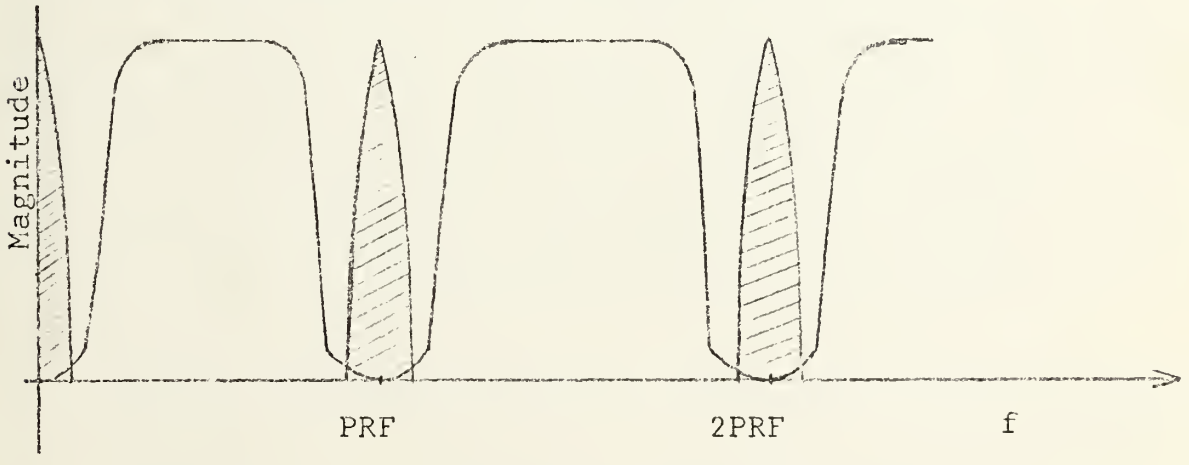

FIGURE 3.12. Comb Filter and Clutter

3. Bandwidth Requirements.

The pulsewidth determines the bandwidth (BW) necessary to reproduce the signal.

$$BW = \frac{1}{2PW}$$

The employed delay lines have 96 stages each. The necessary clock frequency, f_c, is then:

$$f_c = PRF \cdot 96$$

For PRF = 800 HZ, f_c = 76.8 KHZ, which is the effective sample frequency (f_s).

Using Nyquist's Sampling Theorem, $f_s = 2BW$.

The maximum bandwidth that can be faithfully reproduced is then 38.4 KHZ. This corresponds to PW = 13 μsec, which is quite wide and unrealistic. Thus delay lines with considerable larger number of stages are needed.

B. EXPERIMENT

1. Simulation of Radar Return Signal

Since the size of the delay line was limited to 96 stages it was decided to simulate the radar signal for which the delay line was able to respond. The objective was to provide radar return signals simulating fixed and moving targets with variable PRF and number of hits per scan.
The simulation of PRF was implemented using a Beckman 9030 function generator controlled by a sinewave generator (Wavetek Model 142).
The function generator produces a square pulse whose lenght and amplitude can be varied for every period of the sinewave. Thus the PRF may be controlled by changing the Wavetek frequency (Figure 3.13).

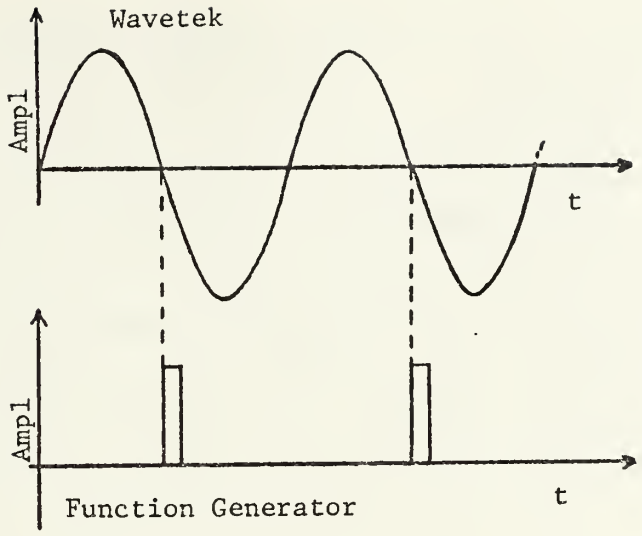

FIGURE 3.13. Time Relationship Between Output from Function Generator and Sinewave Generator

The pulse train thus obtained is the simulation of clutter, or fixed targets, since each pulse is equal in amplitude.

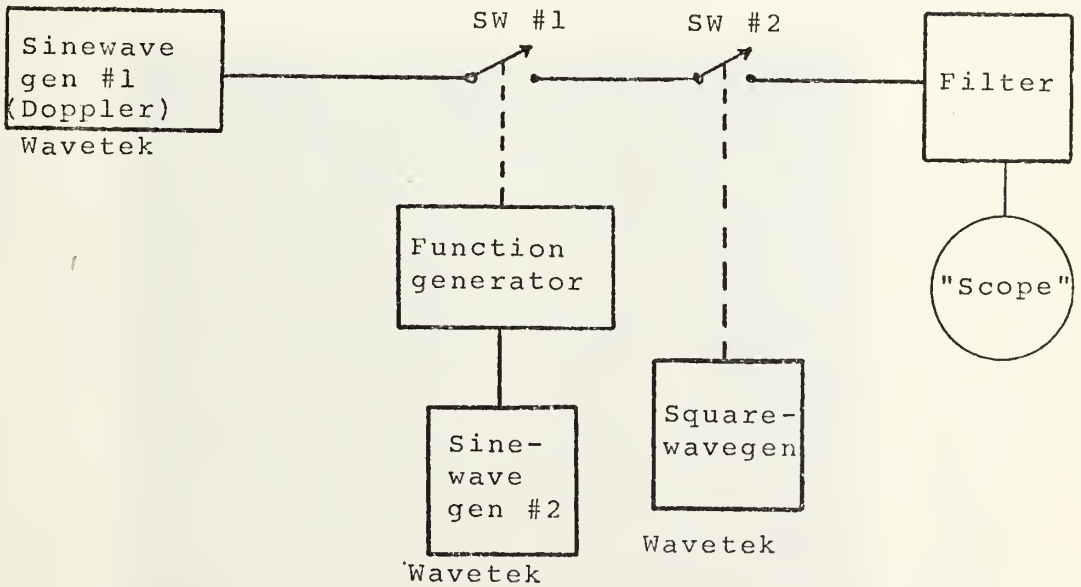

FIGURE 3.14. Block Diagram of Simulation Configuration

Figure 3.14 illustrates the simulation setup. A National Semiconductor MM 4616A switch (Figure 3.15) was used to perform the switching functions. The specifications of this arrangement is that each pulse through this switch had a different amplitude, simulating the moving target signal. On the oscilloscope, this signal should exhibit the "butterfly effect" {6}. If needed, both stationary and moving target signals could be fed into the filter simultaneously. The second switch was operated by another Wavetek M142, which was set such that the positive part of the squarewave was much shorter than the negative part. The positive part would turn the switch on, letting a finite number of pulses from switch one through. This was the simulation of the antenna sweep. However, the present simulation of this effect is limited because it has not been possible to simulate the long time between two series of radar hits.

2. Results.

a. Stationary Targets with PRF = 800 HZ

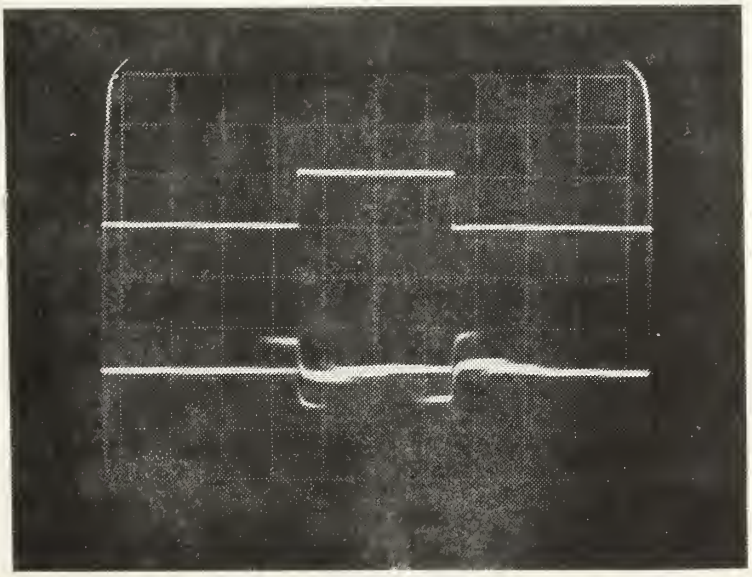

FIGURE 3.17. Cancelling of "Stationary" Target, Horizontal: 10 μsec/cm. Vert: .5V/cm

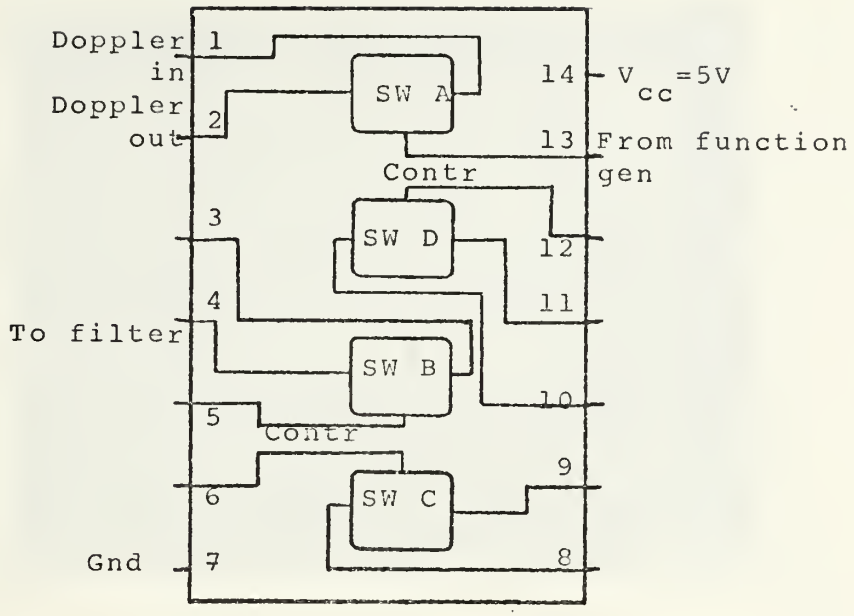

FIGURE 3.15. Analog Switch Schematic.

TABLE IV

Typical Radar Charachteristics

Band:	L-band	S-band	C-band	X-band	K-band
Frequency (GHZ)	1 - 2	2 - 4	4 - 8	8-12.5	12.5-18
Typical PRF	200-500	300-600	500-1000	800-3000	2000-5000
PRI= $\frac{1}{PRF}$	2-5 msec	1.67-3 msec	1-2 msec	333-1250 usec	200-500 usec
Maximum Theoretical Range n.m.	162-405	135-270	81-162	27-101	16.2-40.5
Typical PW	3-5 usec	1-3 usec	0.5-4 usec	.05-1.5 usec	.01-0.5 usec

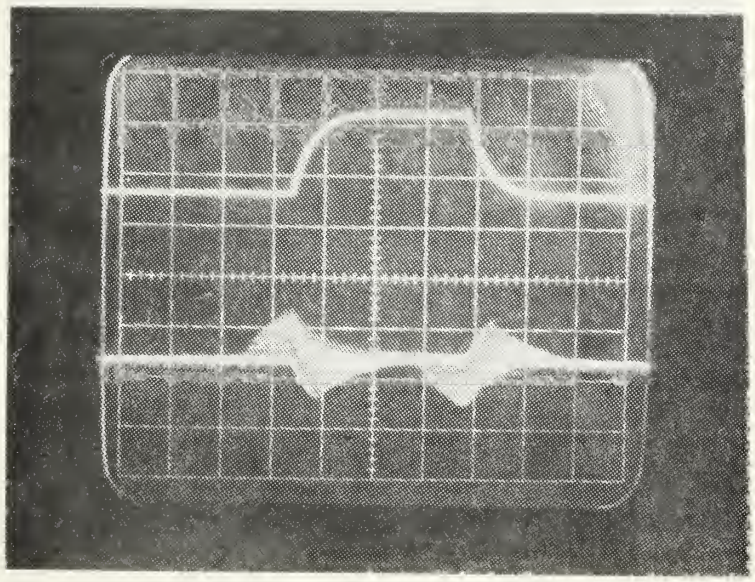

FIGURE 3.18. Cancelling of Stationary Target.
PRF= 800HZ. Horizontal: 10 usec/cm.

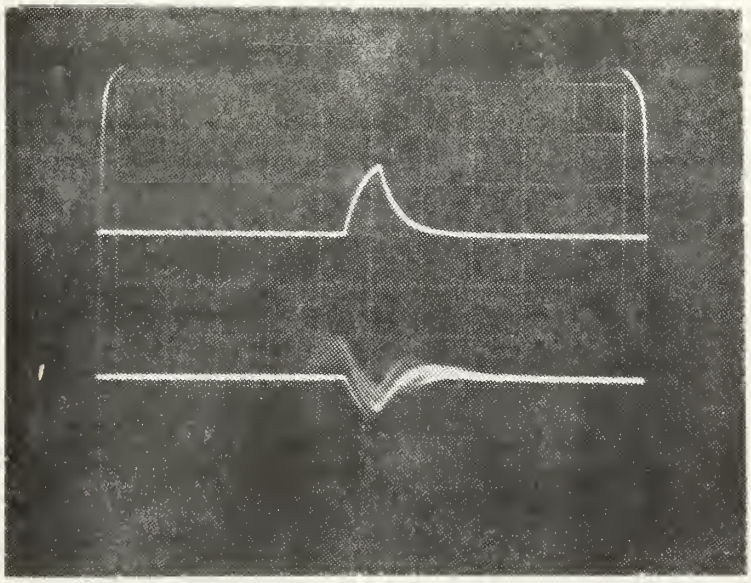

FIGURE 3.19. Cancelling of Narrow, Stationary Target.
PRF = 800HZ. Horizontal: 10 usec/cm.

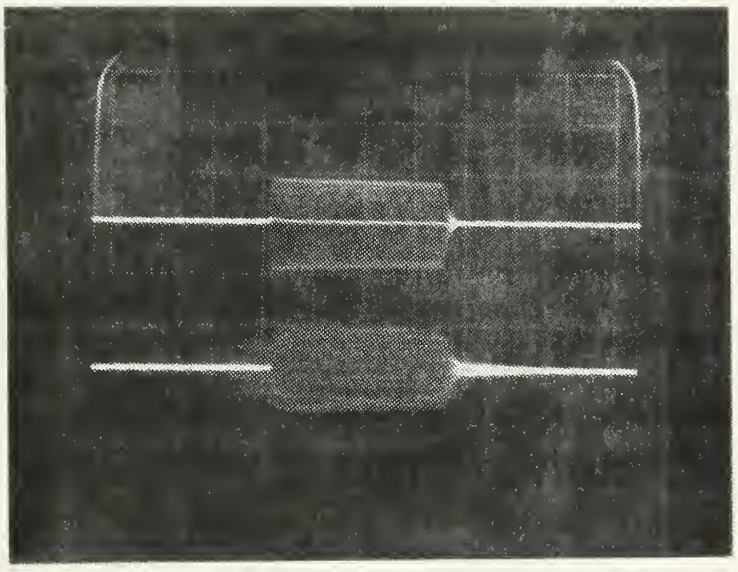

FIGURE 3.20. Moving Target Signal. PRF= 800 HZ
Horizontal: 10 μsec/cm

Figure 3.20 shows a "moving target" signal. The doppler frequency was at the center of first comb tooth of the filter. It can be seen that the combfilter did not cancel the signal. The insertion loss was quite small.

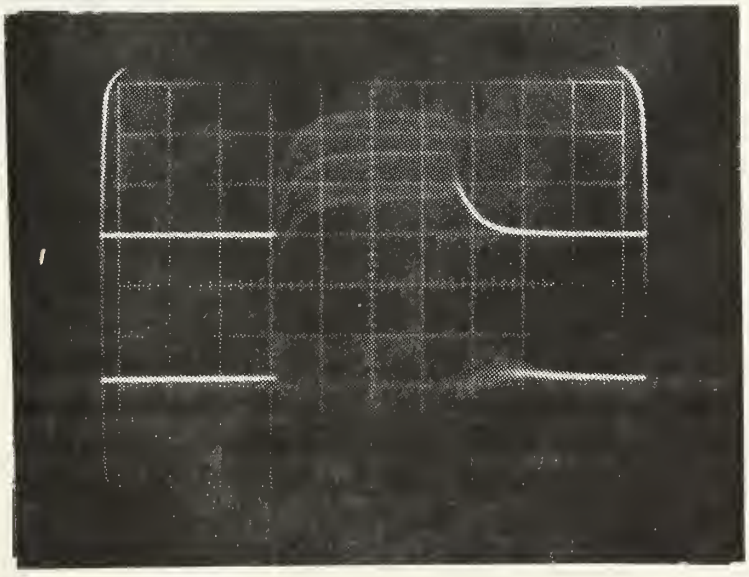

FIGURE 3.21. Moving and Stationary Targets. PRF= 800 HZ
Horizontal: 10 μsec/cm

c. Both Stationary and Moving Signals, PRF = 800 HZ

Figure 3.21 shows an input consisting of both moving and stationary target signals. It can be seen that only the moving signal is passed.

d. Fixed and Moving Targets. PRF = 10 KHZ

To try to eliminate some of the glitches, the effective clock frequency was increased to 288 KHZ, so that the nulls of the comb filter appeared at multiples of 10 KHZ. The set of coefficients for the following results were (potentiometer settings):

$a_o = 0.6885$, $a_1 = 0.975$, $a_2 = 0.87$, $b_1 = 0.5475$, $b_2 = 0.498$.

For all the pictures the vertical scale is 0.5 V/cm.

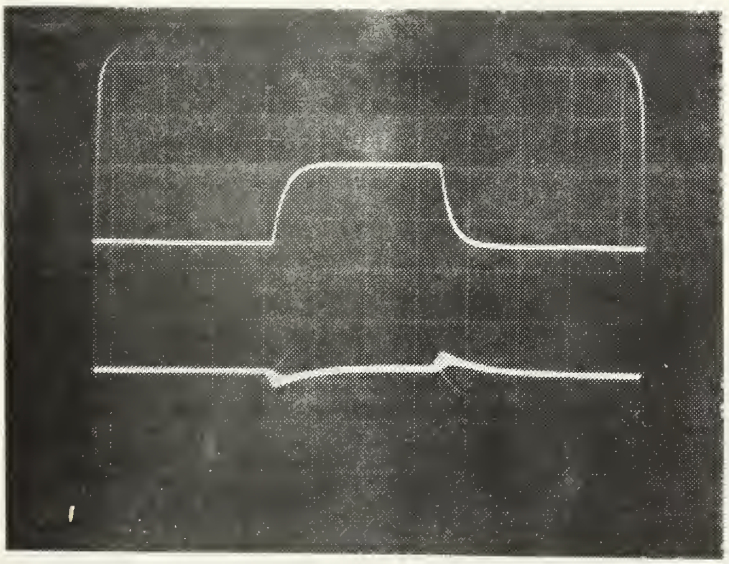

FIGURE 3.22. Stationary Target Signal. PRF = 10 KHZ. Horizontal scale: 50 μsec/cm.

Figure 3.22 corresponds to Figure 3.18, the difference being that now the PRF was 10 KHZ instead of 800 HZ. Note that the glitches were much smaller in amplitude at higher clock frequency.

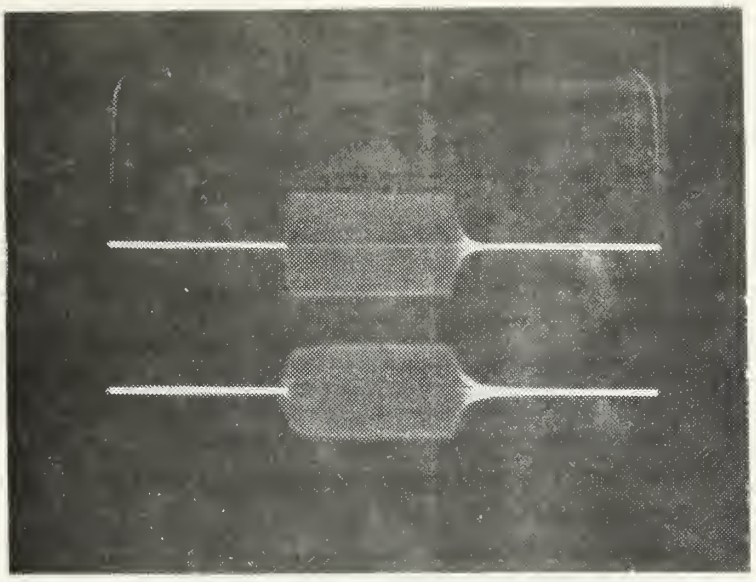

FIGURE 3.23. Moving Target Signal only. PRF = 10 KHZ
Horizontal scale: 50 μsec/cm.

e. Moving Target. PRF = 10 KHZ.

Figure 3. 23 shows a moving target only, with doppler frequency, f_d = 5 KHZ. Again it is noted that the moving target signal passed through the comb filter with low insertion loss.

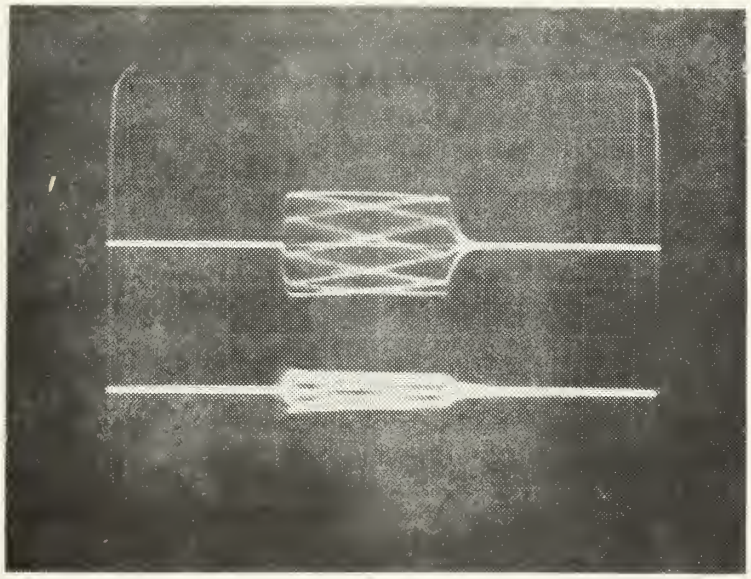

FIGURE 3.24. Moving Target, f_d = 8.5 KHZ. PRF+ 10 KHZ.
Horizontal: 50 μsec/cm/

f. Moving Target with Doppler Frequency Close to the First Null

Figure 3.24 shows that the output amplitude indeed was attenuated when f_d was close to the blind speed. In this case the first blind speed was the radial velocity of the target corresponding to f_d = 10 KHZ.

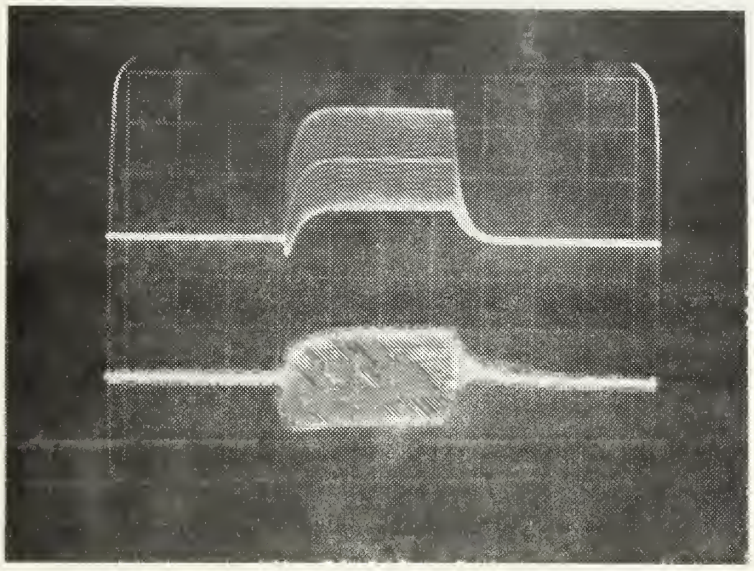

FIGURE 3.25. Moving Target and Stationary Target, f_d = 5 KHZ, PRF = 10 KHZ. Horizontal: 50 μsec/cm.

g. Stationary and Moving Targets, PRF = 10 KHZ

Figure 3.25 shows that when the input consisted of both stationary and moving targets, only the moving target signal was passed. In this case f_d = 5 KHZ which was midband.

h. Stationary and Moving Targets, Doppler Frequency at First Null

Figure 3.26 depicts the same situation as in Figure 3.25, only now f_d= 10 KHZ which was the first blind speed. Both targets were suppressed, and the glitches are seen. The output was almost identical to the output in the stationary target case (Figure 3.22)

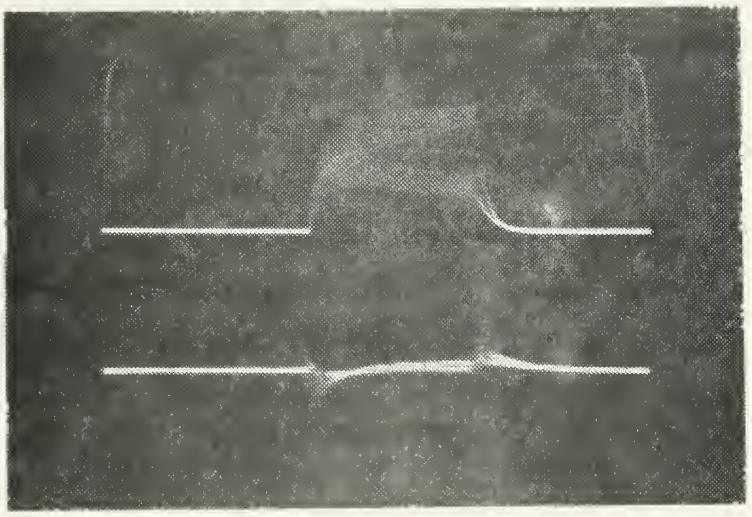

FIGURE 3.26. Moving and Stationary Targets Superimposed. f_d = 10 KHZ, PRF = 10 KHZ. Horizontal: 50 μsec/cm.

i. The Effect of a Finite Number of Stationary Target Signals.

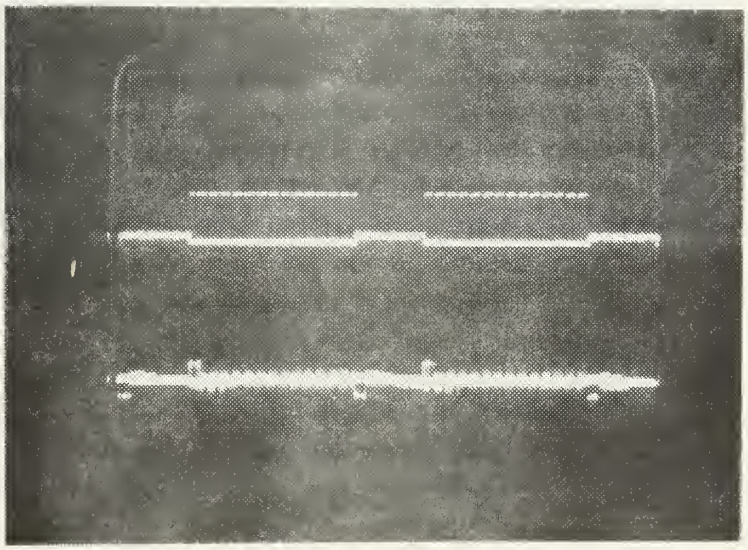

FIGURE 3.27. Truncated Series of Fixed Targets (15 hits) Horizontal: 0.5 msec/cm.

Figure 3.27 shows the input and output of the comb filter in the case where Switch 2 (Figure 3.14) was operated by a low

frequency asymmetrical squarewave, to simulate finite number of "hits" on the target during one period of the antenna scan. The input to the switch was an infinite train of fixed amplitude pulses. The oscilloscope was synchronized to the switch controlling waveform. Note that the first and last pulses in each truncated series of radar hits were passed by the comb filter. This was in agreement with the time analysis. The rest of the pulses were cancelled, except for the glitches, which appeared quite pronounced in this picture. Additional study is necessary to determine the cause of the glitches and their elimination.

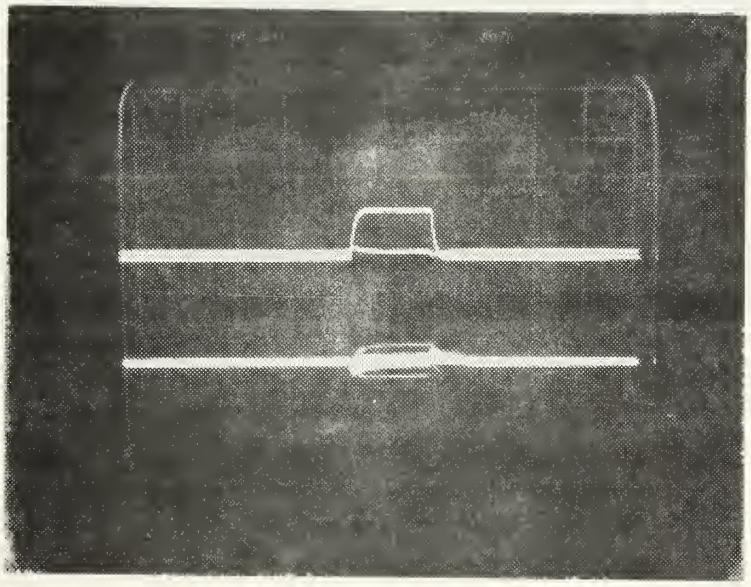

FIGURE 3.28. One Pulse from Figure 3.27.
Horizontal scale: 10 μsec/cm.

Figure 3.28 shows one of the individual pulses in the truncated trains of radar hits from Figure 3.27. The oscilloscope was now synchronized to the function generator (Figure 3.14). It is noted that the cancellation was poor, verifying the analysis of section III.A.1.a, which predicted that energy would leak into sidebands when a finite number of hits were being processed, causing false alarm.

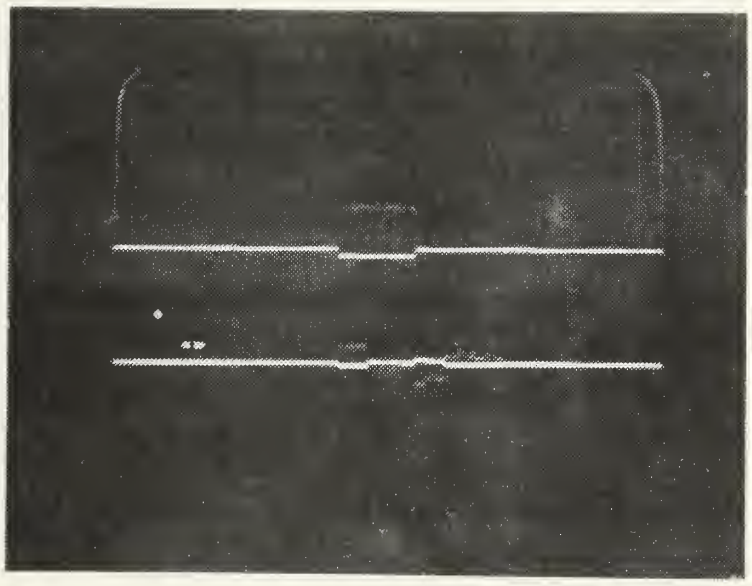

FIGURE 3.29. Truncated Series of Fixed Targets (3 Hits). Horizontal: 20 μsec/cm.

Figure 3.29 shows a truncated series of only 3 hits. The oscilloscope was now synchronized to the squarewave generator controlling Switch 2, and the three hits cannot be seen clearly on this picture for that reason. Note that the first two pulses were passed and the last pulse was also passed as well as several recirculated pulses, causing a smearing of the trailing edge. This phenomenon was desribed in section III.A.1.b., and is caused by recirculation of the signals. The signal will die out gradually depending upon the size of the feedback coefficient.

Figure 3.30 shows one of the individual pulses shown in Figure 3.29. Although this pulse was similar to Figure 3.28, it should be quite different. More pronounced false alarm was expected in Figure 3.30 than in Figure 3.28. The reason for the poor result here was that the individual truncated series were too close, so that several consecutive series were superimposed on the scope. This was also the reason for the base line to appear even under the pulse in both Figures 3.28 and 3.30.

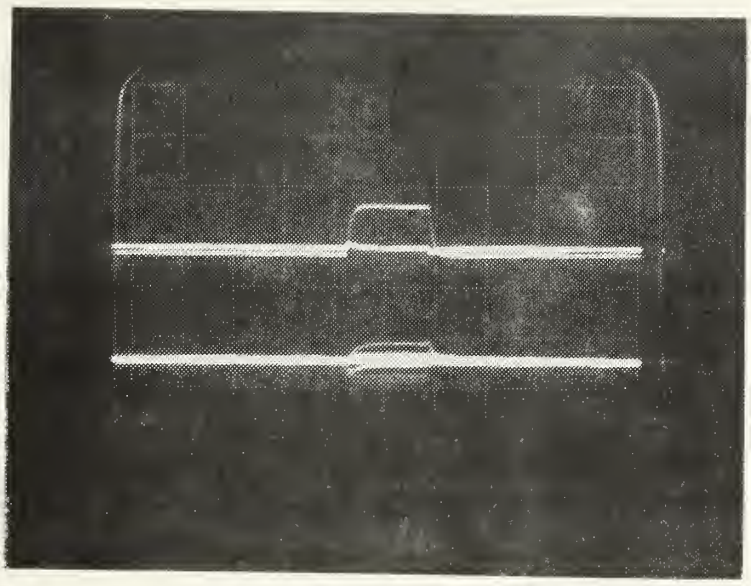

FIGURE 3.30. One pulse from Figure 3.29.
Horizontal: 10 μsec/cm.

The relative brightness of the pulse itself and the base-line under the pulse in Figure 3.28 indicated that there were more oscilloscope sweeps for pulses than for base line.
But in Figure 3.30 the situation was reversed. This was reasonable, since here most of the time-axis was a base-line.

A. CONCLUSIONS OF EXPERIMENTS

1. Filter Experiments

It has been shown that the CTD-device can be used for implementing second order comb filters.

2. MTI-Radar Simulation Experiment.

Most of the simulation objectives were met except for the simulation of antenna rotation. Due to the limitation of instrumentation, the time between two series of radar hits is too short. A more realistic case would be to have a series of radar hits appear every two seconds.

A major unresolved problem encountered in this study was the observed glitches. It must be solved before the sampled analog recursive CTD comb filter may be successfully employed in real radar systems.

Characteristics of the present CTD-devices do not yet allow for enough bandwidth. More delay stages are needed.

Until then only simulated results may be obtained, with rather restrictive ranges of pulsewidths and PRF's.

However, deviations between theory and measured results have been noticed. It was found that both the delay line and its peripheral electronics do not have adequate bandwidths. Consequently, the coefficients used in experimental studies vary with frequency. It is believed that this is one of the major causes of deviation of experiment from theory.

B. RECOMMENDATIONS

1. Research Topics Directly Related to Present Thesis.

In the filter study of chapter II, more work is needed to achieve implementation of frequency independent coefficients. Perhaps voltage controlled operational amplifiers should be used instead of potentiometers, and

also a frequency independent delay-line and its peripheral circuitry.

In the MTI- simulation study, the problem is the glitches. To find the causes, and to eliminate them is important. Another area is to build a better simulation setup for examining the effect of finite number of returns.

2. Proposed Application to Staggered/Jittered PRF MTI-Radar.

Not too many military MTI-radars today will be built that do not include either jitter PRF or stagger PRF capabilities. One of the major attractions of CTD-delay lines is the ease and speed with which the clock-frequency, and thereby the delay time, may be changed. Consequently, the null frequencies of the comb filter can be easily changed by changing the clock frequency.
But there are major problems in applying the CTD-filter to such cases. This is because in jitter, or staggered PRF-radar, the PRI changes from pulse to pulse, and thus the clock frequency of the delay line must be changed for every PRI. It is seen that information which has already been fed into the delay-line (memory device), will be clocked out at a different clock frequency and then added in the output summer (Figure 2.3) with a signa employing a third PRI. The result would be meaningless.
Figure 4.1 is a proposal to employ clocked CTD-delay lines in a jitter PRF tracking filter which could overcome this problem. It may solve the undesirable effects of long settling time associated with high feedback coefficients, as stated in section III.A.1.b.
A short explanation using difference equations, of this circuit follows:

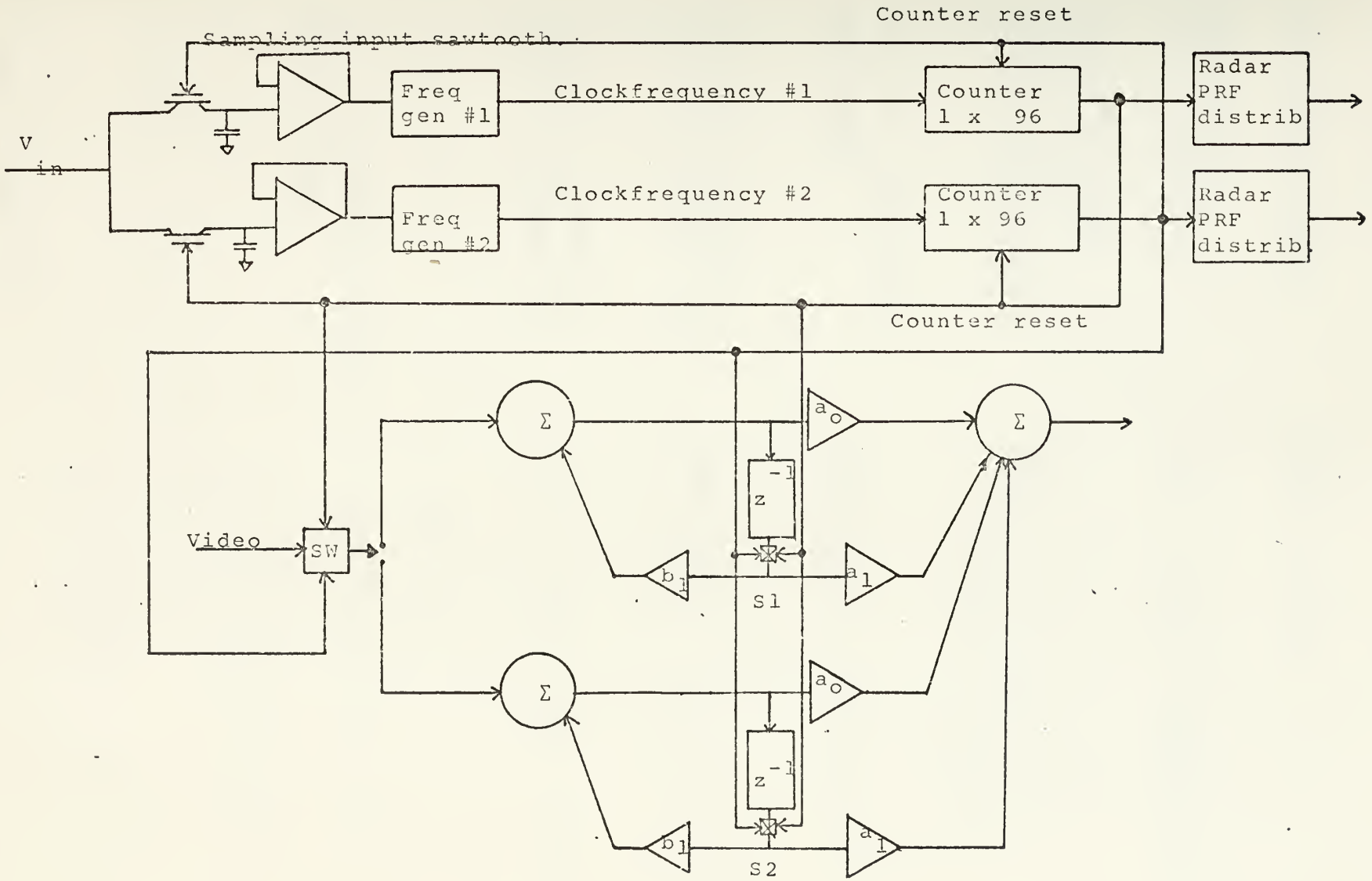

FIGURE 4.1. First Order CCD Jitter PRF MTI-Filter

1st pulse arrives: $Y(0) = a_o X(0)$

Upper part of filter effective: $Y(1) = a_o X(1) + (b_1 a_o + a_1) X(0)$

Video into lower circuit, still tapping upper part: $Y(2) = a_o X(2) + (b_1 a_o + a_1) X(1) + b_1^2 a_o X(0) + a_1 b_1 X(0)$

S1 opens. Video into upper part: $Y(3) = a_o X(3) + (b_1 a_o + a_1) X(2)$

S1 closes, S2 opens, Video into lower part: $Y(4) = a_o X(4) + (b_1 a_o + a_1) X(3)$

S1 opens, S2 closes Video into upper part: $Y(5) = a_o X(5) + (b_1 a_o + a_1) X(4)$

etc

If the video train input is a train of fixed amplitude pulses, then:

$$Y(n) + X(n)\{(a_o(1+b_1))+a_1\}$$

There will be perfect cancellation if:

$$a_o(1 + b_1) + a_1 = 0$$

Circuit operation:

V_{in} is a sawtooth waveform. A sample and hold circuit is used to establish a DC-voltage level which determines the frequency output of the voltage controlled frequency generators. Starting with frequency generator # 1, assuming that the video is being fed into the upper part of the filter, the binary counter will count 96 periods and then generate a trigger pulse, which controls the radar transmitter and all radar timing circuits and the various switches in the filter itself. The functions of this trigger pulse in the filter are to:

- Reset the lower counter to zero.
- Sample V_{in} to establish a new f_{c2} .
- Switch the video to the lower part of the filter.
- Switch off S2, the output of the lower delay line.
- Switch on S1, the output of the upper delay line.

Next, after another PRI and f_{c2} counted to 96, a trigger pulse appears (the counters will only produce a trigger pulse on the count of 96 after each reset). f_{c1} is then set to a new value, counter # 1 is reset, the video is switched to the upper part of the filter, the switch S1 is opened and S2 is closed. Thus the direct signal will always be summed in one part of the filter with the delayed signal stored in the other part. This scheme may be extended to higher order filters.

APPENDIX A

FILTER DESIGN IN THE Z - DOMAIN

It was desired to design a filter with 100 HZ across the null at an attenuation of at least 20 db down.
From a pole-zero plot in the z-domain Figure A-1), the magnitude of the transfer function can be evaluated for every point on the unit circle, geometrically.
By changing the pole and zero locations within the unit circle in a trial and error manner, and comparing the magnitude of the transfer function with the desired shape of the frequency response curve, it was possible to come fairly close after a rather short time:

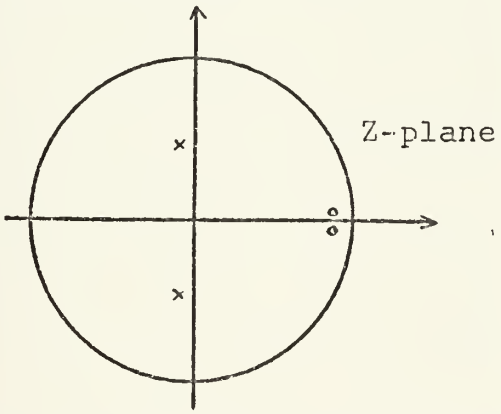

FIGURE A-1. Pole-Zero Plot in Z-Domain.

Results: Zeros: $Z_{12} = 0.8 \pm j0.1$

Poles: $P_{12} = -0.1 \pm j0.5$

This gives the transfer function:

$$H(z) = \frac{0.556 - z^{-1} + 0.4556\ z^{-2}}{1 + 0.14\ z^{-1} + 0.2074\ z^{-2}}$$

A computer simulation of a filter using these cofficients is shown in Figure A-2. The desired width of the stopband, and attenuation was obtained. The filter was also built, and a few data points were plotted, but the implementation of the coefficients were not correct.

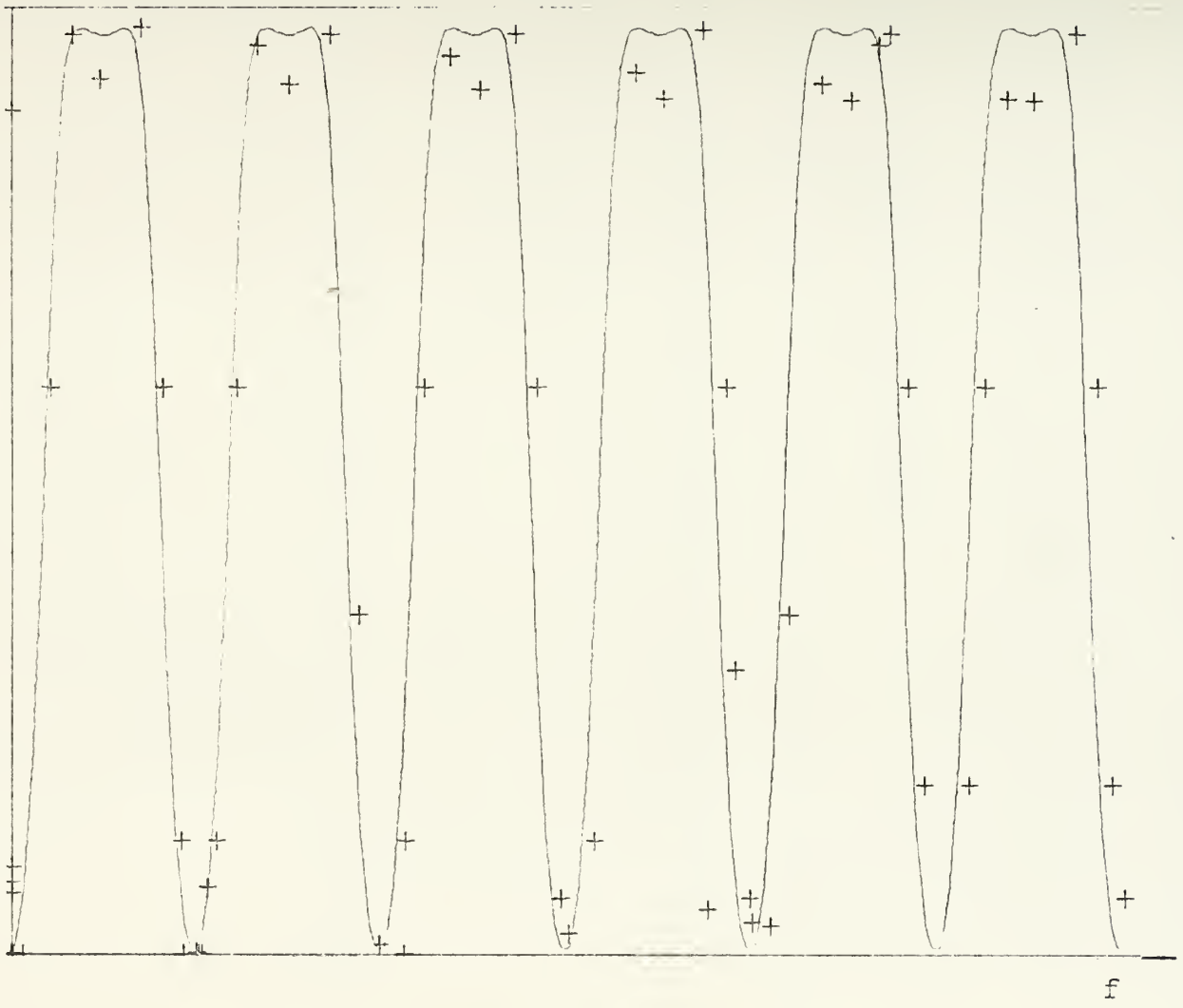

FIGURE A-2. Frequency Response of Filter Using Z-Domain Design

APPENDIX B

```
      THIS PROGRAM CALCULATES THE THEORETICAL RESPONSE OF A SECOND ORDER
      RECURSIVE DIGITAL FILTER.

      THE PROGRAM ALSO READS IN EXPERIMENTAL DATA IN THE FORMAT
      SPECIFIED LATER, AND THEN PRINTS OUT THE EXPERIMENTAL DATA,AND
      ALSO PLOTS BOTH THE THEORETICAL CURVE AND THE EXPERIMENTAL POINTS.

      THE CURVE AND THE POINTS ARE PLOTTED ON THE SAME GRAPH.

      THE FIRST DATA CARD CONTAINS THE COEFFICIENTS OF THE FILTER.
      THE SECOND DATA CARD GIVES THE NUMBER OF POINTS (NPTS), AND THE
      SAMPLING FREQUENCY (FSAMP), WHICH IS THE # OF KHZ BETWEEN THE NULLS
      OF THE FILTER, OR THE PERIOD.

      THE NUMBER OF DATA POINTS MUST ALWAYS BE AT LEAST THE NUMBER
      SPECIFIED BY "NPTS".

      THE NPTS AND FSAMP WILL BE WRITTEN OUT AFTER THE SET OF FILTER
      COEFFICIENTS.

      THE DATA POINTS WILL BE PLOTTED IN GROUPS OF THIRTY.


      DIMENSION FM(350),HM(350),XP(10)
      DIMENSION EP(350),EE(30),EF(30)
      DIMENSION EE(350)
      DIMENSION FX(350),HX(350)
      REAL*8 LABEL/'                '/
      REAL*8 TITLE(12)/'SECOND-ORDER RECURSIVE FILTER    ',
     #2*'                ',
     #'A1= .5    ','A1 =-1.0 ','A2=  0.5','B1 =0.3 ','B2=.2    '/
      REAL*8 TITLE(12)/'SECOND ORDER RECURSIVE FILTER    ',
     #2*'                ',
     #'A1= .5    ','A1 =-1.0 ','A2=  0.5','B1 =0.3 ','B2=.2    ',
     #'                '/
      REAL LABEL/'                '/
      READ(5,51) A0,A1,A2,B1,B2
      READ(5,52) NPTS,FSAMP
      DF=FSAMP/NPTS
      READ(5,52)FX(I),HX(I)
      FX(I)=FX(I)/FSAMP
      DO 3 I=1,NPTS
      PI=3.1415926654
      LP=24

      CALCULATE THE FREQUENCY BETWEEN EACH STEP IN THE THEORETICAL
      CALCULATION OF THE RESPONSE CURVE.

      DW=2.*PI/NPTS
      DF=DW/PI/2.
      NX=NPTS+1
      DO 15 I=1,NX
      FF(I)=(I-1)*DF
5     CONTINUE

      INITIALIZE VARIABLES.

      HMAX=0.
      NM=0.
      EMAX=0.
      NMAX=0.

      CALCULATE MAGNITUDE AND PHASE OF TRANSFER FUNCTION.

      DO 10 I=1,NX
      W=(I-1)*DW
```

```
      C=COS(W)
      CC=COS(2*W)
      S=SIN(W)
      SS=SIN(2*W)
      X2=A0+A1*C+A2*CC
      X1=A1*C+A2*SS
      Y2=1.+B1*C+B2*CC
      Y1=B1*S+B2*SS
      D=X2*Y2+X1*Y1
      N1=X2*Y1-X1*Y2
      N2=Y2*Y2+Y1*Y1
      H(I)=SQRT((1.+C1*C+D1*S)/D)
      HP(I)=ATAN2(N1,N2)
      HD(I)=HP(I)*180/PI
      IF(H(I).GT.HMX)HMX=H(I)
      IF(H(I).LT.HMN)HMN=H(I)
      IF(HP(I).GT.HPX)HPX=HP(I)
      IF(HP(I).LT.HPN)HPN=HP(I)
   10 CONTINUE
      WRITE(6,60)A0,A1,A2,B1,B2
      WRITE(6,62)
      WRITE(6,64)NPTS,FSAMP
      WRITE(6,62)
      WRITE(6,76)
      DO 97 I=1,KPTS
      WRITE(6,77)FX(I),HX(I)
   97 CONTINUE
      WRITE(6,65)
      DO 98 I=1,KPTS
C
C        NORMALIZE THE THEORETICAL VALUES TO ONE.
      HN(I)=H(I)/HMX
   98 CONTINUE
      HMX=1.
C
C        CALL ON THE PLOTTING PACKAGE TO PERFORM THE PLOTTING ,
C
      CALL OPAN(HX,FF,HN,1,0,LABEL,TITL,0,0,0,0,0,0,8,8,0,L)
      MD=2
      DO 30 J=1,10
      JQ=(J-1)*30+1
      IF(JQ.GT.KPTS)MD=3
      CALL OPAN(30,FX(JQ),HX(JQ),MD,2,LABL,TITL,0,0,0,0,0,0,8,8,0,L)
   30 CONTINUE
      WRITE(6,51)
   51 FORMAT(5X,'F',15X,'H')
   52 FORMAT(F15.5,F15.5)
   53 FORMAT(2F15.5)
   54 FORMAT(5X,F10.5)
   60 FORMAT(1H1,1X,'A0 = ',F10.5,5X,'A1 = ',F10.5,5X,'A2 = ',F10.5,
     "5X,'B1 = ',F10.5,5X,'B2 = ',F10.5)
   61 FORMAT(1H1)
   62 FORMAT(1H0)
   65 FORMAT(1H0)
   76 FORMAT(1X,/,/,/,12X,'  NORMALIZED FREQUENCY',5X,
     "'MAGNITUDE',14X,'DB',/)
   77 FORMAT(16X,F10.5,14X,F10.5,14X,F10.5)
  100 FORMAT( 8F10.5)
      STOP
      END
```

LIST OF REFERENCES

1. Oppenheim, A. V. and Schafer, R. W., Digital Signal Processing, Prentice-Hall, 1975.

2. Freund, B. R., Implementation of Comb Filters by Sampled Analog Techniques, Master of Science Thesis, NPGS Monterey 1975.

3. Imsa-ad, V., Discrete Analog Recursive Filters, Master of Science Thesis, NPGS Monterey, 1974.

4. Tao, T. F., and others, Sampled Analog CCD Recursive Comb Filters, Proceedings 1975 International Conference on the application of Charge-Coupled Devices.

5. Buss, D. D. and Bailey, W. H., Applications of Charge Transfer Devices to Analog Signal Processing, 1974 IEEE Intercon Technical Program Papers.

6. Skolnik, M., Introduction to Radar Systems, McGraw-Hill, 1969.

7. Skolnik, M., Radar Handbook, McGraw-Hill, 1972.

8. Kosonocky, W. F. Charge-Coupled Devices - An Overview, 1974 WESCON Technical Papers, Volume 18.

INITIAL DISTRIBUTION LIST

		No of copies
1.	Defense Documentation Center Cameron Station Alexandria, Virginia 22314	2
2.	Naval Headquarters, Royal Norwegian Navy, Oslo Mil Oslo 1, Norway	2
3.	Library, Code 0212 Naval Postgraduate School Monterey, California 93940	2
4.	Department Chairman, Code 52 Department of Electrical Engineering Naval Postgraduate School Monterey, California 93940	2
5.	Assoc. Professor T.F. Tao, Code 52 TV Department of Electrical Engineering Naval Postgraduate School Monterey, California 93940	5
6.	LCDR L.T. Saetre, Royal Norwegian Navy 5075 Haakonshella Norway	2

Thesis
S152145 Saetre
c.1 Sampled analog recursive comb filters and their application to MTI- radar.

Thesis
S152145 Saetre
c.1 Sampled analog recursive comb filters and their application to MTI- radar.